1.0

2.8
3.2
3.6
4.0

2.5
2.2
2.0

1.1

1.8

1.25 1.4 1.6

MICROCOPY RESOLUTION TEST CHART

AFWAL-TR-80-4077

LEVEL

AD A097430

HIGH TEMPERATURE LOW CYCLE FATIGUE DATA FOR THREE
HIGH STRENGTH NICKEL-BASE SUPERALLOYS

J. B. Conway
R. H. Stentz

Mar-Test Inc.
Cincinnati, Ohio

June 1980

TECHNICAL REPORT AFWAL-TR-80-4077

Final Report for Period May 1976 - September 1978

Approved for public release; distribution unlimited.

MATERIALS LABORATORY
AIR FORCE WRIGHT AERONAUTICAL LABORATORIES
AIR FORCE SYSTEMS COMMAND
WRIGHT-PATTERSON AIR FORCE BASE, OHIO 45433

81 4   6 205

REPORT DOCUMENTATION PAGE

READ INSTRUCTIONS
BEFORE COMPLETING FORM

1. REPORT NUMBER	2. GOVT ACCESSION NO.	3. RECIPIENT'S CATALOG NUMBER
AFWAL-TR-80-4077	AD-A097430	

4. TITLE (and Subtitle)
High Temperature Low Cycle Fatigue Data for Three High Strength Nickel-Base Superalloys.

5. TYPE OF REPORT & PERIOD COVERED
Final rept.
May 76 — Sep 78

6. PERFORMING ORG. REPORT NUMBER

7. AUTHOR(s)
J.B. Conway and R.H. Stentz

8. CONTRACT OR GRANT NUMBER(s)
F33615-76-C-5245
F33615-76-C-5191

9. PERFORMING ORGANIZATION NAME AND ADDRESS
Mar-Test Inc.
Cincinnati, OH

10. PROGRAM ELEMENT, PROJECT, TASK AREA & WORK UNIT NUMBERS
23072104 P1

11. CONTROLLING OFFICE NAME AND ADDRESS
Materials Laboratory
Air Force Wright Aeronautical Laboratories
Air Force Systems Command
Wright-Patterson Air Force Base, OH 45433

12. REPORT DATE
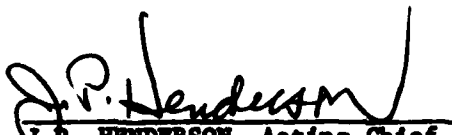June 1980

13. NUMBER OF PAGES

14. MONITORING AGENCY NAME & ADDRESS(if different from Controlling Office)
119

15. SECURITY CLASS. (of this report)
Unclassified

15a. DECLASSIFICATION/DOWNGRADING SCHEDULE

16. DISTRIBUTION STATEMENT (of this Report)

Approved for Public Release; Dist. unlimited

17. DISTRIBUTION STATEMENT (of the abstract entered in Block 20, if different from Report)

18. SUPPLEMENTARY NOTES

19. KEY WORDS (Continue on reverse side if necessary and identify by block number)

Rene 95	Low Cycle Fatigue
AF-115	Crack Initiation
AF2-1DA	Superalloys

20. ABSTRACT (Continue on reverse side if necessary and identify by block number)
This report presents a summary of the high temperature low cycle fatigue data for three high strength nickel-base superalloys, Rene 95, AF-115, and AF2-1DA. The majority of tests were performed in strain control at $1200°F$ and $1400°F$, and at frequencies of 20 cpm, 0.2 cpm, and 0.05 cpm. Conventional triangular waveform was used for most of the testing although strain dwell tests and some SLOW-FAST and FAST-SLOW tests were also included.

DD FORM 1473 EDITION OF 1 NOV 65 IS OBSOLETE
1 JAN 73

The primary purpose of this report is to make these data available in the literature. Some analyses and interpretation of the data are also included along with an original format for data presentation in terms of stress amplitude and mean stress.

FOREWORD

Accession For	
NTIS GRA&I	☑
DTIC TAB	☐
Unannounced	☐
Justification	
By	
Distribution/	
Availability Codes	
Dist	Avail and/or Special
A	

TABLE OF CONTENTS

SECTION I

INTRODUCTION

A major area of concern in the development of recent military turbine
engines has been life cycle management. A part of the technology needed to
optimize the life of components, such as turbine disks, is the ability to
accurately predict their crack initiation lives under typical cyclic conditions.
With the increasing turbine temperatures that accompany performance gains, the
turbine section operating conditions are becoming increasingly severe. Typical
military flight missions include significant dwell periods at high power settings
with the result that time dependent damage mechanisms operate. This has
necessitated modification of existing life relationships previously relied
upon at lower temperature.[1]

Programs have been initiated at the Materials Laboratory and in industry
to develop analytical models for predicting crack initiation in nickel-base
superalloys under creep-fatigue conditions. As part of the effort, this
work was initiated to provide a substantive low cycle fatigue data base
for alloys of particular interest to the Air Force. The alloys that have been
tested extensively under this program are cast and wrought Rene 95, a current
turbine disk alloy rated for 1200°F service, and AF-115 and AF2-1DA, powder
metallurgy superalloys being developed for 1400°F use. The test matrix has
been designed to study the effect of cyclic frequency and dwell period and it
has been necessarily limited to the primary service temperature for each
alloy. Where possible, additional waveforms and temperatures have been included.

The major emphasis of this report is on data presentation. A complete
summary of all the fatigue tests is present in Tables 1 through 6. Some
analysis and interpretation of data trends have also been included.

The evaluations of the data focus on attempts to identify mathematical models for certain materials behavior. An original format for data presentation in terms of stress amplitude and mean stress is described.

The data generated in this program have been the basis for three AFML Technical Reports, (2,3,12) and have been included in the proceedings of an AGARD panel meeting.[4] An extensive review of the analytical models for predicting LCF crack initiation at elevated temperature is the subject of one of the AFML Technical Reports.[2] Another AFML Technical Report gives the behavior of the stresses during many of the fatigue tests.[12]

SECTION II

MATERIALS

1. <u>AF-115</u>

a. Processing

Two vacuum induction melted ingot master heats, V03963 and V03964 were

made in the Carpenter Technology Corporation R&D Center. The chemistries of

these heats are shown in Table 1. The VIM master heats were vacuum induction

remelted as a single atomization heat, A844, which was subsequently argon

atomized. The chemistry of this heat is also shown in Table 1.

Type 304SS canisters were prepared and powder was charged into canisters

(C646 and C655) under vacuum less than 5 microns Hg. The canisters were

compacted in two separate HIP cycles #1474 and #1477 using Industrial Materials

Technology Corporation's 8" x 26" National Forge Unit. The pressing parameters

used were 2175°F/2 Hrs./15 ksi.

Subsequent to compaction, canister C646 was cut into 10 slices. Slices

#3, #5, and #8 were then forged by the Wyman-Gordon Company prior to heat

treatment. The forging practice involved using die shocks heated to 1650-2100°F

at a press head velocity of 1 to 5 inches/minute. A total reduction of 50%

was accomplished.

All ten pancakes (3 forged plus 7 as HIP) were solution-treated at a

temperature of 2175°F (+10, -25) for four hours followed by a fan air-cool. The

aging treatment was 1425°F (+25) for 16 hours followed by an air-cool. The

tensile properties of AF-115 in both the HIP and HIP plus forge conditions are

summarized in Table 2.

3

b. **Microstructure**

The AF-115 alloy was studied in the HIP and heat treated, as well as the HIP plus forged and heat treated conditions. The recommended processing parameters for these treatments resulted in a very similar microstructure, that differed significantly only in grain size. The AF-115 microstructure was dominated by three distinct sizes of γ' precipitate. The irregular shaped unsolutioned γ' precipitates were positioned along the grain boundaries and were approximately 3-10μ along their major axis, and the cooling γ' particles which were contained within the grains were cuboidal in shape approximately .25μ on edge. The ultra-fine aging γ' particles were more shpeherical in shape and had a diameter of .02-.04μ.

AF-115 also contained a small amount of carbides which were approximately 50μ in diameter. The carbides were, in general, uniformly distributed throughout the grain boundaries often lying near the unsolutioned γ' particles. There were observations in isolated areas of carbide particles decorating prior particle boundaries, but this did not appear to be a general problem. Although neither quantitative analysis nor microdiffraction studies were undertaken, the majority of the carbides in AF-115 were believed to be MC type. This was supported by microprobe analysis which indicated that the carbides were rich in MC formers; titanium, columbium, tantalum, and hafnium; and depleted in chromium, a $M_{23}C_6$ carbide former.

The grain size of the as-HIP AF-115 was ASTM #7.0 (30μ diameter), while the HIP plus forged alloy had a grain size of ASTM #8.5 (19μ diameter). The AF-115 alloy was processed into 10 individual pancakes of material. There was uniformity of microstructure and mechanical properties for all pancakes.

c. Powder Metallurgy Defects

There were three distinct defect types that were found in this heat of
AF-115 alloy; pores, nonmetallic inclusions, and hafnium oxide inclusions. Pores
were the most populous of the defects. The porosity is a by-product of the powder
production process. Argon gas is adsorbed onto the powder surface or entrapped in
hollow particles during the argon atomization phase. The gas subsequently expands
during the solution heat treatment which results in the porosity. The level of
porosity is, therefore, a function of atomization processing and solutioning temp-
erature.

The level of porosity in the AF-115 alloy was quantitatively determined
using a thermal induced porosity (TIP) test. This involved measuring the density
of a sample of the billet material before and after the solutioning heat treatment.
The change in density due to the expansion of the gas at high temperature was a
measure of the porosity level.

This heat of AF-115 had a change in density due to thermal induced porosity
of .42% after solutioning at 2175°F. This is considered an abnormally high level.
The pores ranged in size from a few microns in diameter to approximately 130μ in
diameter.

Considerably less populous than the pores was the second most prevalent defect
in AF-115, nonmetallic inclusions. These were tramp pieces of ceramic equipment
liners used in the powder production process. These inclusions were generally
high in concentrations of calcium, silicon, aluminum, and magnesium. These
inclusions were up to 100μ in length and ranged from spherical to elliptical in
shape. The inclusions were often fractured before fatigue testing and were
generally poorly bonded to the matrix.

The final and least populous defect in this heat of AF-115 was the hafnium oxide inclusions (probably HfO_2). These inclusions were plate-like and were up to 125μ in diameter with a thickness of only 5μ. They formed in the melt and were a result of the high hafnium content. HfO_2 particles were normally bonded more strongly to the matrix than the other inclusions.

TABLE 1

AF-115 – CHEMICAL ANALYSES; WT. PERCENT

Element	V03963	V03964	A00884
C	.155	.164	.155
Mn	.01	.01	<.01
Si	<.01	<.01	.03
P	<.005	<.005	<.005
S	.003	.003	.002
Cr	10.80	11.08	10.20
Ni	Bal.	Bal.	Bal.
Mo	2.86	2.90	2.62
Co	15.04	15.30	14.95
Ti	3.92	3.84	3.90
Al	4.00	3.79	3.85
Cb	1.64	1.75	1.62
W	6.05	6.20	5.62
B	.022	.023	.023
Hf	0	0	2.02
Zr	0	0	.045
O	.0006	.0012	.0044
N	.001	.001	.001

TABLE 2

TENSILE PROPERTIES AF-115

PANCAKE	TEMP, °F	0.2% YIELD STRENGTH, ksi	UTS, ksi	ELONGATION, %	RA, %
9 HIP	1400	152.5	172.9	8.9	9.5
2 HIP	1400	143.5	167.7	7.8	11.6
7 HIP	1400	146.9	173.4	7.6	12.9
9 HIP	1500	135.4	146.5	11.7	11.2
5 HIP/Forge	1400	150.8	164.2	8.0	13.1
5 HIP/Forge	1400	151.0	168.8	11.0	12.85

8

2. <u>AF2-1DA</u>

a. Processing

The two AF2-1DA pancakes (B1 and B2) used for this study were produced from Federal Mogal Inc. powder Heat 454. The composition of the powder is contained in Table 3. The powder was 100 mesh argon atomized.

The powder was sealed in a stainless steel can and compacted at 2000°F ±25°F at 30,000 psi for 21 seconds. The compact was then extruded at 2025°F ±25°F. The reduction ratio was 7.3 to 1.0. After extrusion, the compact was superplastically forged at 2025°F ± 15°F, at a strain rate of 0.1 in/in/min.

The forgings were finally heat treated by the following sequence:

      1)   2210°F ± 15°F/2 Hrs./Air Cool

      2)   2050°F ± 15°F/2 Hrs./Air Cool

      3)   1300°F ± 25°F/8 Hrs./Air Cool

      4)   1500°F ± 25°F/8 Hrs./Air Cool

The tensile properties of AF2-1DA are summarized in Table 4.

9

b. Microstructure

The AF2-1DA microstructure also had three sizes of γ' precipitate.
An irregular shaped primary γ' (1-3) decorated the grain boundaries with
cuboidal cooling γ' (.25μ) and aging γ' (.06-.08μ) contained within the grains.

Due to the higher carbon content, there were more carbides in the AF2-1DA
microstructure than in AF-115. The carbides were again rich in MC carbide formers,
and they were evenly dispersed throughout the microstructure.

The grain size for AF2-1DA was relatively large (grain diameter 200μ).
Also prevalent within the grains were annealing twins of varying size.

c. P/M Defects

Although the AF2-1DA powder was also made by the argon atomization technique, the processing of this heat of powder was such that there was no significant level of porosity in the forgings. There were also no hafnium oxide inclusions as in the AF-115 alloy. The only defects were nonmetallic inclusions similar to those in the AF-115 alloy. Their size ranges up to 100μ in length.

TABLE 3

CHEMICAL COMPOSITION - AF2-1DA; WT. PERCENT

(Heat 454)

Cr		12.22	Zr		.084
Ti		2.89	Si	<	0.1
Co		10.10	Fe	<	0.1
W		5.70	B		.016
Al		4.70	C		.31
Mo		3.00	S		.007
Ta		1.90	P	<	.002
Mn	<	0.1	O_2		65 PPM

Balance - Nickel

TABLE 4

TENSILE PROPERTIES - AF2-1DA

PANCAKE	TEMP. °F	0.2% YIELD STRESS (ksi)	UTS (ksi)	RA (%)
B2	1400	131.8	138.9	17.9
B2	1400	130.3	139.8	17.5
B1	1500	126.3	134.4	23.9

3. Rene 95

The two pancakes of cast and wrought Rene 95 used in this program were taken from a vacuum induction melted and vacuum arc remelted ingot approximately 0.228 m in diameter. The alloy composition is given in Table 5. The ingot was given a homogenization anneal in the range 2125°F - 2175°F for four hours and then furnace cooled. The pancakes were subsequently reheated to 2000° - 2080°F and forged to bring the thickness to 40-50% above the final value. This was followed by a recrystallization anneal at 2125°F for one hour. This results in a uniform grain diameter between .064 -.127mm. The forgings were cooled from the recrystallization temperature at a rate greater than 150°F per hour to 1650°F and then air cooled and taken to final processing. The forgings were reheated to 1975° - 2025°F and the final reduction was applied, resulting in a further 40-50% decrease in thickness. The pancakes were then partially solutioned at 2000°F, oil quenched to a temperature below 900°F, and aged at 1400°F for 16 hours. This processing resulted in a duplex microstructure consisting of warm worked grains surrounded by a necklace of very fine recrystallized grains.

The Rene 95 forgings have been characterized in terms of microstructure, tensile behavior, and room temperature LCF crack initiation mechanisms.[5,6,7] The tensile and creep properties of Rene 95 are summarized in Table 6.

14

TABLE 5

CHEMICAL COMPOSITION OF RENE 95*

Nickel	61
Chromium	14
Cobalt	8
Tungsten	3.6
Aluminum	3.6
Molybdenum	3.5
Niobium	3.5
Titanium	2.5
Carbon	0.15
Iron	0.13
Silicon	< 0.10
Manganese	< 0.10
Zirconium	0.04
Boron	0.012
Phosphorus	< 0.01
Nitrogen	0.003
Sulfur	0.002
Lead	< 0.001
Oxygen	7 ppm
Silver	< 5 ppm
Bismuth	< 1 ppm

---

*WT %

TABLE 6

AVERAGE TENSILE PROPERTIES OF RENE 95 AT 1200°F

Yield Stress:	175 ksi
Ultimate Stress:	210 ksi
Modulus of Elasticity:	25.4×10^3 ksi
% Reduction in Area:	12
% Elongation:	11

RENE 95 CREEP TESTS AT 1200°F

| Specimen	Stress (ksi)	Secondary Creep Rate (in/in/min)	Time to Failure (min)
C-1-B	180	5.26×10^{-4}	94
C-2-B	171	4.85×10^{-5}	433
C-4	171	6.90×10^{-5}	430
219	160	4.00×10^{-5}	960

SECTION III

## TEST PROCEDURES

1. SPECIMENS AND EQUIPMENT

Strain-controlled low-cycle fatigue evaluations were performed on two different specimen configurations (see Figure 1). Hourglass-shaped specimens were used with the Rene 95 material and uniform gage length, parallel-sided specimens were used with the AF-115 and AF2-1DA materials. All specimens were heated inductively using specially developed induction coils that have been demonstrated to produce very flat temperature profiles within the gage section of the specimen.

Test temperatures were controlled using spot-welded chromel-alumel thermocouples and solid state controllers. The thermocouples were attached just assure that the desired test temperature level and profile were established in the gage section.

In preparing for each test, the specimens were cleaned with Freon and the thermocouples were spot-welded at the proper locations. Then the specimens were connected to the load train and positioned within the induction coil. For the threaded specimens used in these tests special adapters were employed which contain precision machined flat surfaces for mating with the top and bottom surfaces of the specimen. The buttonhead ends of the adapters were mounted in the specimen holding fixture on the test machine using a split collet type of assembly. Buttonhead specimens were loaded directly into these fixtures. A leveling device was employed to assure that the specimens were installed perpendicular to the platen on the machines. Before any load was applied to the specimen, a visual inspection of the final load train connection was made. This was done by comparing the alignment and parallelism of two closely spaced, precision ground, flat surfaces before they were bolted together. In this

17
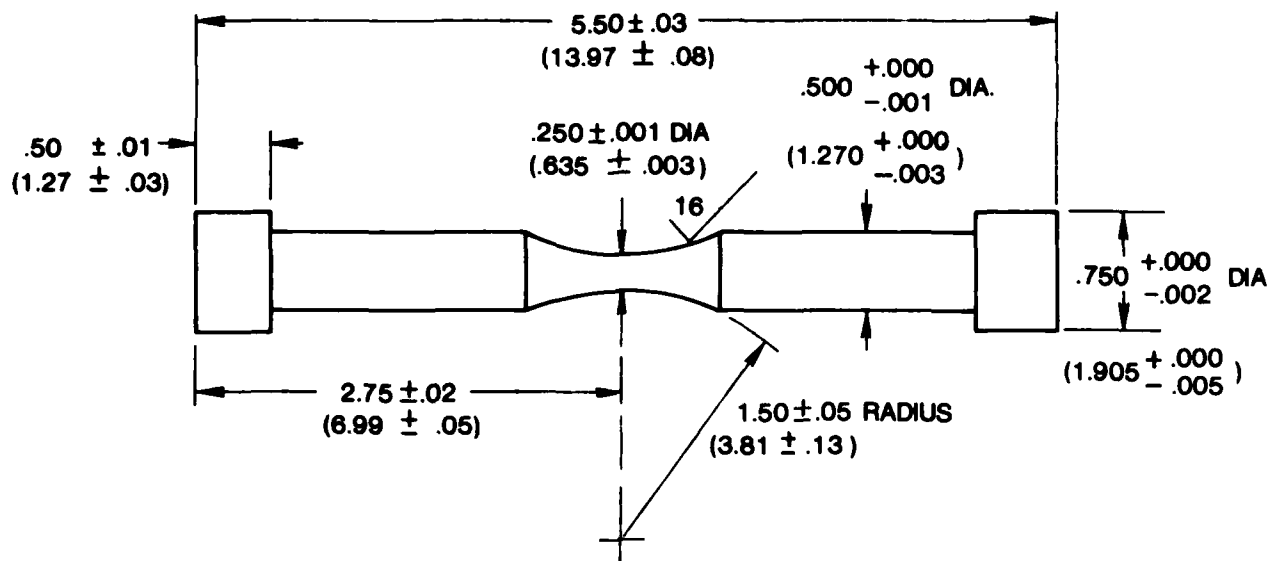
(a) HOUR GLASS-SHAPED SPECIMEN
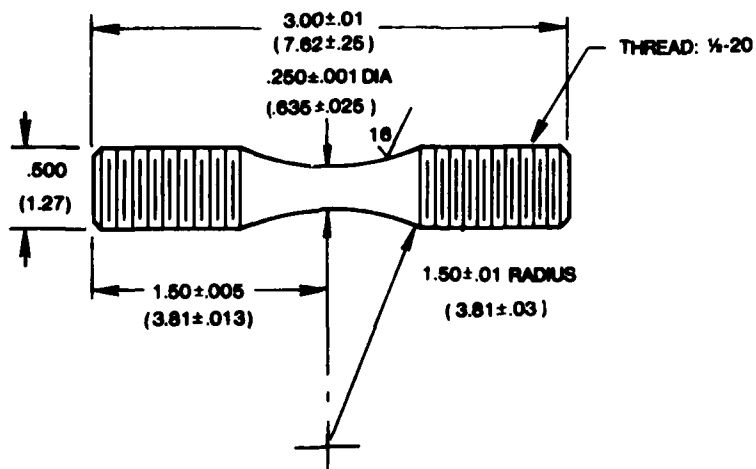
(b) Uniform Section Specimen
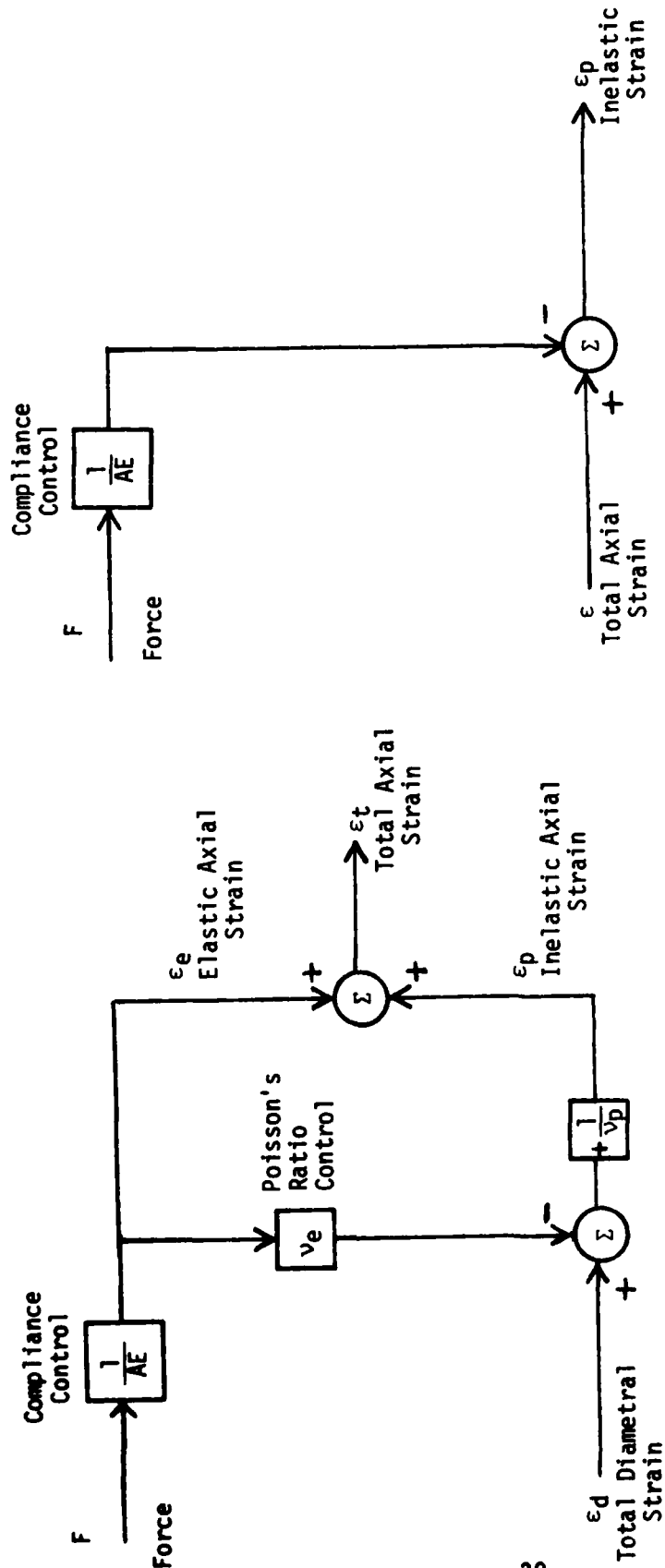Fig. 1 Test Specimen Designs Used in this Study

18

manner, the specimen alignment in each and every specimen installation was checked prior to the test. The final bolting operation was performed with the system in load control so that the specimen was not subjected to any extraneous forces during this final assembly operation.

At this time the extensometer was attached to the specimen. For the hour-glass-shaped specimens, the diametral extensometer was attached to the minimum diameter which automatically established the gage section. For the uniform gage specimens, a previously established electronic calibration was used to position the extensometer tips over a length that would yield a gage section of exactly 0.500 inch when the specimen was heated to test temperature.

Before any hourglass specimens were tested, the analog strain computer was calibrated by making use of the specimen cross-sectional area (A) and the value for Young's Modulus (E) at the intended test temperature. The values of A and E were used as shown in the block diagram in Figure 2 to generate axial strain values corresponding to measured values of diametral strain and force. This diagram provides an aid to an understanding of the computer calibration procedure which is based on using the values of A and E and adjusting the compliance control to establish the followin equality:

$$AE = \frac{F}{\varepsilon_e} \tag{1}$$

Prior to heating a specimen to the desired test temperature, the system was placed in force control. This automatically kept the force at zero by gradually lowering the movable platen to account for the thermal expansion of the specimen as the temperature was increased. When the test temperature was obtained, the calibration of the analog strain computer was continued. The specimen was cycled elastically and the inelastic strain output was set to zero. This procedure established the correct value for Poinsson's ratio elastic, ν_e, and calibrated the inelastic strain signal with hourglass specimens. The same procedure was used

19

Compliance Control

$$\frac{1}{AE}$$

F
Force

ϵ
Total Axial
Strain

$+$

$-$

Σ

ϵ_p
Inelastic
Strain

b. Block Diagram of a Strain Computer
Used with an Axial Extensometer

Compliance Control

$$\frac{1}{AE}$$

F
Force

ϵ_e
Elastic Axial
Strain

Poisson's
Ratio
Control

ν_e

$+$

Σ

$+$

ϵ_t
Total Axial
Strain

$$\frac{1}{\nu_p}$$

ϵ_p
Inelastic Axial
Strain

$-$

Σ

$+$

ϵ_d
Total Diametral
Strain

a. Block Diagram of Strain Computer Used with
A Diametral Extensometer

FIG. 2. Schematic Diagrams of Operation of Computer
used in Strain control testing.

20

to calibrate the inelastic strain signal when uniform gage specimens were tested. At this point, the computer was completely calibrated and capable of furnishing the strain components of interest.

Two strip chart recordings were made during start-up, one of the axial force on the specimen and the other of the total axial strain. In addition, a X-Y recorder was used to plot the initial hysteresis loops. The system was placed in number strain control keeping the force at a minimal level by using a by-pass valve. The desired cyclic strain was then gradually established in the specimen. After all final manual adjustments were made to the test machine, the test conditions were automatically held constant until failure.

Hysteresis loops were obtained on the X-Y recorder during the first few cycles and at frequent intervals thereafter. In addition, a continuous recording was made of the applied force and the associated inelastic strain.

After failure occurred, determined either by complete specimen separation or some pre-determined stage of specimen cracking, the shut-down circuit automatically de-energized the entire system including the hydraulic solenoind, induction generator, timing device, cycle counter, and recorders.

2. WAVEFORMS

Various waveforms were used in the course of this data generation program. The majority of specimens, however, were tested using continuous cycling (triangular waveform) and simple strain hold cycles. The continuous cycling tests were run at frequencies of 20 cycles per minute (cpm), 0.2 cpm, and 0.05 cpm. A schematic of this waveform is shown in Figure 3. The simple strain hold cycles included hold times in tension, compression, and tension and compression. These waveforms are also shown in Figure 3 and the nomenclature is further explained in Table 7.

A limited number of tests was also performed on Rene 95 using less conventional waveforms including SLOW-FAST and FAST-SLOW cycling and unsymmetrical strain holds. These waveforms are also illustrated in Figure 3 and further described in Table 7.

TABLE 7

DESCRIPTION OF FATIGUE CYCLES AND NOMENCLATURE

| Symbol	Description
20 cpm, 0.2 cpm, 0.05 cpm	Continuous cycling at a frequency of 20 cycles/min, 0.2 cycles per minute, and 0.05 cycles per minute.
1-0	1-min. hold time at maximum strain in tension. 20-cpm ramps for the strain reversals.
10-0	As in 1-0, except 10-min. hold time instead of 1 min.
0-1	1-min hold time at maximum strain in compression. 20-cpm ramps for the strain reversals
0-10	As in 0-1, except 10-min hold time instead of 1 min.
1-1	1-min hold time at maximum strain both in tension and compression. 20-cpm ramps for the strain reversals.
10-10	As in 1-1, except 10-min hold time instead of 1 min.
20-0.05 cpm	Continuous cycling at two frequencies. The positive strain rate was 20-cpm and the negative strain rate was 0.05-cpm. The changes in strain rate occurred at the peak tensile and compressive strains.
20-1/2-0.05 cpm	As in 20-0.05-cpm, except the change from the fast to the slow strain rate occurred halfway between the peak tensile and zero strain.

TABLE 7 (Con't)

Symbol	Description
0.05-20-cpm	Continuous cycling at two frequencies. The positive strain rate was 0.05-cpm and the negative strain rate was 20-cpm. The changes in strain rate occurred at the peak tensile and compressive strains.
0.05-1/2-20-cpm	As in 0.05-20-cpm, except the change from the fast to the slow strain rate occurred halfway between the peak compressive strain and zero strain.
1-1/2-20 cpm	As in 0.05-1/2-20-cpm, except the slow strain rate was 1-cpm.
11-0	1-min hold time before the peak tensile strain. 20-cpm ramps for the strain reversals.
0-11	1-min hold time before the peak tensile strain. 20-cpm ramps for the strain reversals.
10-1	10-min hold time at the peak tensile strain and 1-min hold time at the peak compressive strain. 20-cpm ramps for the strain reversals.
1-10	1-min hold time at the peak tensile strain and 10-min hold time at the peak compressive strain. 20-cpm ramps for the strain reversals.

CONTINUOUS STRAIN CYCLING (20 CPM, .05 cpm)
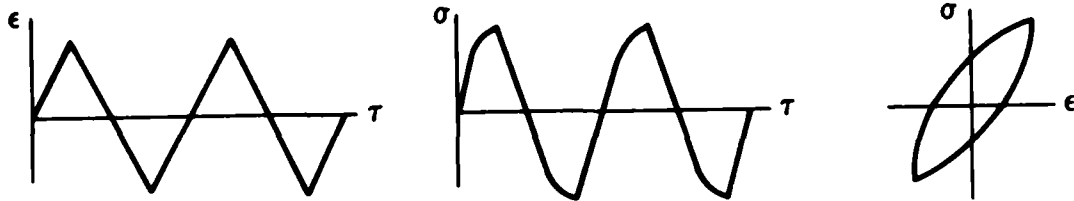
TENSION STRAIN HOLD (CP - 1/0, 10/0)
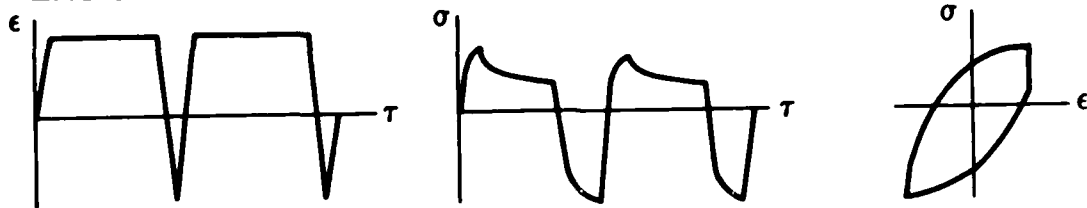
COMPRESSION STRAIN HOLD (PC - 0/1, 0/10)
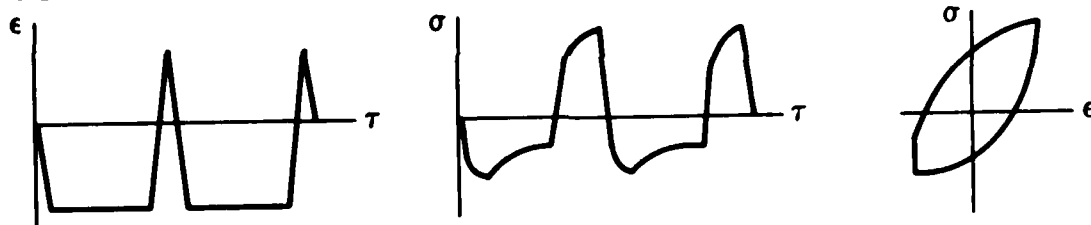
TENSION AND COMPRESSION STRAIN HOLD (CC - 1/1, 10/10)
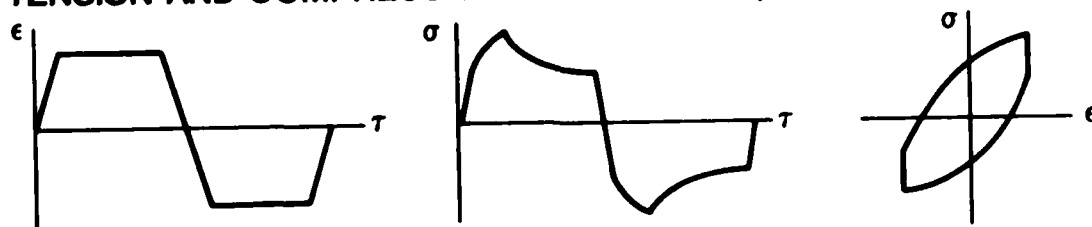
Figure 3   Waveforms and Hysteresis Loops of Fatigue Tests

FAST/SLOW (F/S, 20 - 0.05cpm)
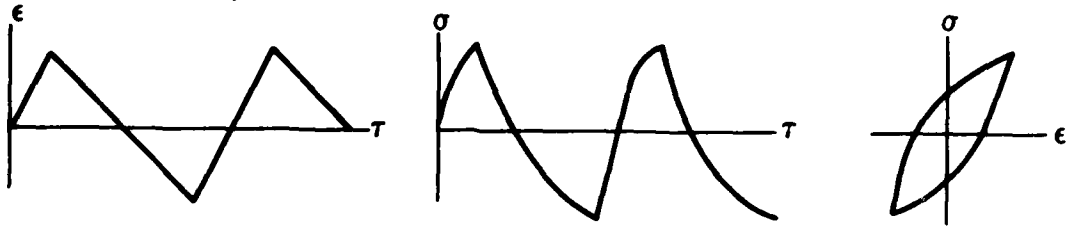
FAST/SLOW (F/S, 20 - ½ - 0.05 cpm)
WITH RATE CHANGE HALFWAY BETWEEN MAX. AND ZERO STRAIN
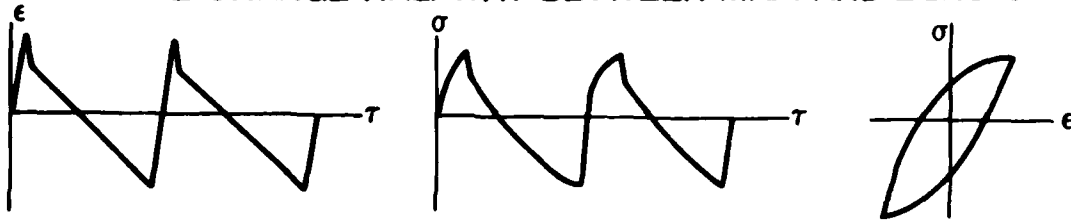
SLOW/FAST (S/F, 0.05 - 20 cpm)
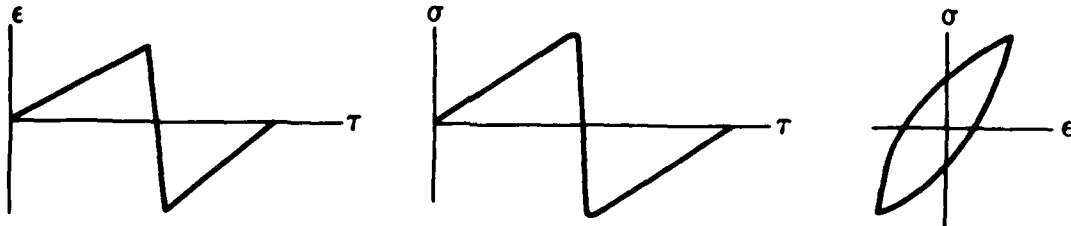
SLOW/FAST (S/F, 0.05 - ½ - 20 cpm, 1 - ½ 20 cpm)
WITH RATE CHANGE HALFWAY BETWEEN MIN. AND ZERO STRAIN

FIG. 3 (Con't)

26
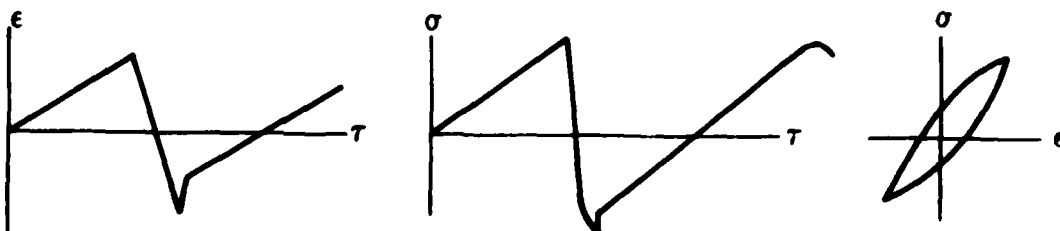
UNSYMETRICAL STRAIN HOLD (10/1)
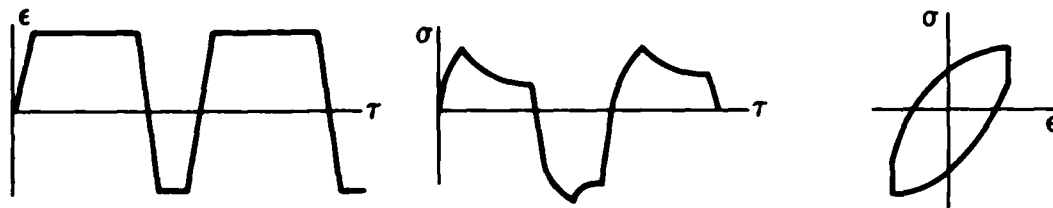
UNSYMETRICAL STRAIN HOLD (1/10)
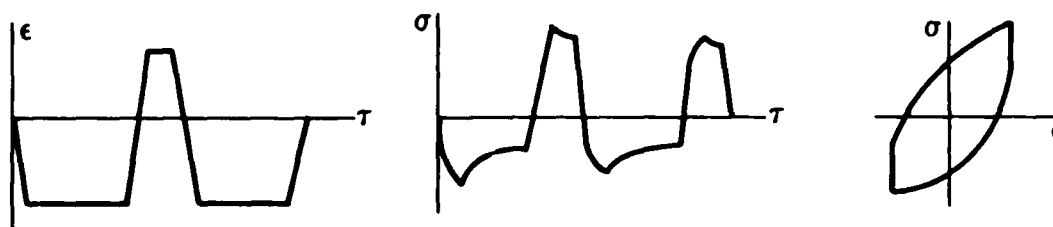
INTERMEDIATE TENSILE STRAIN HOLD (11/0)
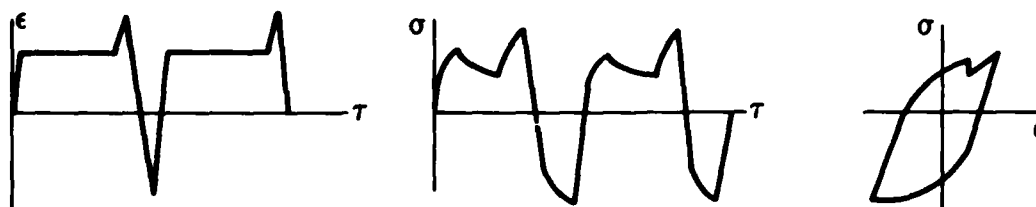
INTERMEDIATE COMPRESSIVE STRAIN HOLD (0/11)

Figure 3 (continued)

27

SECTION IV

RESULTS AND DISCUSSION

1. AF2-1DA

A summary of the test data generated in the evaluation of the alloy,
AF2-1DA is presented in Appendix A. These tests employed uniform gage section
specimens tested using axial strain measurement and control. It will be noted
that 60 tests were performed, all with an A-ratio* (on strain) of unity, with
the distribution shown in Table 8.

A semilogarithmic plot of $\Delta\epsilon_t$ vs. N_f for the AF2-1DA alloy is presented
in Figure 4 to define the behavior at 1400°F for a test frequency of 20 cpm.
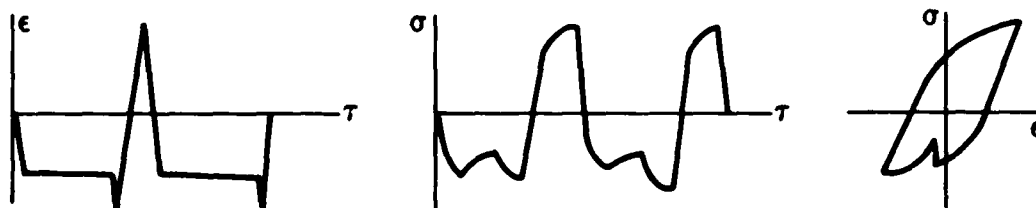Within reasonable scatter these data can be represented by two linear segments
intersecting near a strain range of 0.73%. This behavior pattern persists to
a fatigue life of about 100,000 cycles which represents the range of the
experimental data. Beyond this regime the fatigue response has not been
defined but it will probably not be respresented by an extension of the linear
segment defined in the range from 10,000 to 100,000 cycles. It is expected
that eventually the data will tend toward an endurance limit and a fatigue life
in excess of that corresponding to the linear extension just described.

An overall comparison of all the continuous cycling data is presented in
Figure 5. It is to be noticed that the data at 1400°F for a frequency of 0.2 cpm
fall very close to the bilinear representation defined in Figure 4 indicating
little to no frequency effect over this frequency range. This conclusion should
be restricted to the strain ranges tested, however, since no tests were preformed
below a strainrange of 0.70% to determine if this type of frequency response will
continue to be exhibited out to 100,000 cycles. A test at 0.2 cpm near a strain
range of 0.60 or 0.65% would be needed to complete this definition of frequency
response.

*A - ratio can be used in terms of stress or strain and is defined as
the alternating component divided by the mean value, or, mathematically,
as: $(\sigma_{max} - \sigma_{min})/(\sigma_{max} + \sigma_{min})$ or $(\epsilon_{max} - \epsilon_{min})/(\epsilon_{max} + \epsilon_{min})$

TABLE 8 - DISTRIBUTION OF LOW-CYCLE FATIGUE TESTS PERFORMED FOR AF2-1DA ALLOY

	Number of Tests			
	1500°F	1400°F	1200°F	R.T.
20 cpm	7	19[a]	9	2
0.2 cpm	4	6	2	—
4.95 minutes Hold in Tension	1	5[b]	1	—
4.95 minutes Hold in Compression	—	1	1	—
1 minute Hold in Tension	—	1	—	—
1 minute Hold in Compression	—	1	—	—
	12	33	13	2

a) One test was in load control.

b) One test was a void test.

29

FIGURE 4
STRAIN RANGE VS N_F
AF2-1DA

1400°F 20 cpm A = +1.0

Figure 5
Strain Range vs N_F
AF2-1DA

$A = +1.0$

	20 cpm	0.2 cpm
1400°F	◁	○
1200°F	□	
R.T.	▷	
1500°F	▽	▽

FROM FIGURE 4

$\Delta \epsilon_t$, %
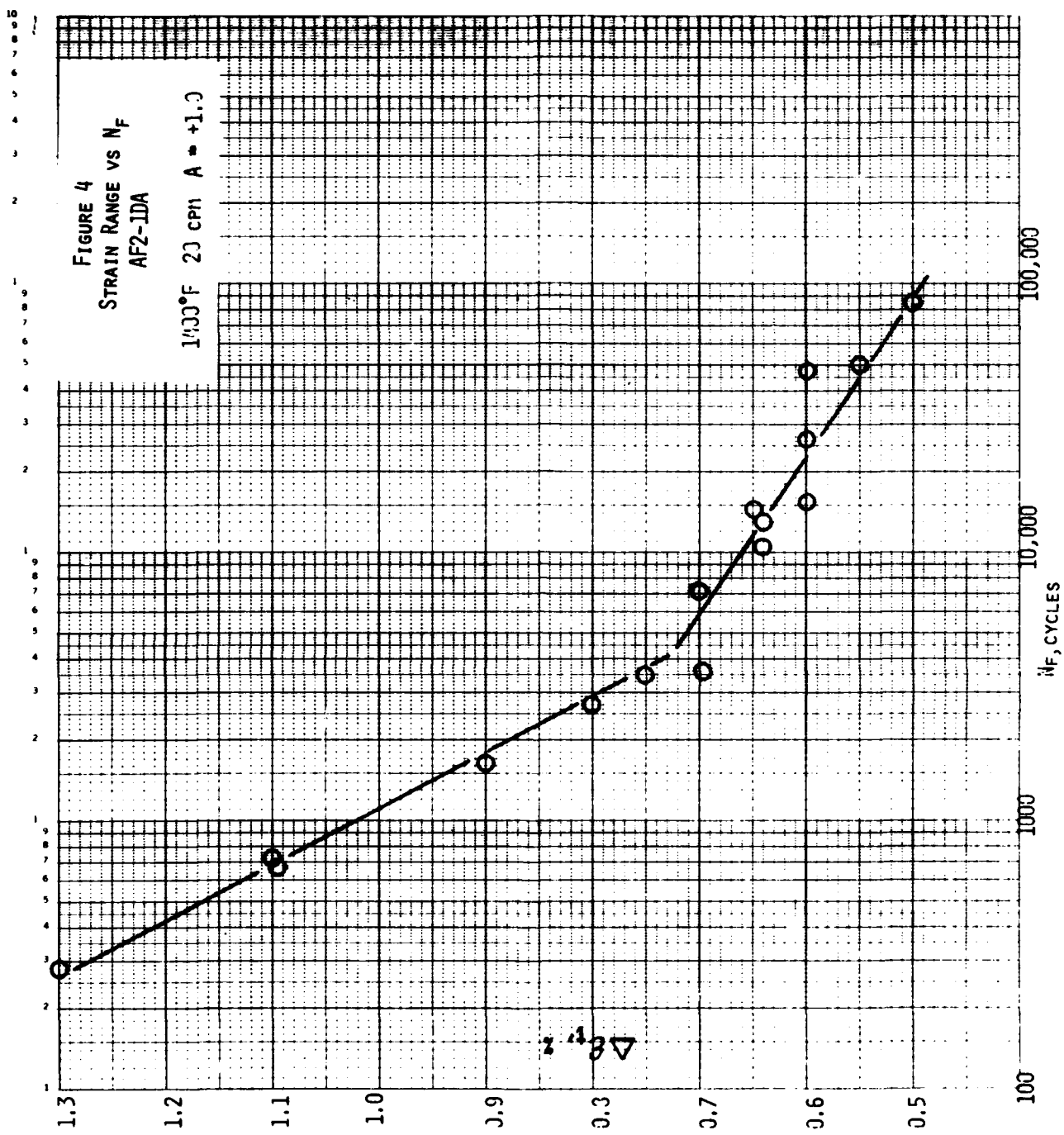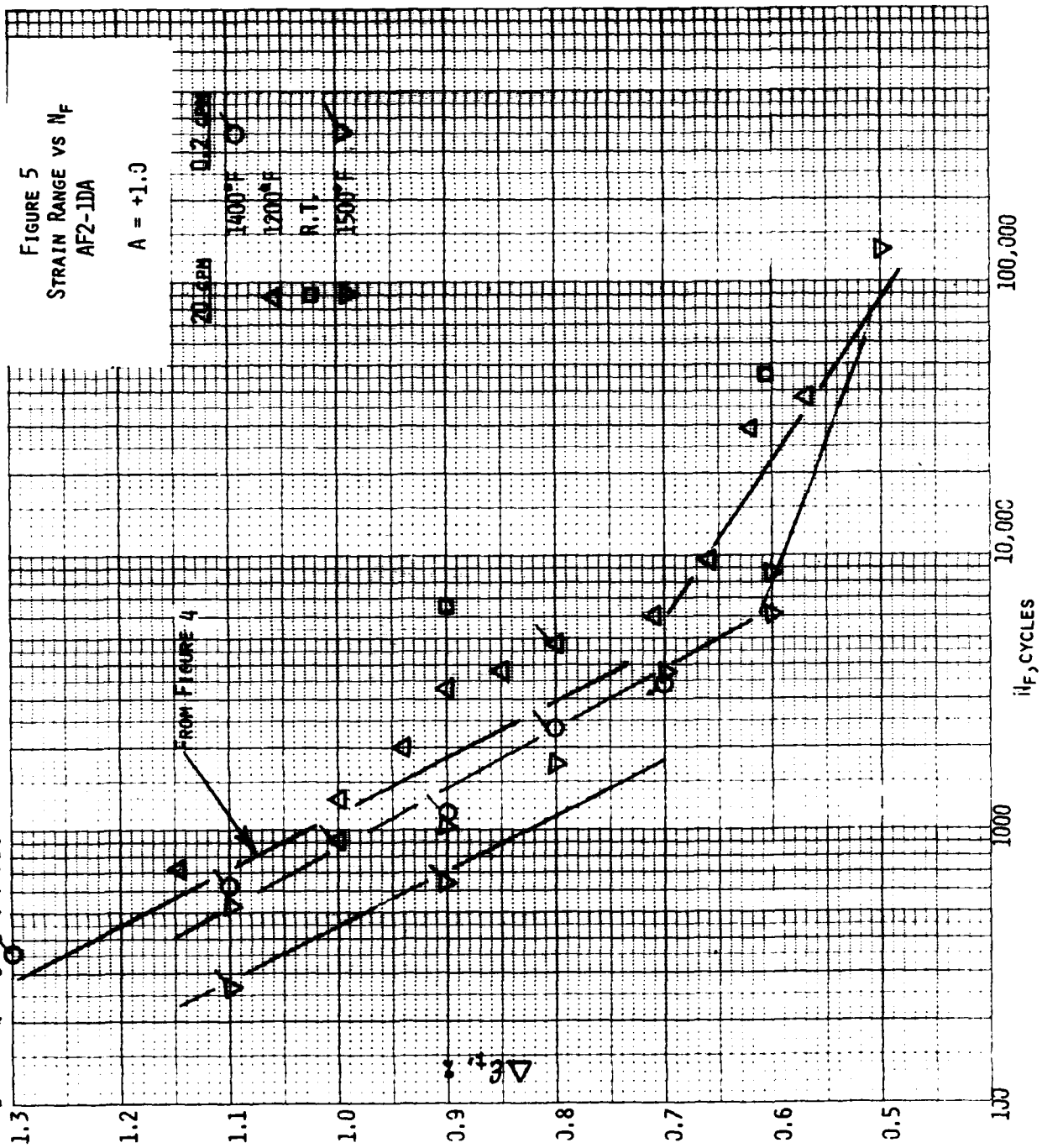
N_F, CYCLES

Another interesting observation associated with Figure 5 involves temperature

effects. At 1200°F, the bilinear representation of Figure 4 defines the data

at 1200°F fairly well, especially in the life regime beyond 6,000 cycles. At

lower cyclic life values the bilinear representation for 1400°F lies just below

the data at 1200°F but it would predict the 1200°F data well within a factor

of two. Also to be noted, is the absence of a frequency effect at 1200°F

which, of course, would be expected since little to no frequency effect was

noticed at 1400°F. Finally, the data at 1500°F fall slightly to the left of

the bilinear relationship established at 1400°F although there does seem to

be a tendency for the fatigue behavior at 1500°F to approach that at 1400°F

in the long life regime. This behavior at 1500°F has been approximated by the

bilinear construction shown in Figure 5. Included in this construction is

a separate dashed line for the data at 1500°F and a frequency of 0.2 cpm.

A definite frequency effect is apparent at 1500°F although the effect seems to

be well within a factor of two compared to the data at 20 cpm.

In view of the limited number of data points at room temperature no

discussion of these results is offered. It will be noted, though, that the two

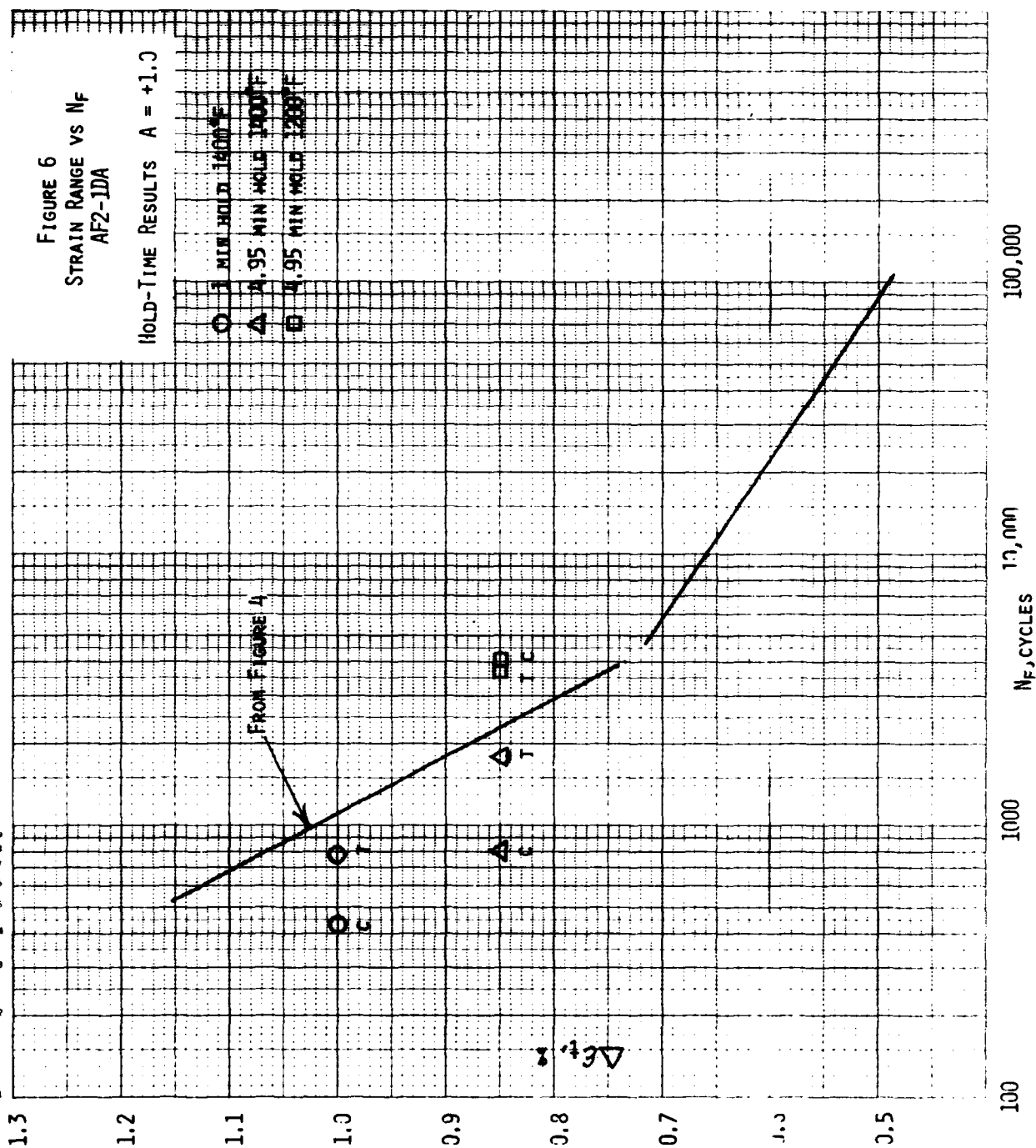tests that were performed led to fatigue life values that were not significantly

greater than those observed at 1400°F (Figure 5).

A limited number of hold-time tests was performed for the AF2-1DA alloy so

no extensive conclusions can be drawn. It was noticed that for both the 1-minute

and 4.95 minute hold-times, the hold period in compression was more damaging

than the hold period in tension. This behavior was also observed for the other

alloys and will be discussed in a later section. The hold-period test points

are ploted in Figure 6 and compared to the bilinear plot of Figure 4. It

can be noted that the 1-minute hold period in compression at a strain range

of 1.0% leads to a fatigue life that is about 40% of the continuous cycling

value for this strain range. This is about the same amount of fatigue life

32

FIGURE 6
STRAIN RANGE VS N_F
AF2-1DA

HOLD-TIME RESULTS A = +1.0

○ 1 MIN HOLD 1400°F
△ .95 MIN HOLD 1200°F
□ .95 MIN HOLD 1200°F

33

reduction obtained with a 4.95 minute hold period in compression at a strain range of 0.85%. This result is somewhat unexpected although it might represent a saturation effect for hold-time damage. More test information will be needed in order to confirm this tentative interpretation. At 1200°F no hold-time effect is evident since the fatigue life with 4.95 minute hold times was found to be essentially identical to the continuous cycling fatigue life.

Cyclic stress-strain behavior for th. AF2-1DA alloy, based on half-life information, is presented in Figures 7 and 8. A comparison with the limited room temperature data is included in each figure as is the effect of frequency. Frequency is seen to have little effect at 1200°F and a small but noticeable effect at 1400°F and 1500°F.

A plot of the AF2-1DA data at 1400°F is shown in Figure 9 where a well-defined linear relationship between log $\Delta\sigma$ (based on $N_f/2$ information) and log N_f is noted. This linearity persists over the range from about 200 to 100,000 cycles and exhibits a slope of approximately -0.12. Data for the other test temperatures are presented in Figure 10 and compared to the linear relationship described in Figure 9. It appears reasonable to represent the data at each temperature with a straight line having the same slope as that assigned in Figure 9, although at 1500°F a definite break in the linear trend seems to develop based on the point near 130,000 cycles. Converting the stress range data of Figures 9 and 10 to elastic strain range by dividing by the elastic modulus provides for some degree of correlation of the temperature dependence noted in Figure 10. This result is shown in Figure 11 based on an average modulus value from the data shown in Appendix A. While this type of plot provides for some normalization of the data a very definite temperature effect is still noticeable as indicated by the lines drawn to represent that data for the temperatures involved. Some further correlation of the temperature effect is

FIGURE 7
STRESS RANGE VS STRAIN RANGE
AF2-1DA

A = +1.0

FIGURE 8.
STRESS RANGE VS STRAIN RANGE
AF2-1DA

A = +1.0 ; 1400°F AND R.T.

FIGURE 9.
STRESS RANGE VS N_F
AF2-1DA

1400°F   A = +1.0

slope = -0.12

N_f, cycles

$\log \Delta\sigma$ (at $N_f/2$)

Figure 10
Stress Range vs N_F
AF2-1DA

$A = +1.0$
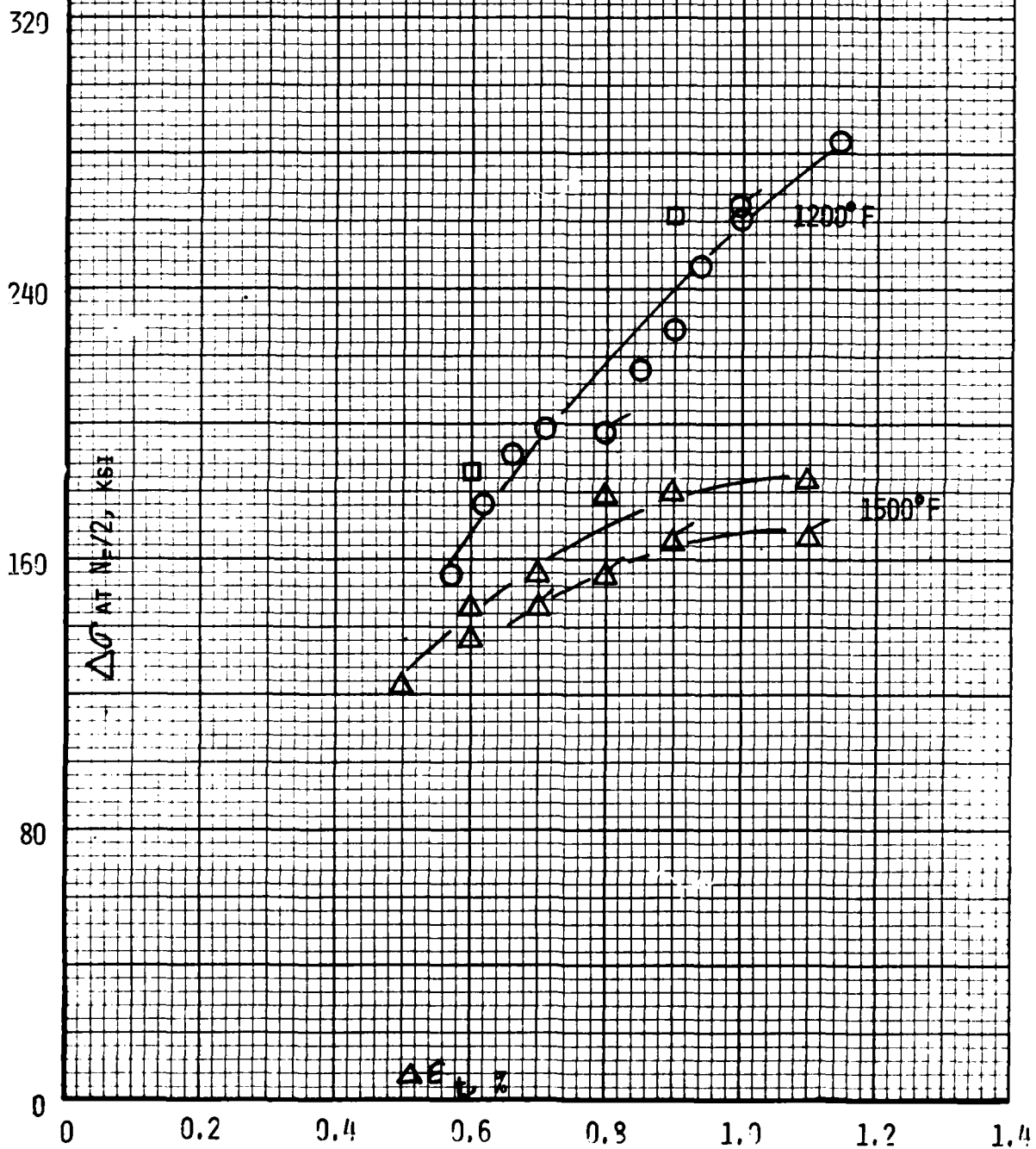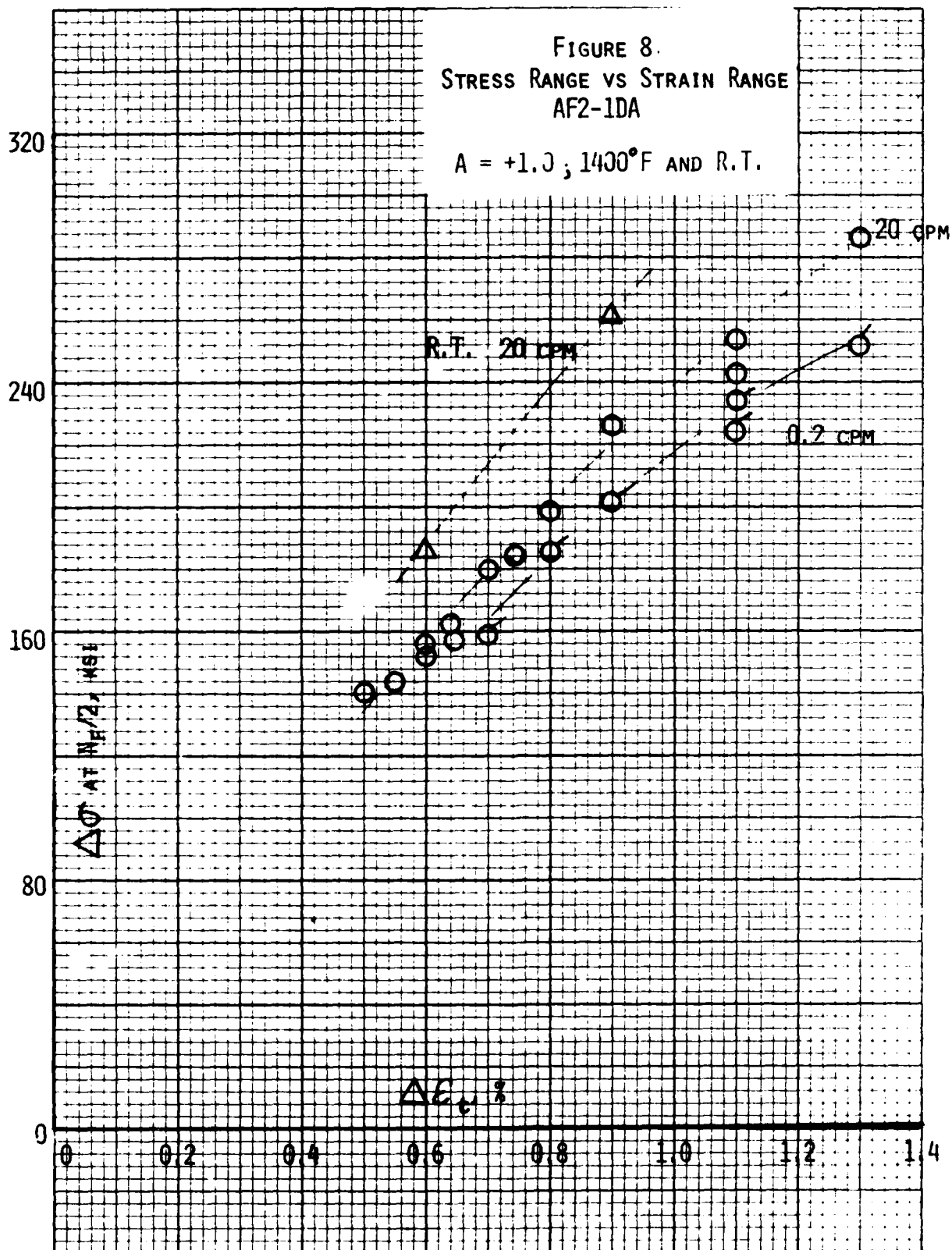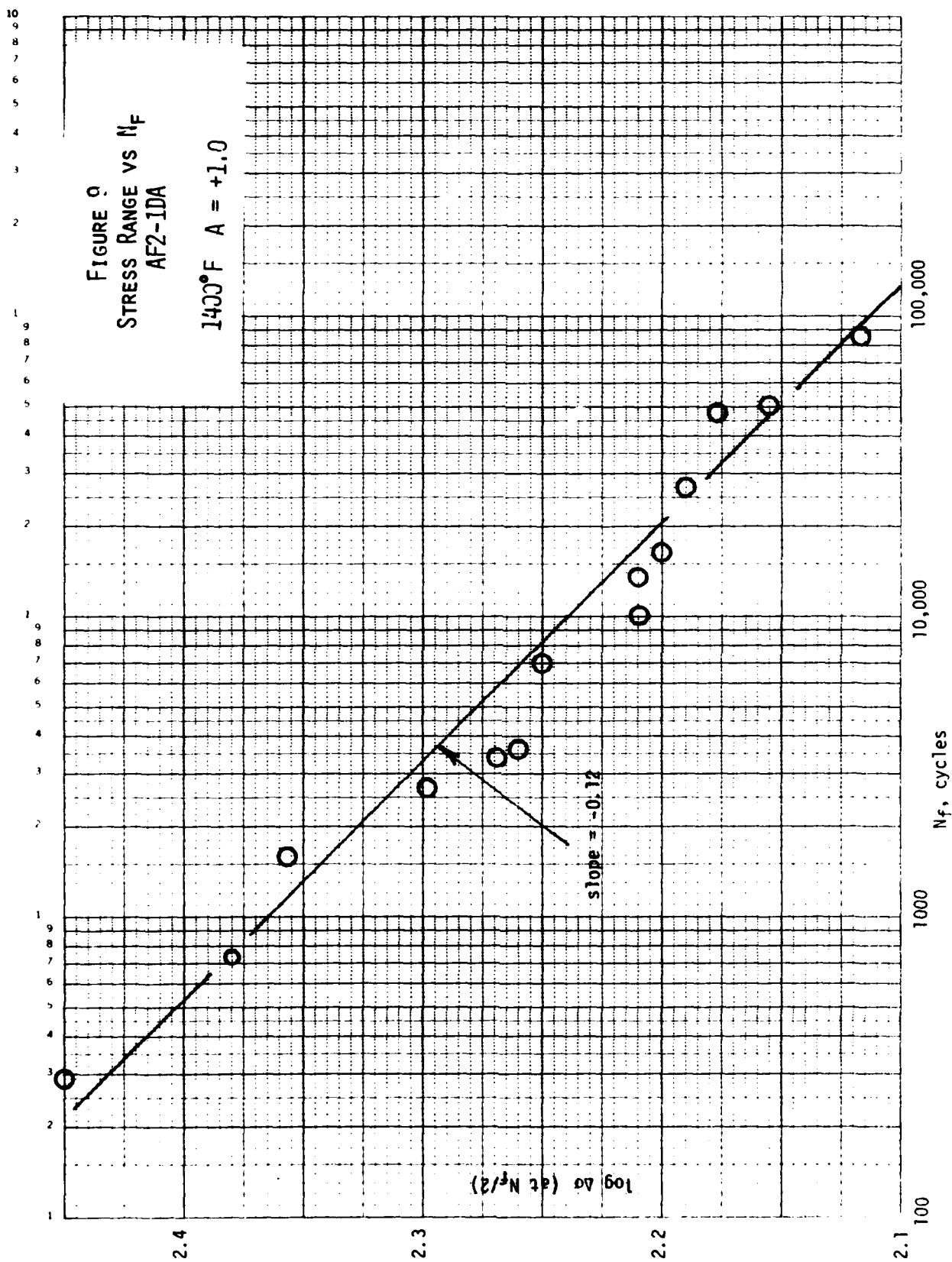
warranted and a logical approach might be that offered in the Universal Slopes[8] equation where the elastic strain range is represented in terms of the ultimate tensile strength divided by the elastic modulus. It is recommended that this evaluation be performed in a subsequent analysis of these results.
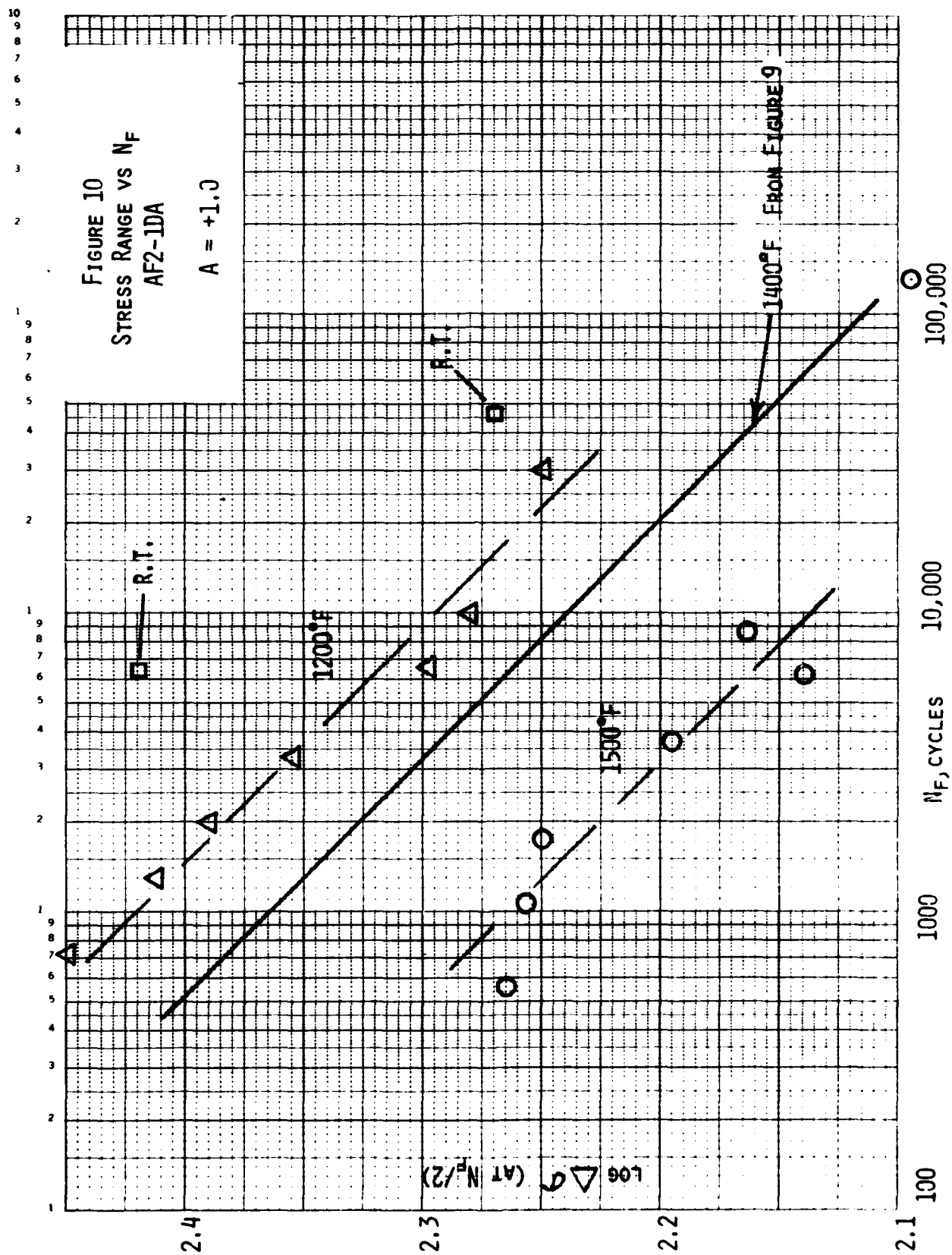
In Figure 11 the two available data points at 1200°F and a frequency of 0.2 cpm indicate no effect of frequency on fatigue life. At 1400°F a small frequency effect appears to be developing. Data at 1500°F are presented in Figure 12 to identify the development of a definite frequency effect as the frequency is reduced from 20 to 0.2 cpm. Additional data will be required to determine if this type of effect is still present in the lower strain range regime (for example, at the point corresponding to a fatigue life of 130,000 cycles at 20 cpm).

An evaluation of the plastic strain range results led to the plot shown in Figure 13. In the regime near 10,000 cycles the value of the plastic strain range approached 0.01%. At such levels, the reliability for these values is low and it becomes difficult to establish a dependable relationship between plastic strain range and fatigue life. For this reason, only those tests were included in Figure 13 that had plastic strain range values greater than 0.02%. Based on the data at 1200°F, 1400°F, and 1500°F, a series of parallel lines represents the behavior pattern fairly well, for this limited range of fatigue life. It is also noted that the slope of the line defined by the data at 1200°F is very close to a value of -1.0. Lines having this same slope have been drawn at 1400°F and 1500°F and predict the data within a factor of $\pm$ 2. This slope of -1.0 represents a more negative value than that associated with the Coffin-Manson relation. A slope of -1.0, of course, establishes a unique relationship between $\Delta\epsilon p$ and N_f in the form:

$$\Delta\epsilon p \times N_f = \text{constant} \qquad (2)$$

Intercept calculations in Figure 13 lead to values for this constant of 74, 110,

and 135 for test temperatures of 1200°F, 1400°F, and 1500°F respectively. These values will be discussed again in a latter section dealing with similar data for Rene 95.

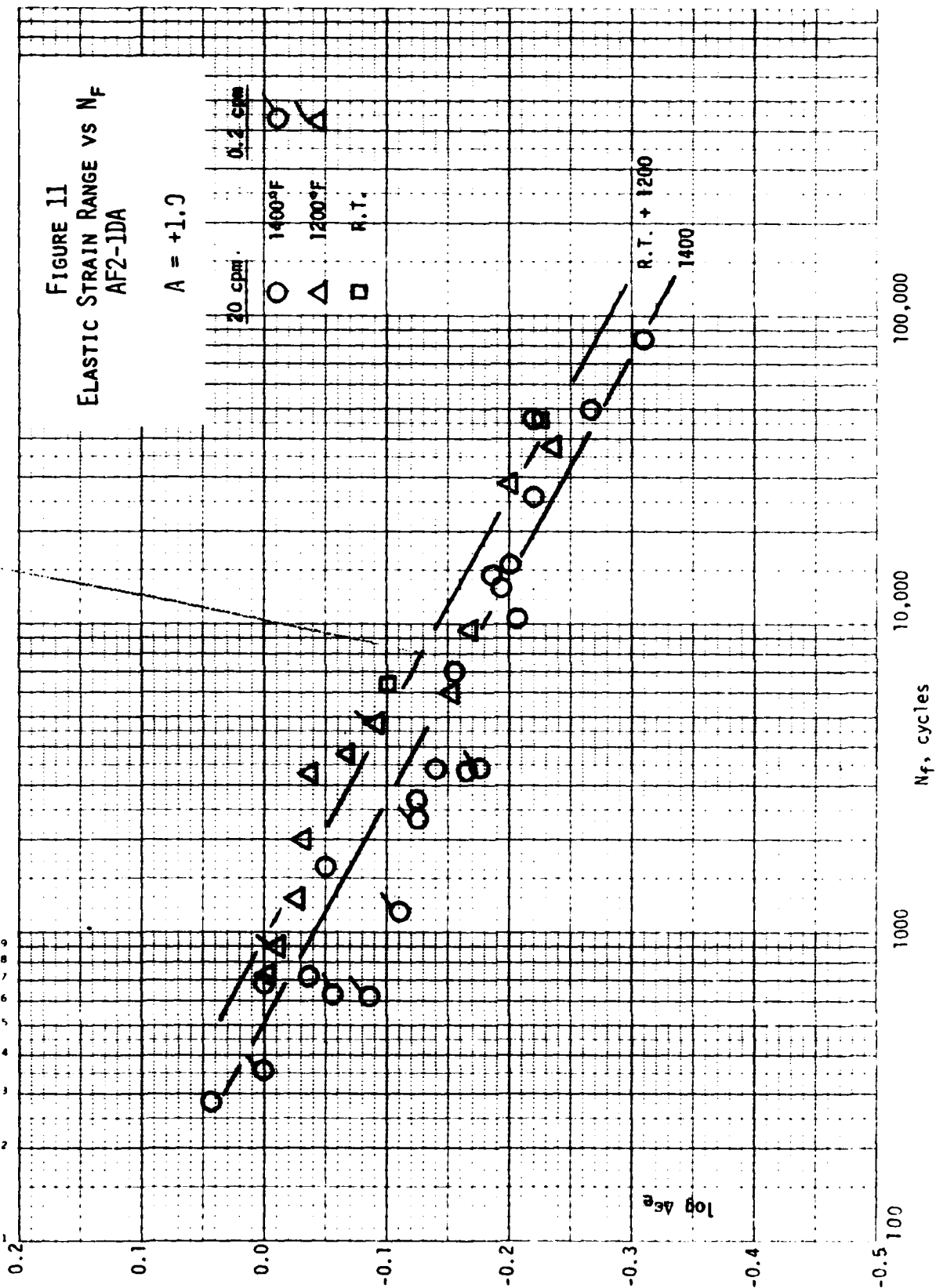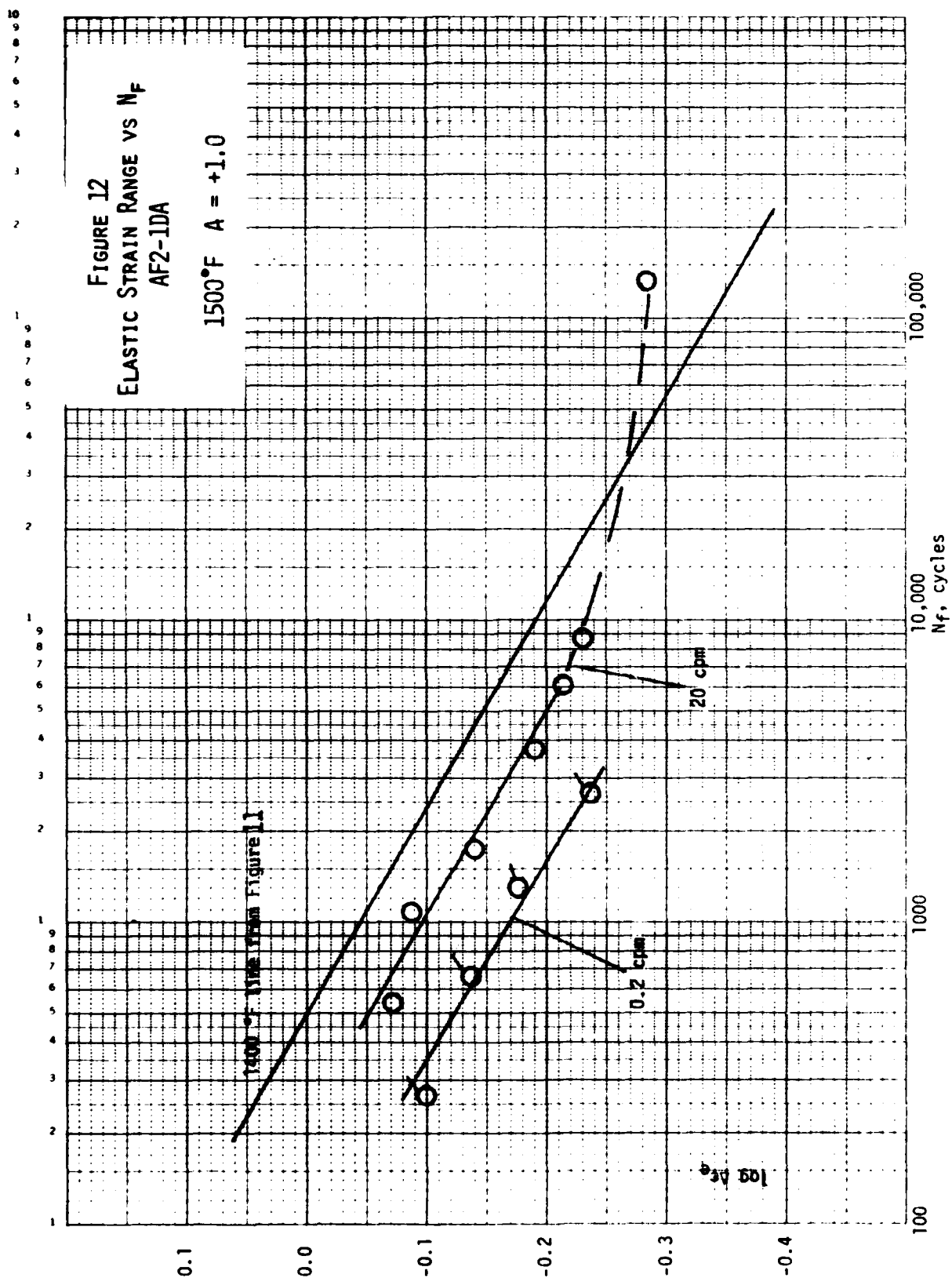FIGURE 11
ELASTIC STRAIN RANGE VS N_F
AF2-1DA

$A = +1.0$

41

FIGURE 12
ELASTIC STRAIN RANGE VS N_F
AF2-1DA

1500°F   A = +1.0

FIGURE 13
PLASTIC STRAIN RANGE VS N_F
AF2-1DA

20 CPM   A = +1.0

○ 1200°F
△ 1400°F
□ 1500°F

N_F, CYCLES

43
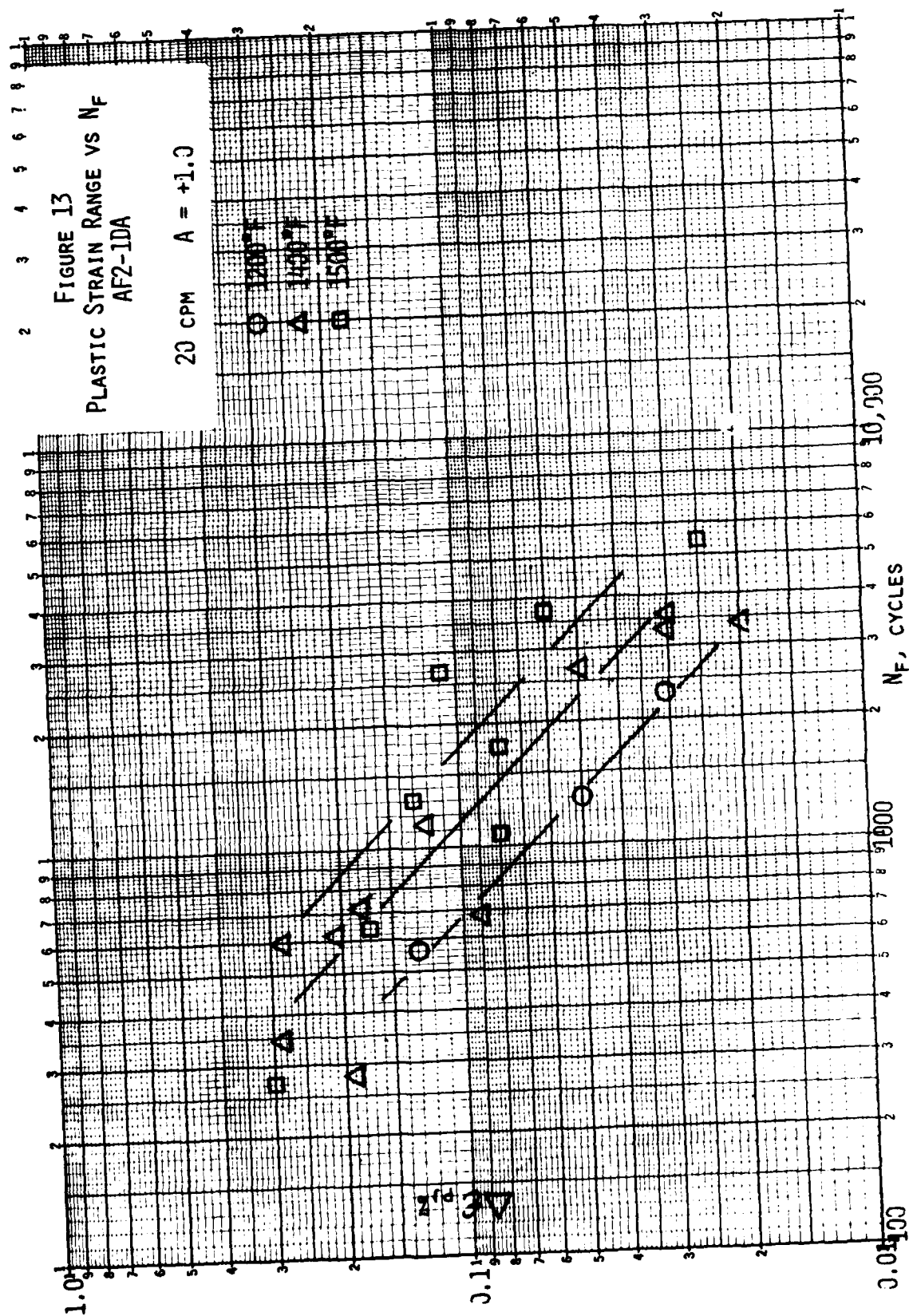
2. AF-115

AF-115 was tested in much the same way as the AF2-1DA alloy. Uniform gage section specimens were employed and the tests were performed using axial strain measurement and control. Further more, the test temperatures were essentially the same as those employed in the evaluation of the AF2-1DA alloy and, with one exception, the A - ratio (on strain) was equal to unity. The evaluation of frequency and hold-period effects was also patterned after that followed in the study of the AF2-1DA alloy. A summary of the results obtained in the 100 tests performed in the evaluation of the AF-115 alloy is presented in Appendix B. These tests correspond to the distribution shown in Table 9.

There were two processing conditions of the primary heat of AF-115, HIP and HIP plus forge. The LCF behavior for both conditions was approcimately the same as shown in Figure 14. In addition, some specimens from a second heat of AF-115, identified in Appendix B as pancake 3, (300 series), were also tested and their fatigue behaviors were also similar (Figure 14). Since the fatigue responses of the different conditions of AF-115 were approximately equal, these tests will be treated as one population in this analysis.

A semilogarithmic plot of $\Delta\epsilon_t$ versus N_f for the AF-115 alloy at 1400°F and a frequency of 20 cpm is shown in Figure 15. The bilinear representation for the AF2-1DA alloy from Figure 4 is also included in Figure 15 for comparison purposes. It will be noted that the behavior patterns for the two alloys are quite similar.

All the data in Figure 15 have been combined with the AF-115 data at 1400°F and a frequency of 0.2 cpm to yield the plot shown in Figure 16. In analyzing these results, there was no significant frequency effect on fatigue life at this

44

TABLE 9 - DISTRIBUTION OF LOW-CYCLE FATIGUE TESTS PERFORMED FOR AF-115 ALLOY

	Number of Tests				
	1500°F	1400°F	1200°F	1000°F	R.T.
20 cpm	12	30[2]	6	2[1]	2
1 cpm	---	2	---	---	---
0.2 cpm	9	22	3	---	---
4.95 minutes Hold in Tension	2	4	---	---	---
4.95 minutes Hold in Compression	---	2	---	---	---
1 minute Hold in Tension	---	2	---	---	---
1 minute Hold in Compression	---	2	---	---	---

1 Tests performed in an argon environment using computed axial strain control.

2 Includes one test with A-ration (on strain) of infinity and one test in load control at 60 cpm.

45

Figure 14
Strain Range vs N_F
AF-115

1400°F A = +1.0

AS-HIP
AS-HIP
HIP + FORGE
(PANCAKE)

AF-115
AF-115
AF-115

N_F, CYCLES

$\Delta\varepsilon_t$, %

1.3
1.2
1.1
1.0
0.9
0.8
0.7
0.6
0.5

130
1000
10,000
100,000

46
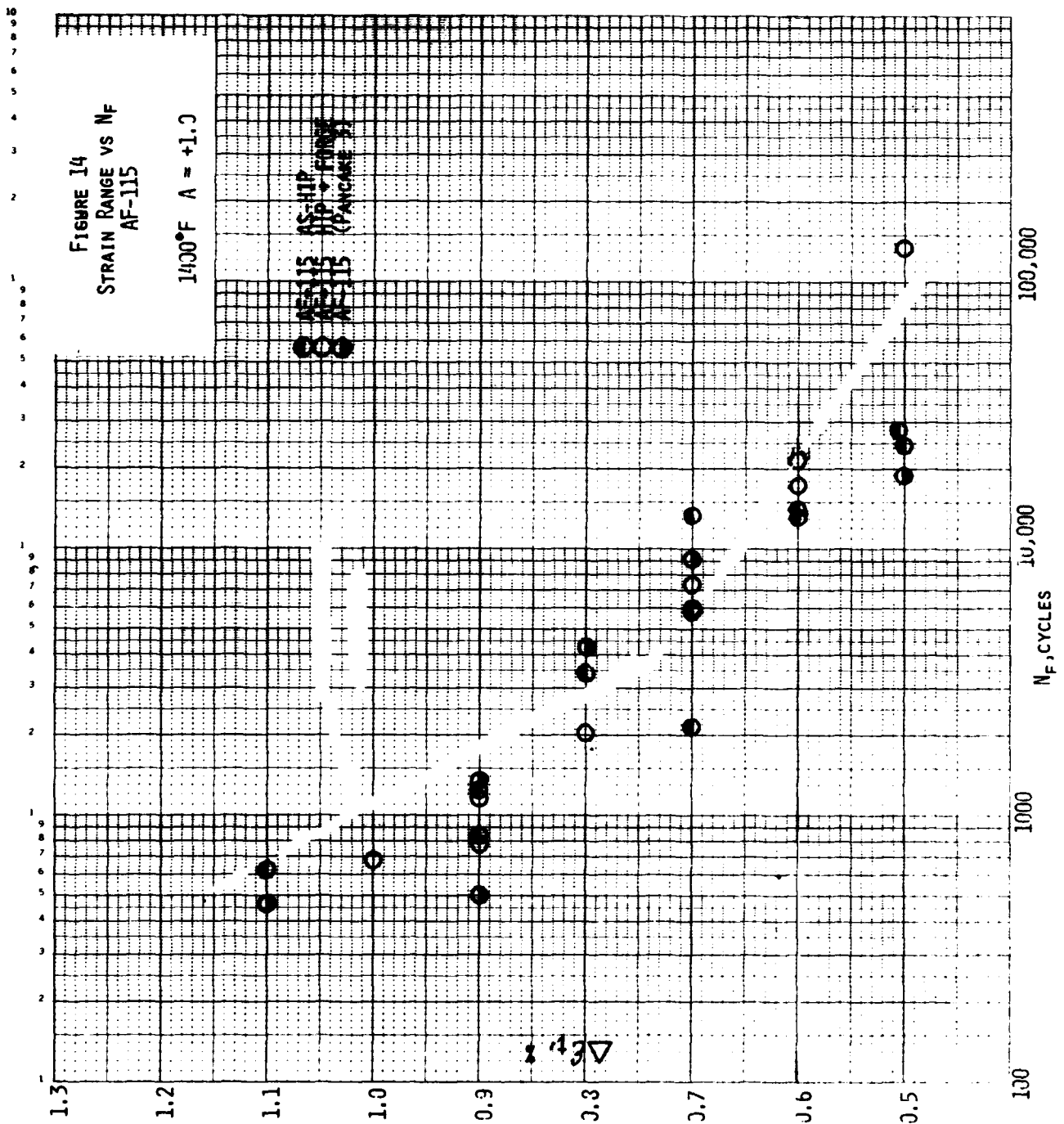
FIGURE 15
STRAIN RANGE VS N_F
AF-115
1430°F A = +1.0

From FIGURE 4
For AF2-1DA

$\Delta\varepsilon_t$, %
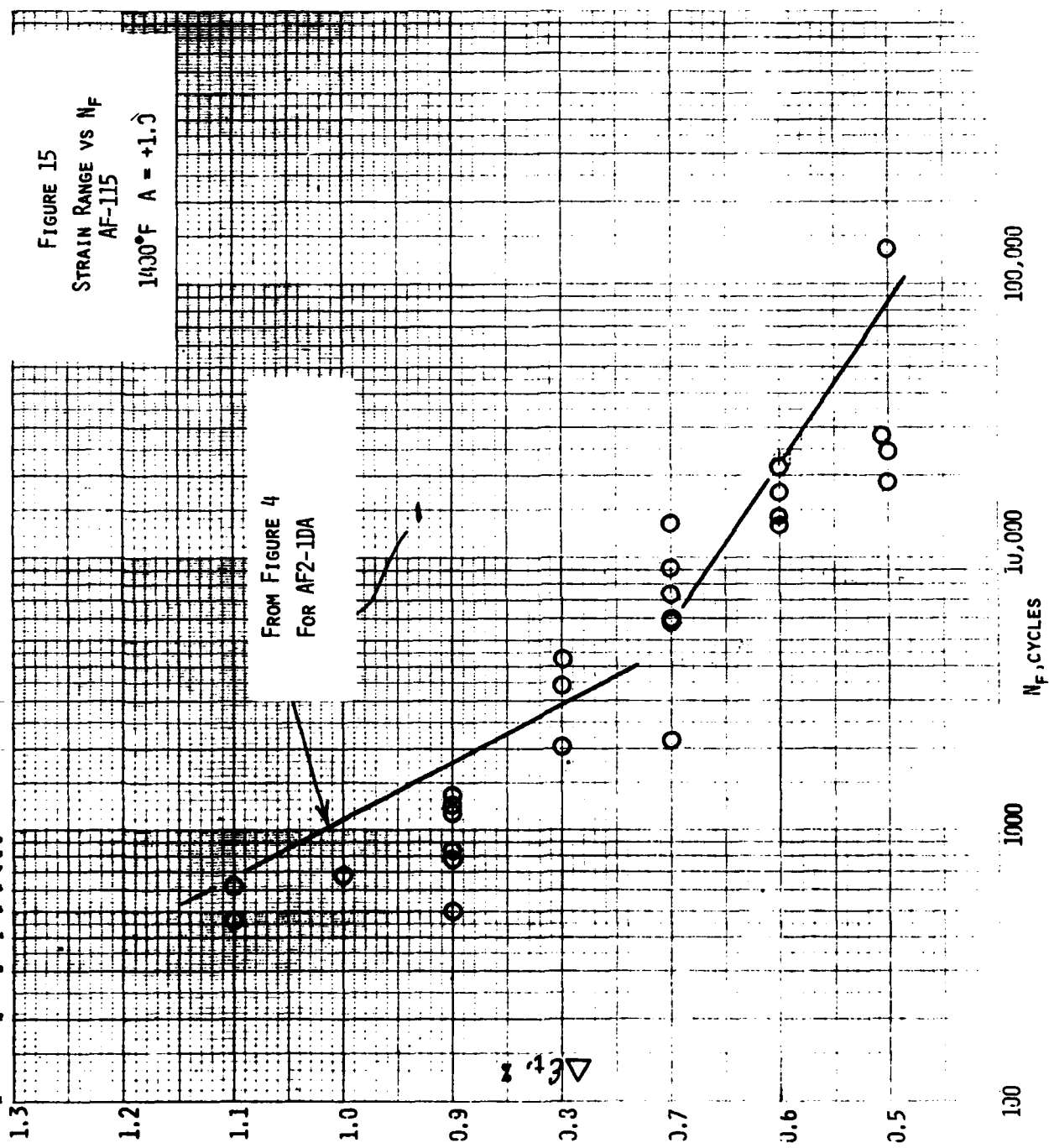
N_F, CYCLES

temperature. It was also noted that within reasonable scatter the entire data set could be represented by a straight line (the point at 130,000 cycles is an obvious exception to this linear data trend and, in the absence of further testing in this strain range regime, should probably be viewed as an unusually long fatigue life for a strain range of 0.50%. This line in Figure 16 was used in Figure 17 to provide a comparison of the temperature effect identified in these tests of the AF-115 alloy. Even though the data scatter is quite substantial, a definite temperature dependency is noted and it appears reasonable to represent the data with the linear and parallel isotherms that are shown. Each line can be described by an equation of the form:

$$N_f = Ae^{-b\Delta\epsilon_t} \tag{3}$$

and since the slopes are the same, the value of "b" is independent of temperature. An extension of this analysis led to an evaluation of the temperature dependency of the value of A in Equation 3 and this led to the following:

$$N_f = 8150 \ e^{\frac{8580}{T^{\circ R}}} \ e^{-7.1 \ \Delta\epsilon_t} \tag{4}$$

This expression has been used to position the lines in Figures 16 and 17, and within the limits of the data, provides a good description of the data at 20 cpm, being within a factor of 2 in most instances. Of course, since no frequency effect is observed at 1200°F and 1400°F, this equation can also be applied over the frequency regime from 0.2 to 20 cpm at these two temperatures. At 1500°F, a frequency effect (see points in Figure 17) is observable and some reduction in life is noted as the frequency is reduced from 20 to 0.2 cpm.

It is to be emphasized that Equation 4 was developed using data corresponding to an A - Ratio (on strain) of unity and should not be applied at any other A - ratio. Although Equation 4 will probably yield reasonable

estimates of fatigue life for an A - ratio of infinity in the regime of high
strain ranges, it can be expected to underestimate the fatigue life as the one
word strain range is reduced. For example, the test of Spec. 2-16 led to a
fatigue life of 285,877 cycles at 1400°F, $\Delta\epsilon_t$ = 0.55%, 20 cpm and A = ∞. This
life is substantially longer than the value of 16,500 cycles that is obtained
from Equation 4 for these conditions at A = +1.0. Some additional studies
would be needed before a term for A - ratio effects could be introduced
into Equation 4.

FIGURE 16
STRAIN RANGE VS N_F
AF-115

1400 F A = +1.0

50

Figure 17
Total Strain Range vs N_F
AF-115

$A = +1.0$ 20 CPM
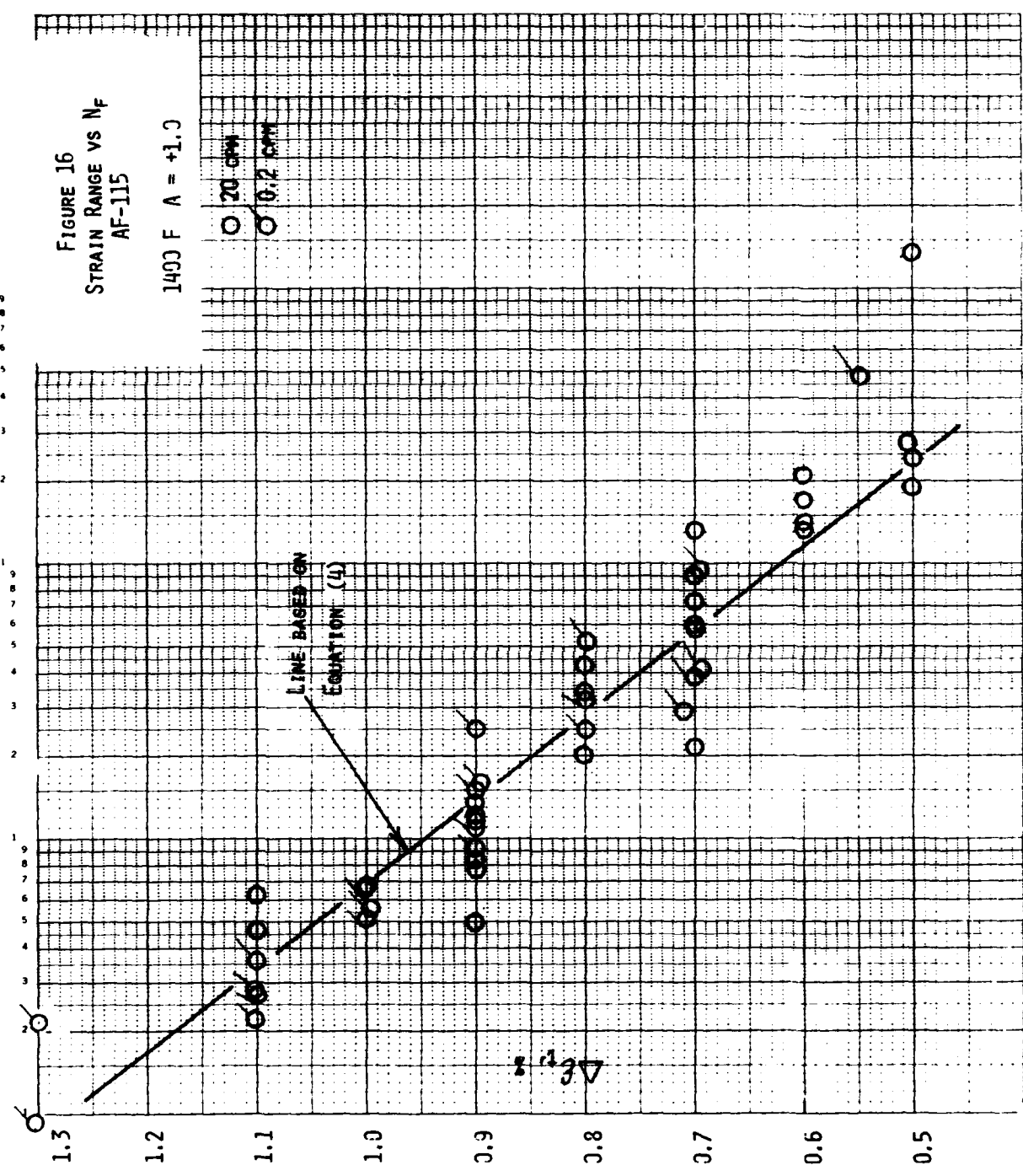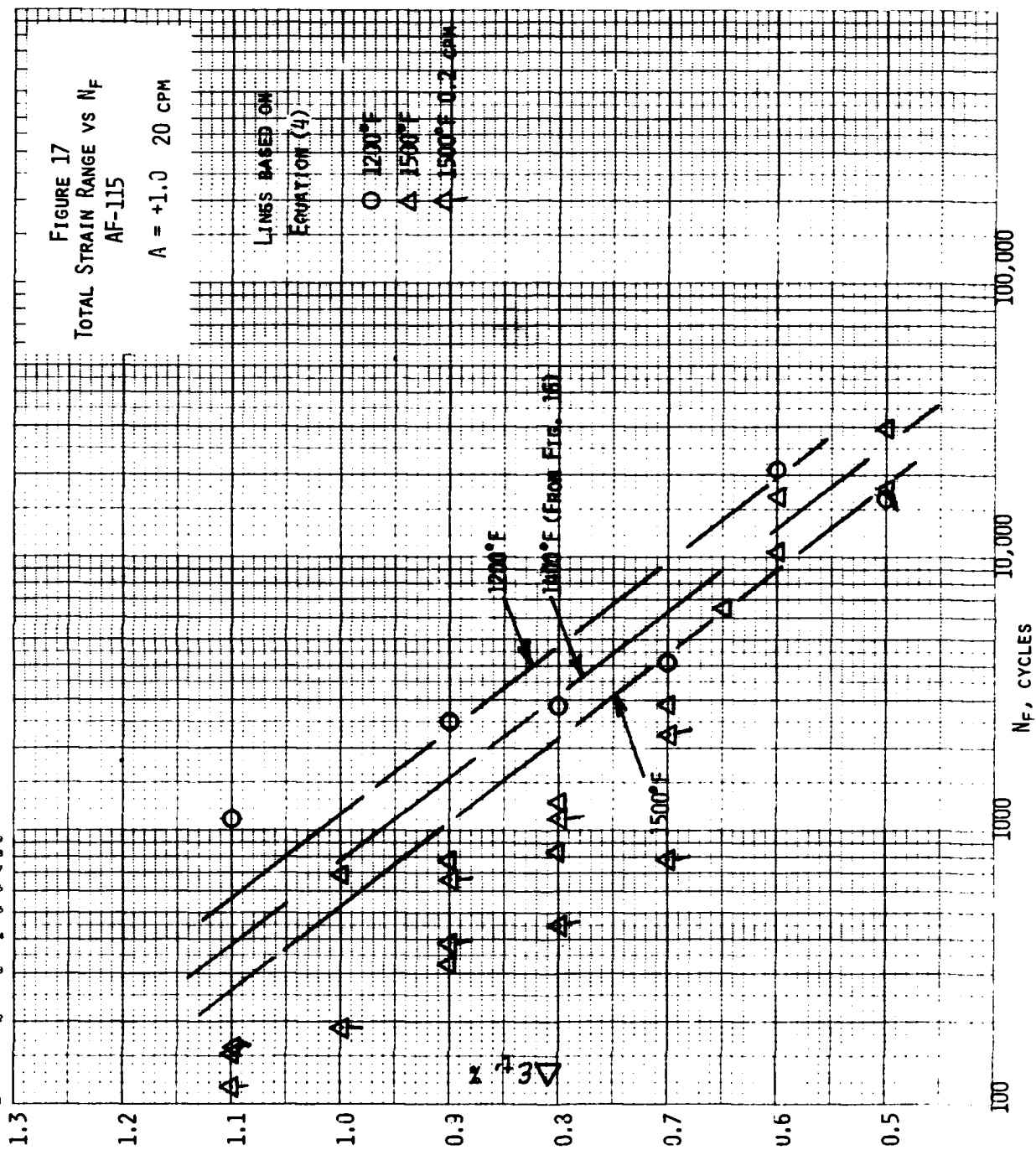
As indicated in Table 8, only 12 hold-time tests were employed in this
evaluation of the AF-115 alloy. For this reason, nothing more than trend
behavior was identified. A comparison of the results obtained at 1400°F is
presented in Figure 18. Within the scatter of the continuous cycling data
the hold periods in tension (both 1 minute and 5 minutes) indicate no
reduction in fatigue life due to the presence of a hold period. As a
matter of fact, there is some indication that hold periods in tension actually
lead to an increase in fatigue life. However, a factor of two reduction
in fatigue life results when a hold period of 1 or 5 minutes is imposed in
compression. This behavior is quite similar to that noted in the tests of
the AF2-1DA alloy and again, hold periods in compression appear to be more
damaging than periods in tension. At 1500°F only two hold-period tests
were performed (both 5-minute hold periods in tension) and the effect is
essentially the same as that noted at 1400°F for tension hold-periods.

Cyclic stress-strain behavior for the AF-115 alloy at 1400°F is shown
in Figure 19 for the two frequencies employed in these evaluations. As
will be noted, no frequency effect appears evident at this temperature.
A similar conclusion regarding frequency effect follows from the data shown
at 1200°F in Figure 20. At 1500°F, however, the data shown in Figure 20
reveal a noticeable development of a frequency effect. The effect, however,
is mild and is seen to amount to about a 10% reduction in stress range as
the frequency is reduced from 20 to 0.2 cpm. A comparison of the cyclic
stress-strain behavior for the AF-115 material with that for the AF2-1DA
alloy in Figures 7 and 8 indicates very similar behavior although the small
frequency effect noted at 1400°F in Figure 8 is not observed in Figure 19.

Figure 18
Total Strain Range vs N_F
AF-115

1100°F   A = +1.0

T – Tensile Dwell
C – Compressive Dwell

Line from Figure 16
1100° Continuously Cycling Data

$\Delta \varepsilon_t, \%$

N_F, Cycles to Failure
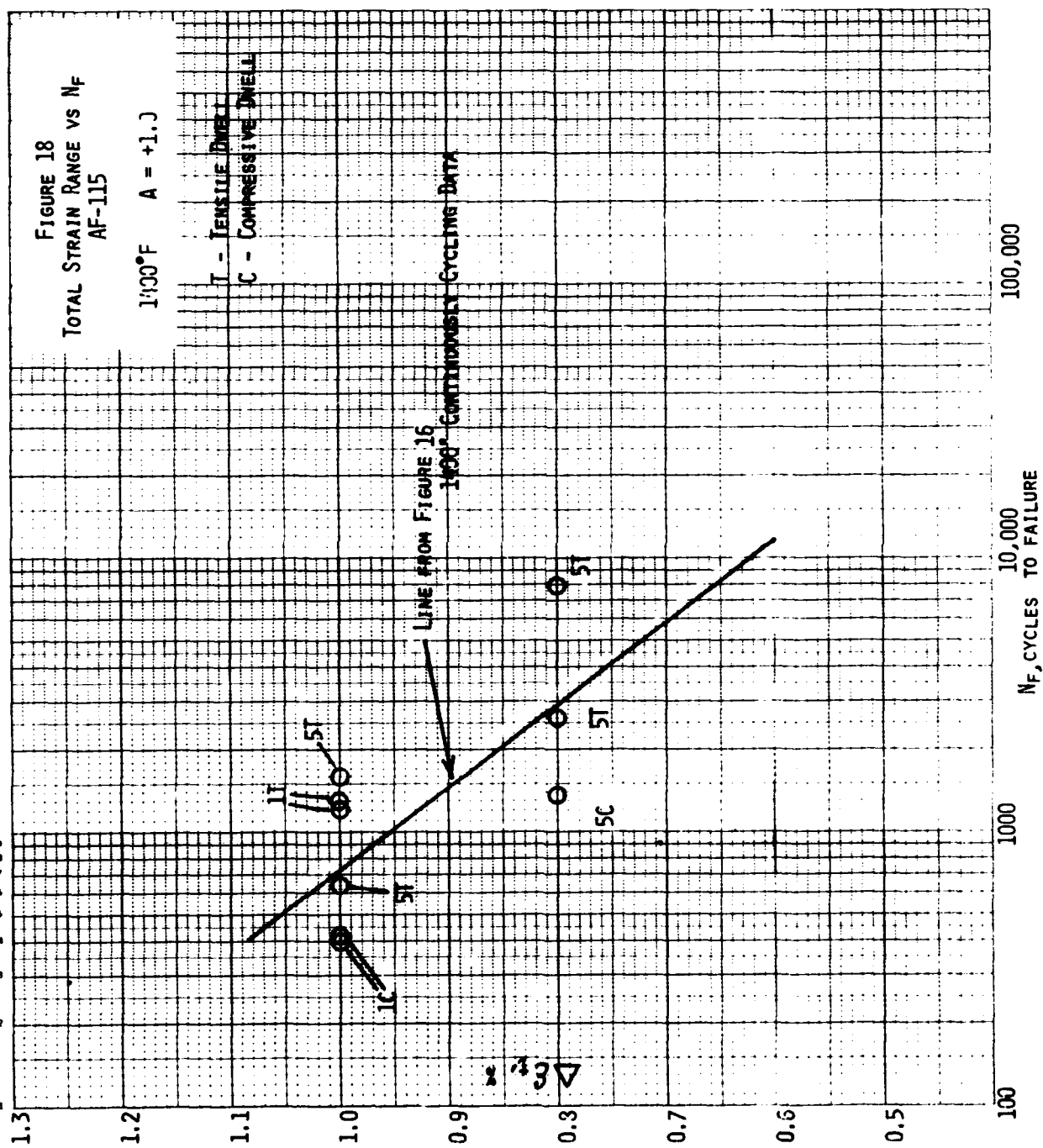
FIGURE 19
STRESS RANGE VS STRAIN RANGE
AF-115

$1400°F \quad A = +1.0$

○ 20 CPM
♂ 0.2 CPM

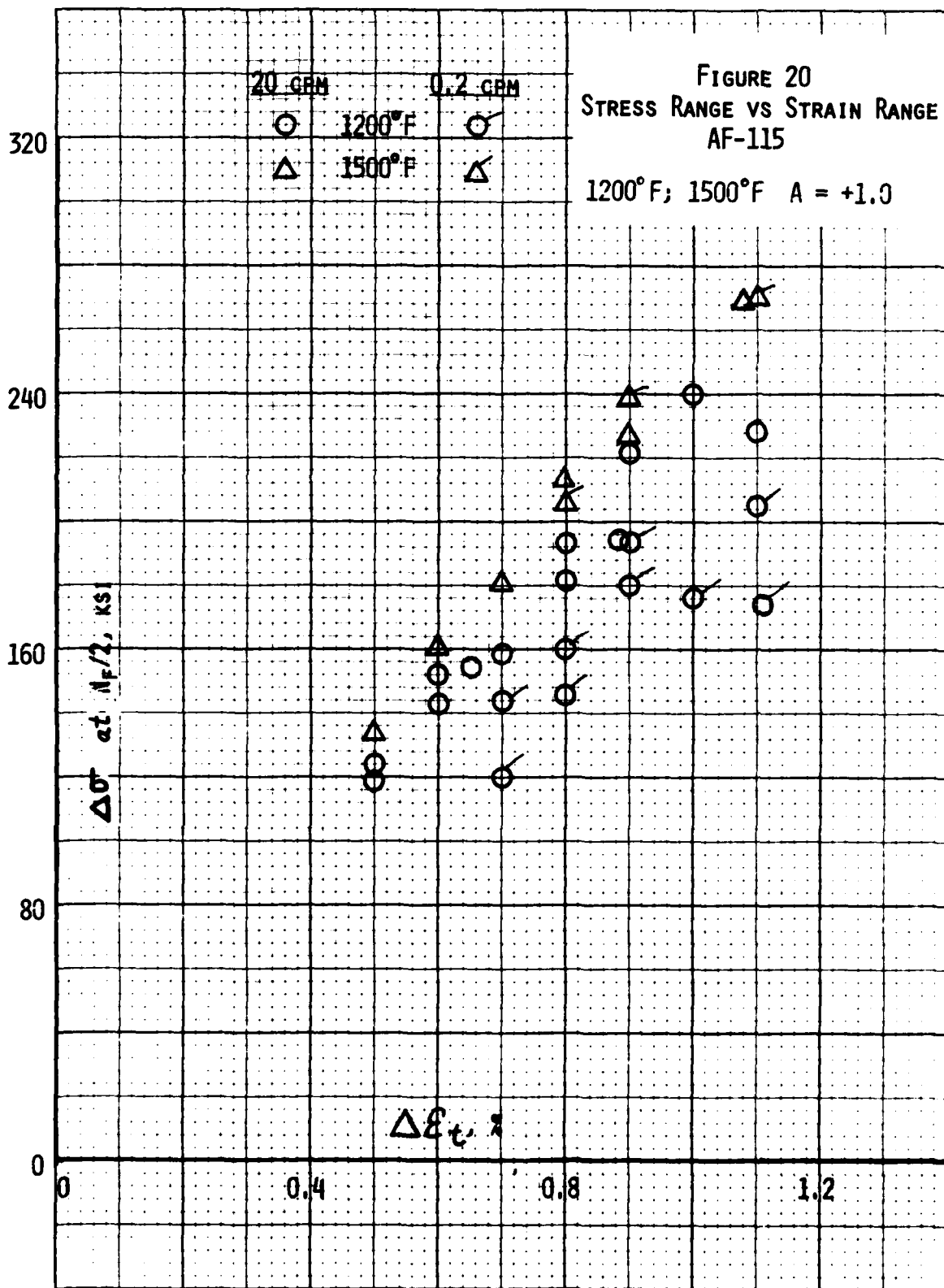Stress Range at $N_F/2, \Delta\sigma$, KSI

$\Delta\epsilon t, \%$

FIGURE 20
STRESS RANGE VS STRAIN RANGE
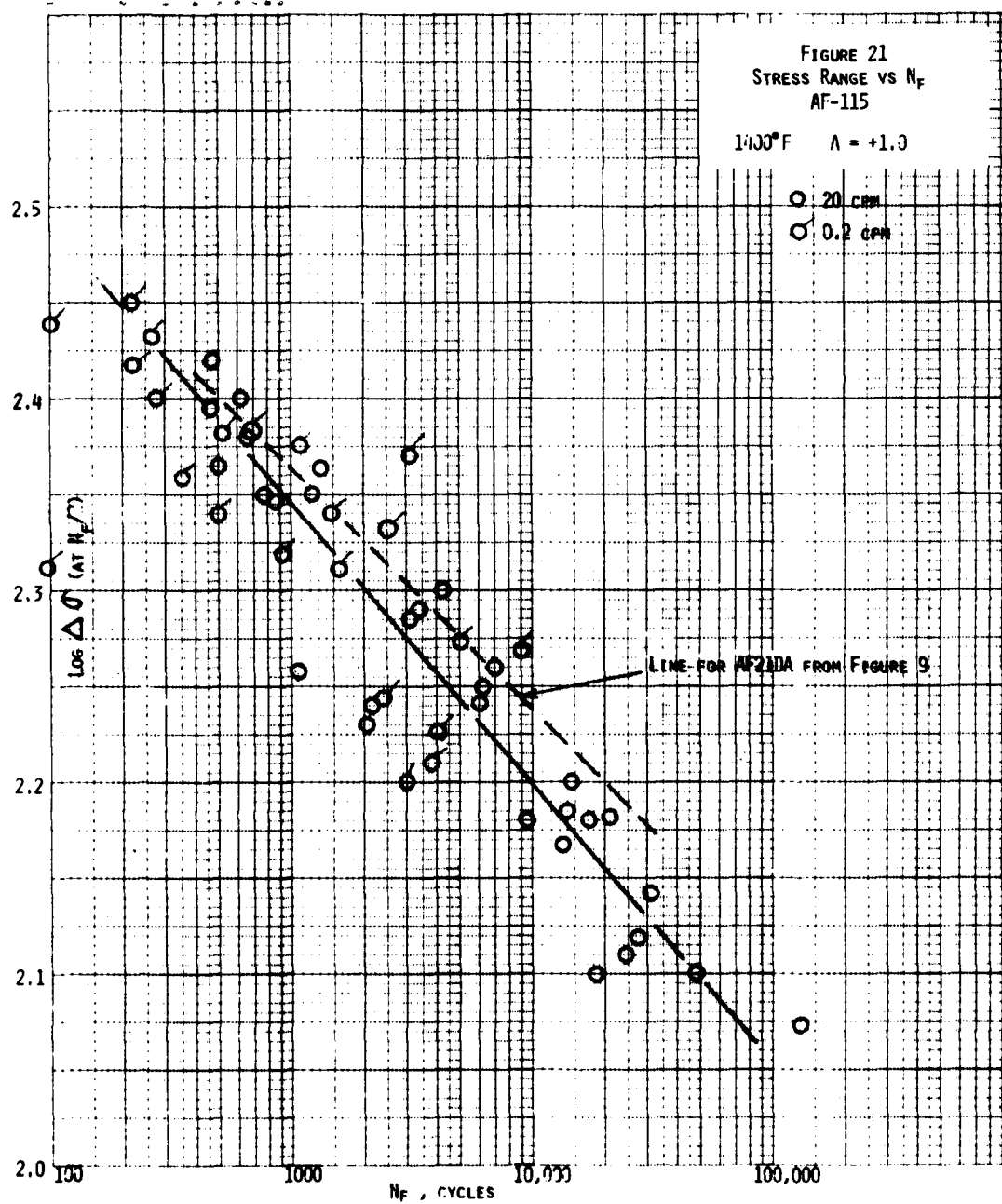AF-115

1200°F; 1500°F   A = +1.0
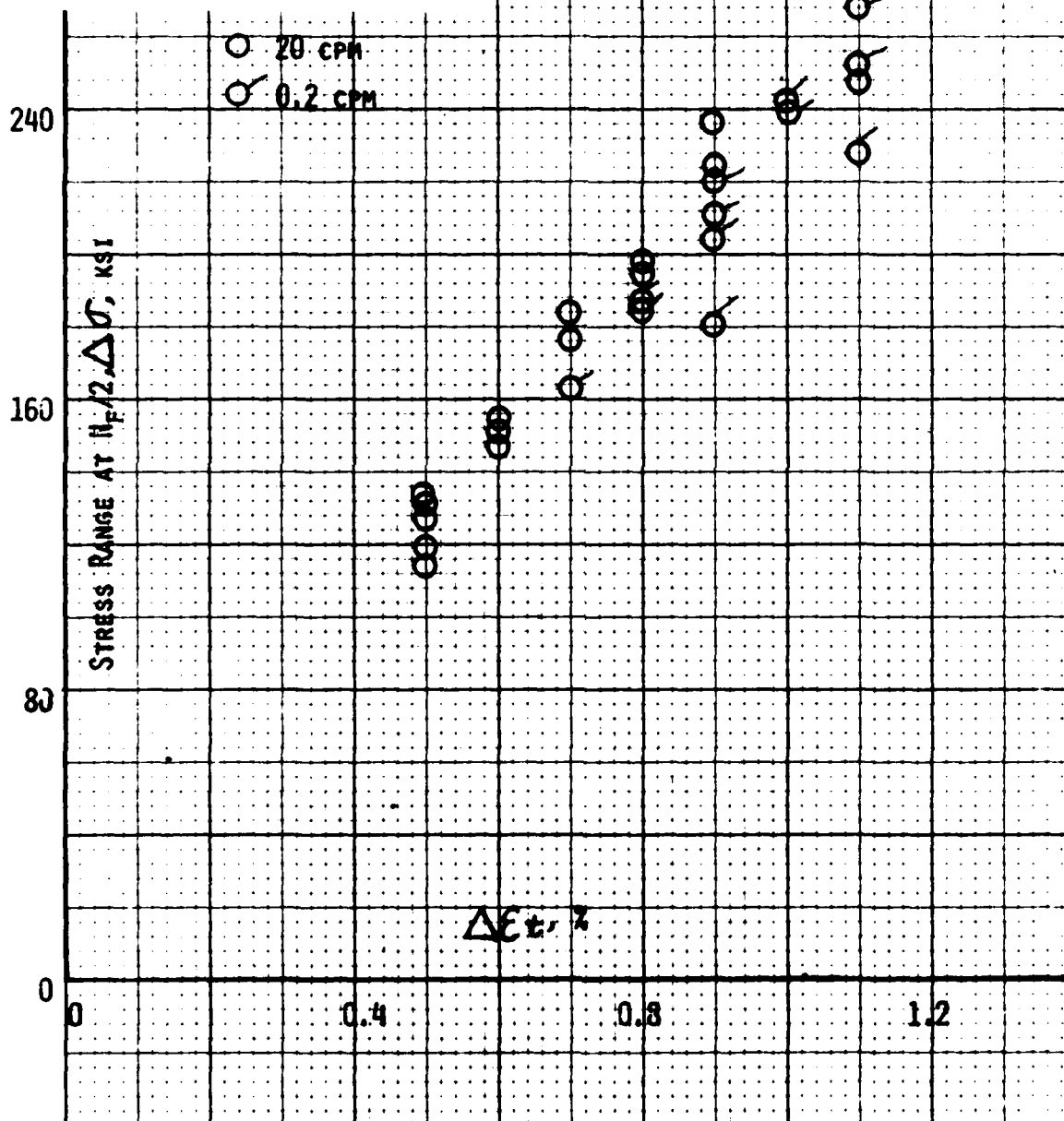
An analysis of the stress range (at $N_f/2$) data for the AF-115 alloy at 1400°F led to the plot of Log $\Delta\sigma$ versus N_f shown in Figure 21. This result is very similar to that noted in Figure 9 for the AF2-1DA alloy. Within reasonable scatter, the plot is linear over almost three orders of magnitude and the slope of this linear relation is close to -0.14. As in the case of the AF2-1DA alloy, the data in Figure 21 show a negligible effect of frequency at 1400°F over the range from 0.2 to 20 cpm. A dashed line has been included in Figure 21 based on the relationship identified for the AF2-1DA alloy in Figure 9. This comparison reveals that the two alloys exhibit very similar stress rnage versus fatigue life relationships.

Another similarity exists in the temperature dependence exhibited by the two alloys. In Figure 22, the AF-115 relationship from Figure 21 is positioned to provide a comparison of the AF-115 results at 1400°F with data obtained at 1200°F and 1500°F. Linear and parallel isotherms provide a reasonable representation of the data and this behavior pattern is very similar to that noted in Figure 10 for the AF2-1DA alloy. It should also be noted in Figure 22 that the effect of frequency becomes apparent at 1500°F. This, too, is similar to the behavior pattern observed for the AF2-1DA alloy.

A different representation of the stress range data shown in Figures 21 and 22 is provided in terms of elastic strain range in Figures 23 and 24. As should be expected, the behavior patterns noted are identical to those noted for the stress range behavior. In Figure 23, for example, the line drawn to represent all the data at 1400°F reflects the same type of result discussed in connection with Figure 21. Also, the result in Figure 24, associated with parallel isotherms and the development of a frequency effect at 1500°F, is identical to that identified for the stress range behavior of Figure 22.

FIGURE 21
STRESS RANGE VS N_F
AF-115

1400°F   A = +1.0

○ 20 cpm
♂ 0.2 cpm

LINE FOR AF2IDA FROM FIGURE 9

N_F, CYCLES

Log $\Delta \sigma$ (AT $N_F/2$)

57

FIGURE 22
STRESS RANGE VS N_F
AF-115

$A = +1.0$

FIGURE 23
ELASTIC STRAIN RANGE VS N_F
AF-115

$1400°F \quad A = +1.0$

59

FIGURE 24
ELASTIC STRAIN RANGE VS N_F
AF-115

$\Lambda = +1.0$

60
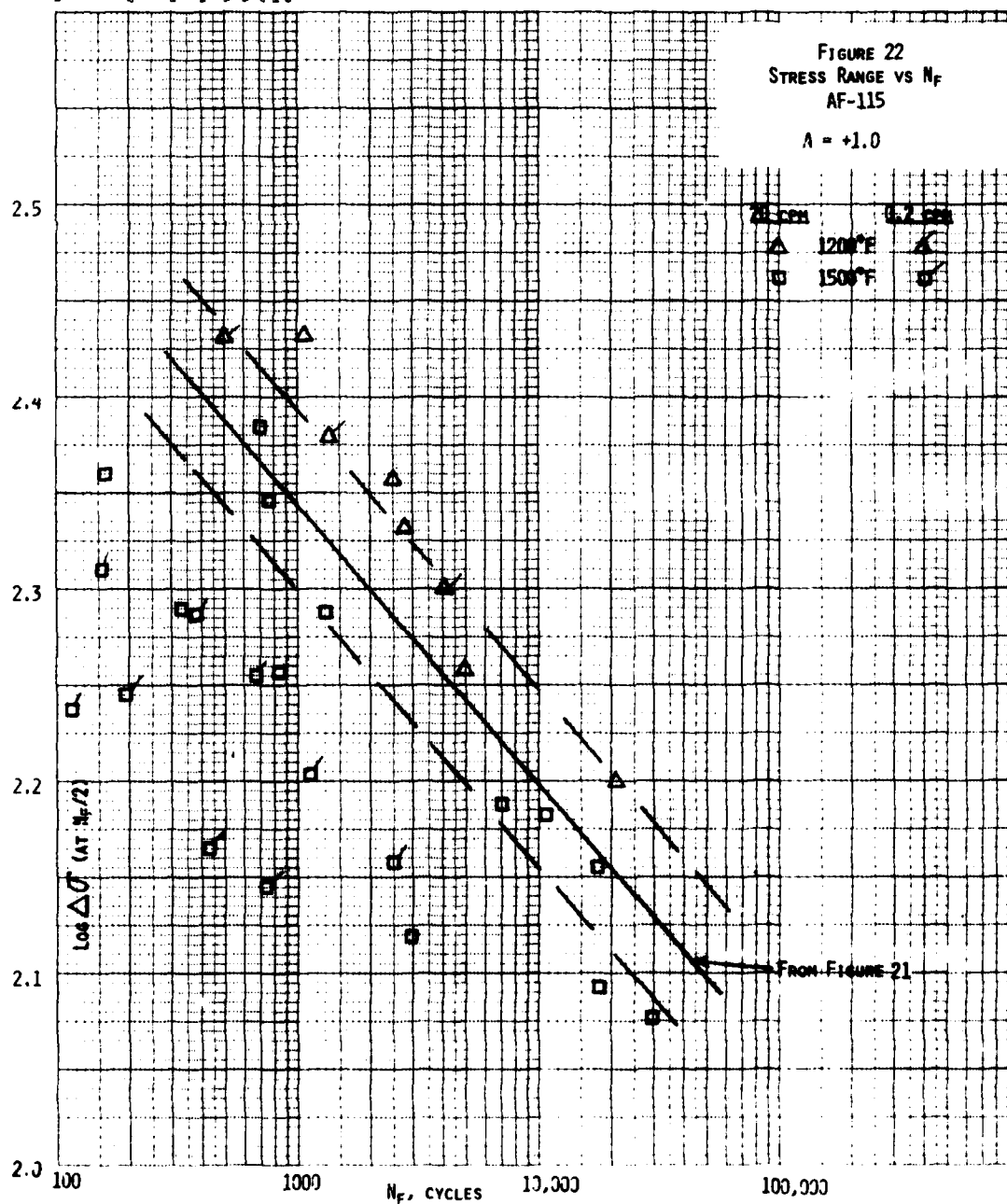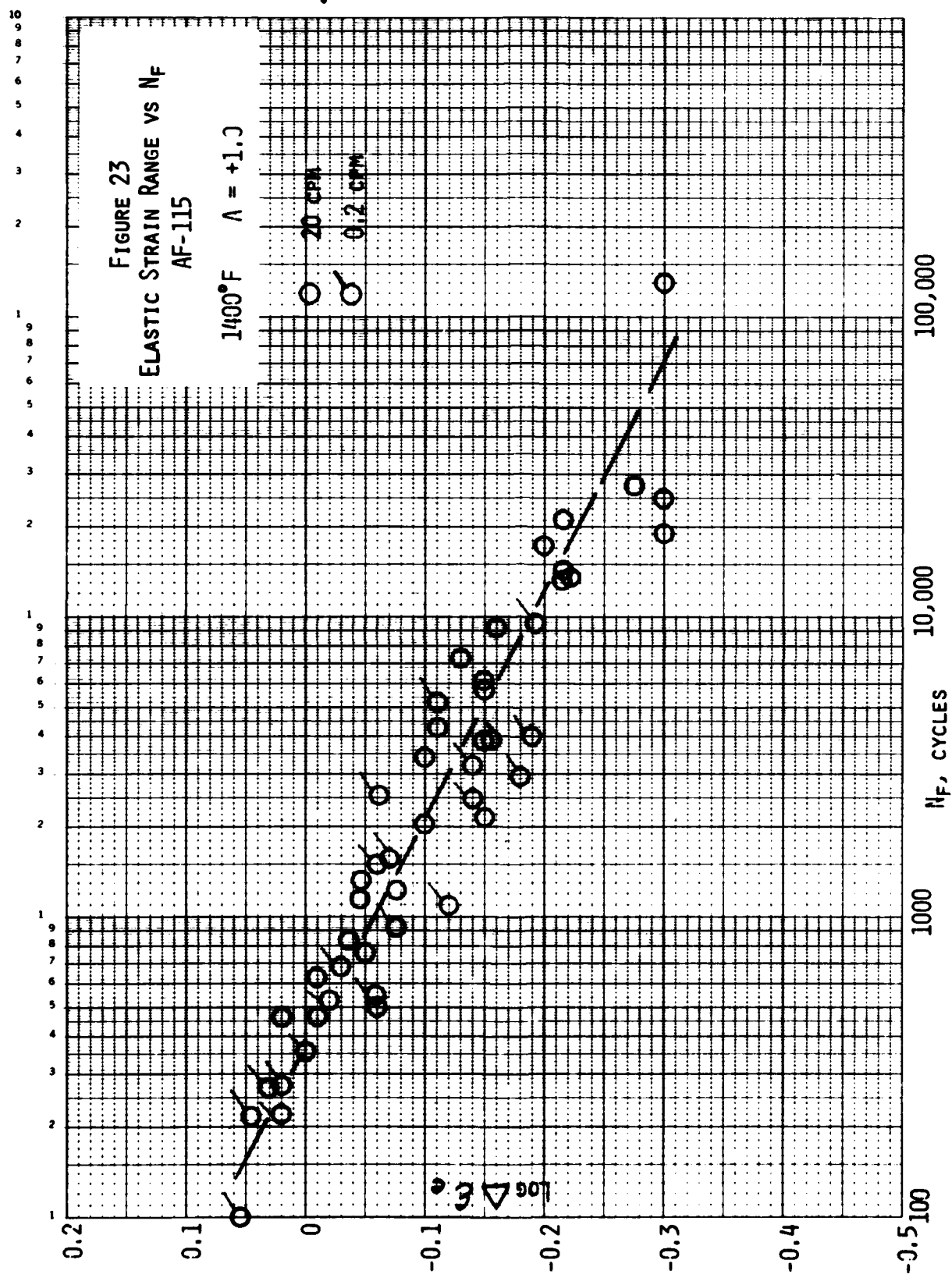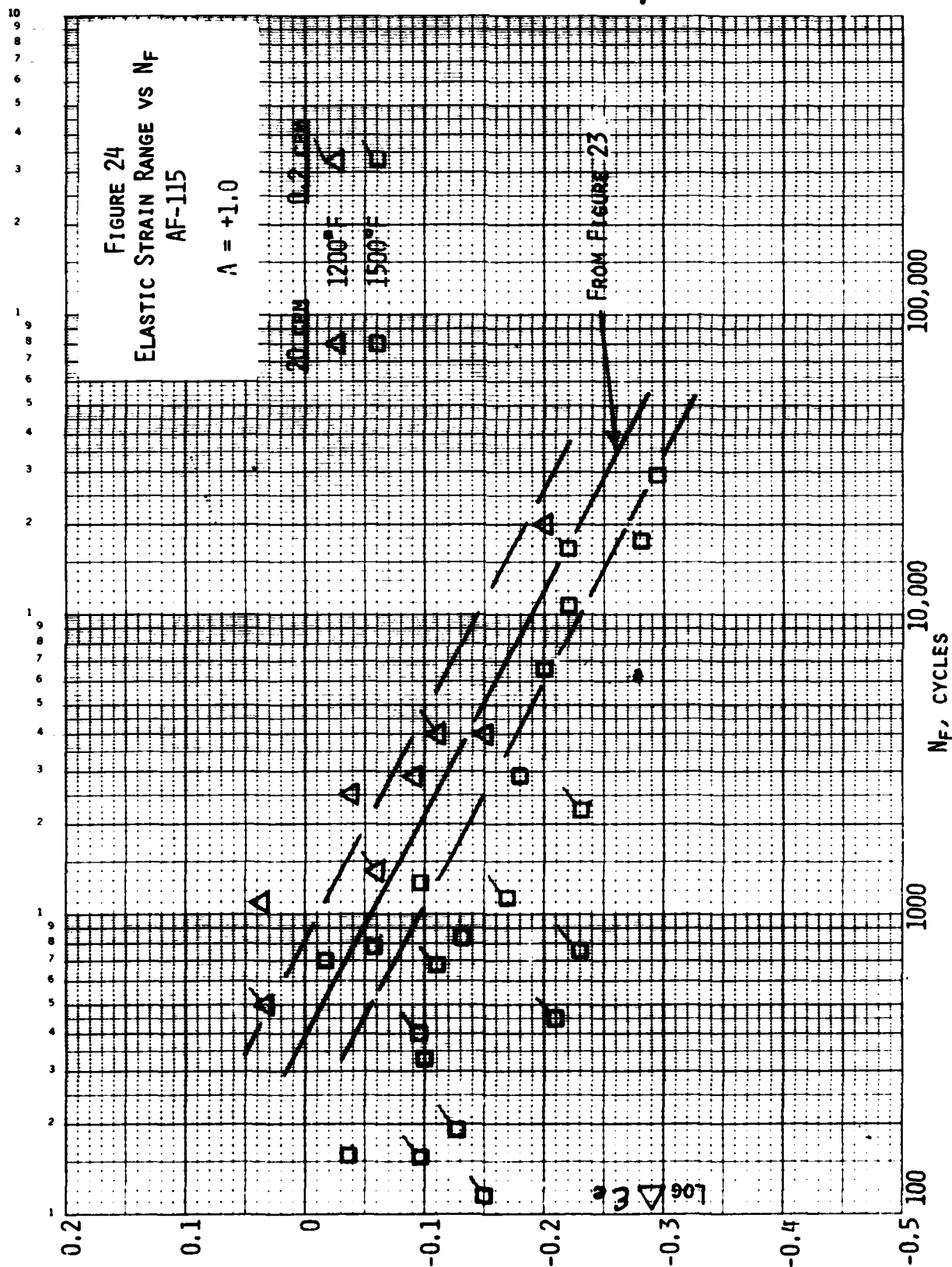
The plastic strain range behavior for the AF-115 alloy is not as well defined as that for the AF2-1DA alloy even in the range below 10,000 cycles. However, based on the data available (Figure 25) some general comments can be made. At 1500°F, and to some extent at 1400°F, the shorter fatigue life (below about 2000 cycles) results appear to define the same type of linearity (i.e. slope of -1.0) noted in Figure 13. It will be noted, though that this persists to a fatigue life value that is far below that observed at 1500°F (and 1400°F) in Figure 13. Furthermore, the estimated isotherms for 1400°F and 1500°F in Figure 25 are positioned noticeably to the left of the corresponding isotherms for the AF2-1DA alloy. Beyond the life regime of about 2000 cycles the plastic strain range vs. life relationship appears to be defined by a line (or curve) having a very shallow slope. This aspect of the fatgieu characteristics of the AF-115 alloy appears to warrant additional study.

FIGURE 25
PLASTIC STRAIN RANGE VS N_F
AF-115
A = +1.0

○ 1200 F
△ 1400 F
□ 1500 F

N_F, CYCLES

$\Delta\varepsilon_{pl}$, %
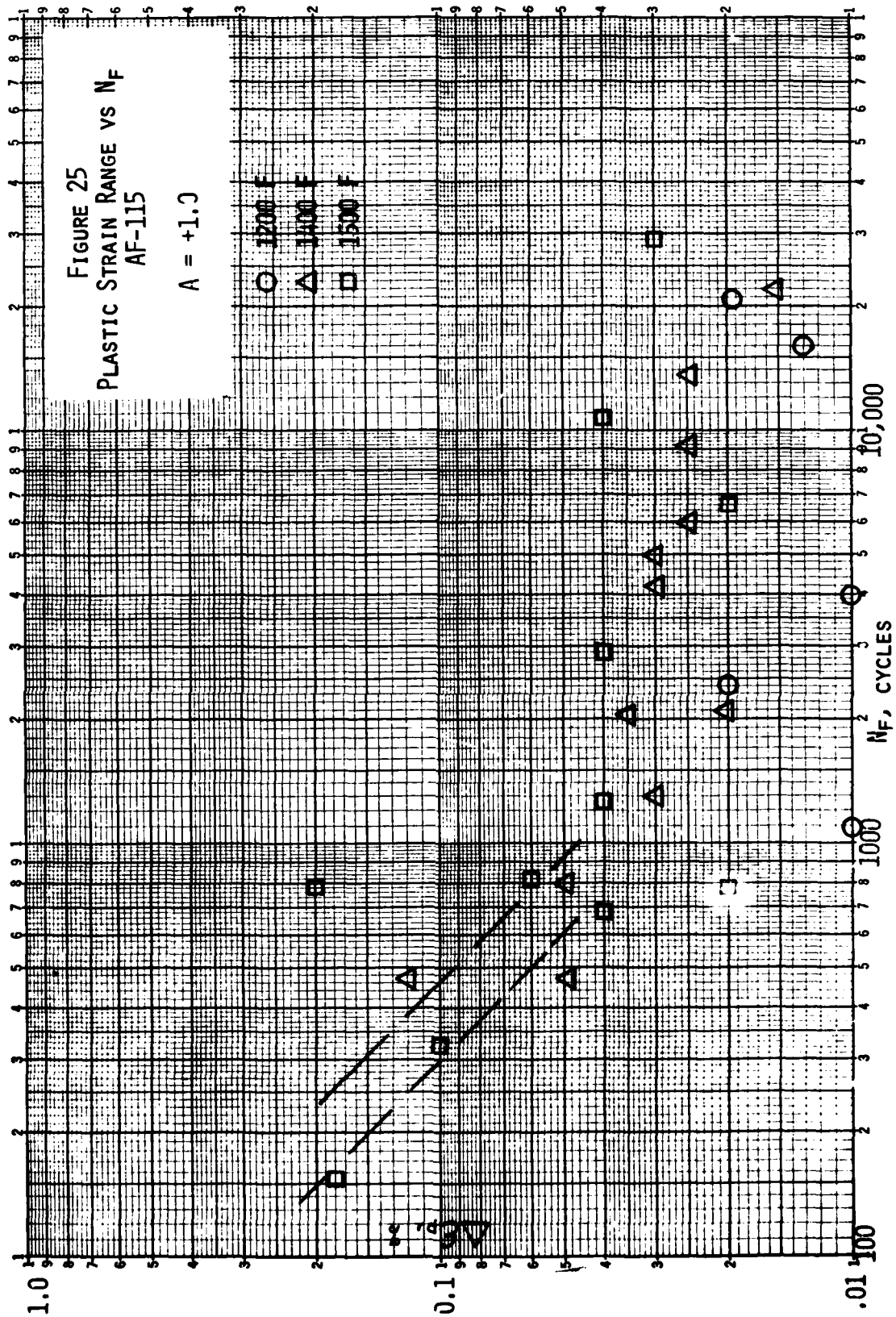
3. RENE 95

With the exception of four tests at 1300°F, all the low-cycle fatigue
evaluations of the Rene 95 alloy in this program were performed at 1200°F.
The total effort on Rene 95 at Mar-Test Inc. involved 101 individual tests.
(Appendix C) It is also to be noted, that, except for one test (Spec. No. 46),
all the low-cycle fatigue evaluations employed hourglass-shaped specimens
and computed axial strain control. In this way, then, these tests differed
from those performed in the evaluation of the AF2-1DA and AF-115 alloys.
Another difference is related to the A – ratio (on strain) employed.
In the Rene 95 tests, the A – ratio was equal to infinity in most cases
except for one test at A = +1.0, one test at A = -1.0, and a series of six
tests in which A – ratio values of +1/3, -1/3, +1/5, and -1/5 were investigated.
In addition, a series of special waveforms was evaluated using selected
versions of slow-fast and fast-slow cycling. A final observation relating to
the Rene 95 evaluations concerns hold-time effects as these were investigated
in much more detail than they were in the case of the two other alloys.

An evaluation of the low-cycle fatigue behavior of the Rene 95 alloy
in terms of total strain range is presented in Figure 26. A well-defined
curvature on this semilogarithmic plot describes the behavior at 1200°F
over the range from 200 to about 400,000 cycles. Also to be noted is an
apparent approach toward an endurance limit in the strain range regime near
0.85%. Also, at 1200°F a slight frequency effect is noted. As the frequency
was reduced from 20 to 0.05 cpm a life reduction factor of approximately 2.0 was
realized over the range studied. Tests in the strain range regime near 0.9%
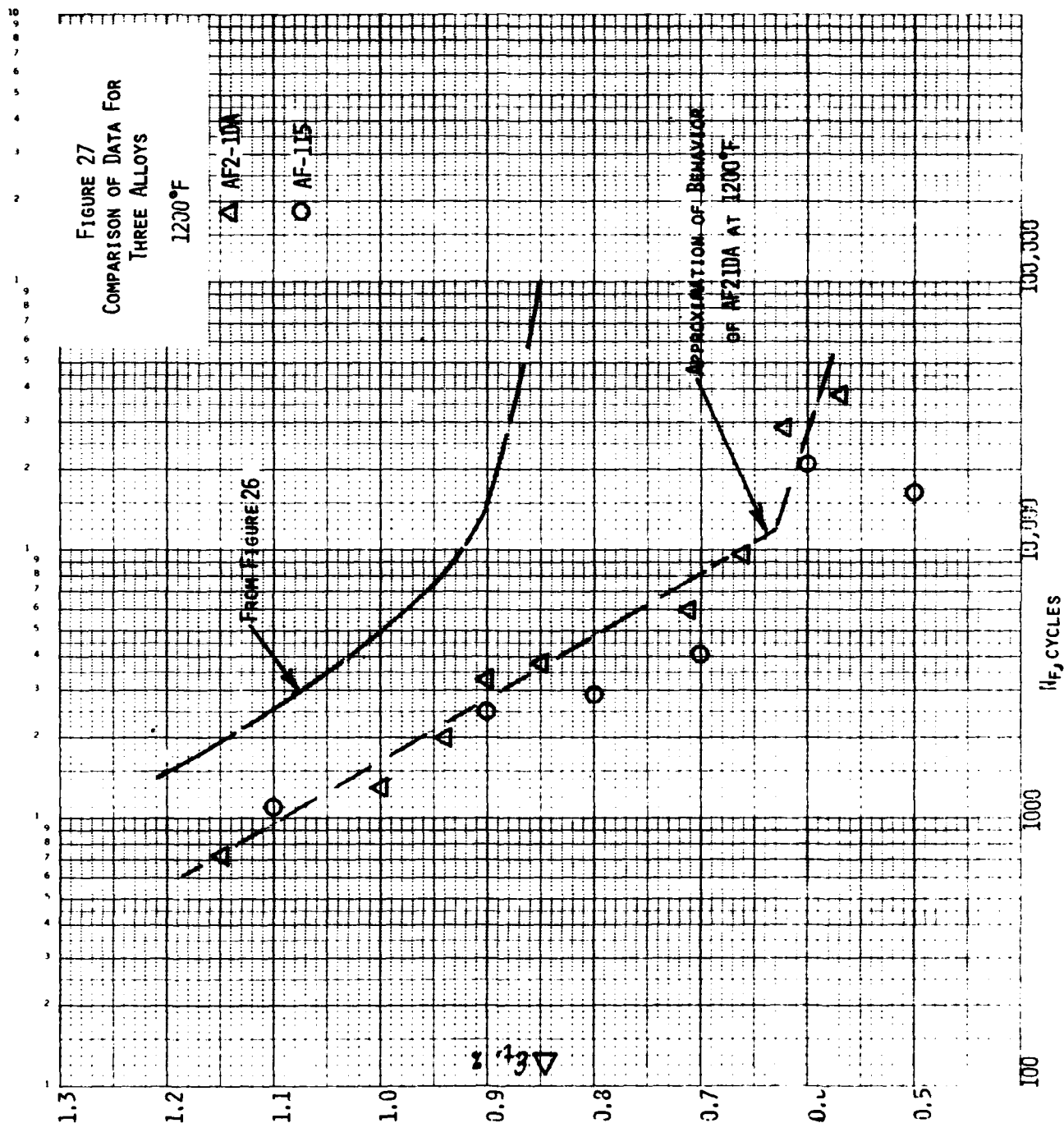are needed to develop an understanding of this behavior.

Another point to be made in connection with Figure 26 concerns temp-
erature effects. While only a few data points are available at 1300°F, it
appears that there is a reduction in life with increased temperature. These

63

Figure 26
Strain Range vs N_F
Rene 95
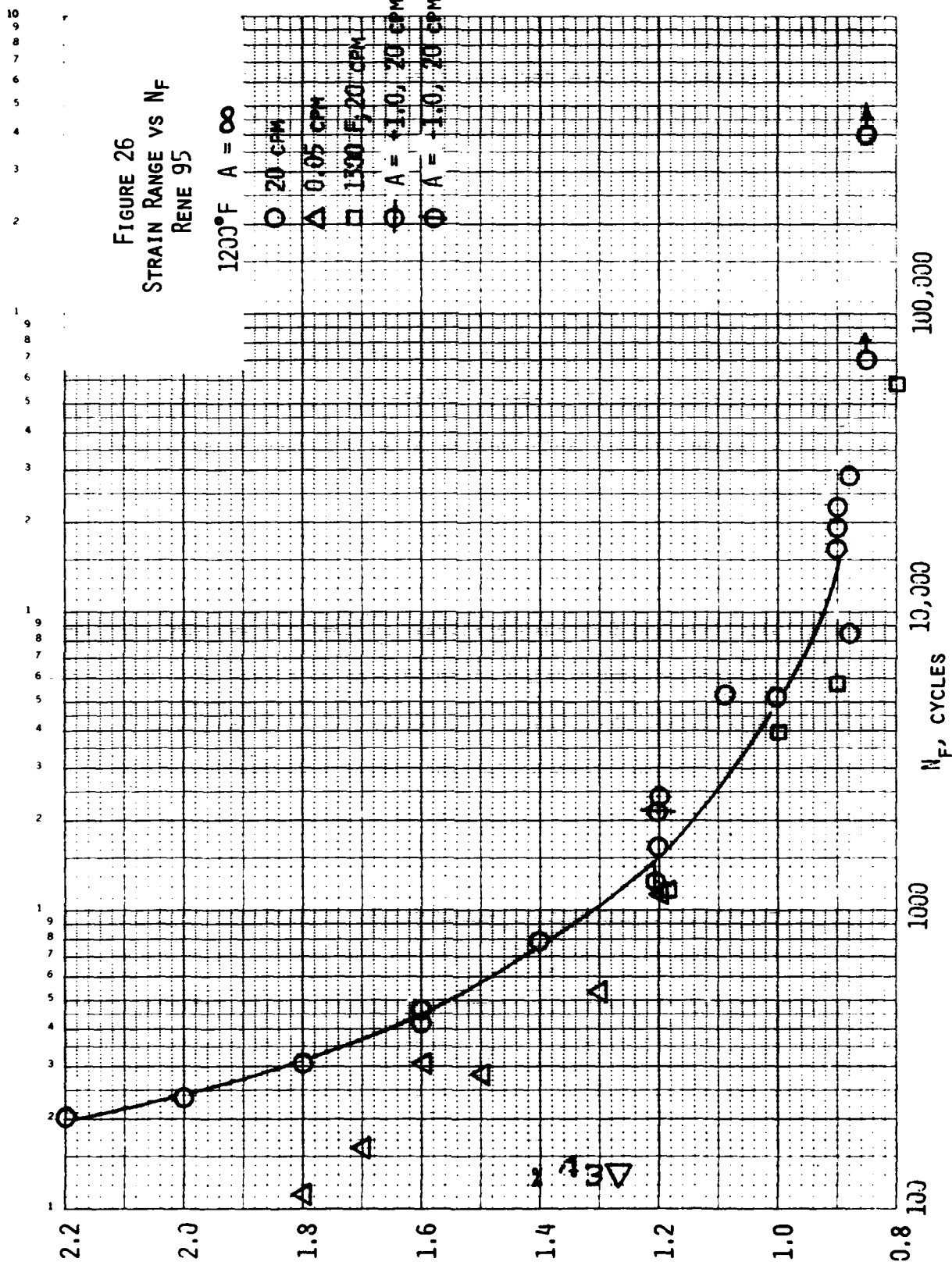
1200°F   A = ∞

tests at 1300°F also suggest that a reduction in the endurance limit will be encountered as the temperature is increased from 1200°F to 1300°F.

Two data points at 1200°F for an A - ratio other than infinity are included in Figure 26; one for A = +1.0 and one for A = -1.0. At a strain-range of 1.2% only a small effect on fatigue life is noted. For A = +1.0, a small reduction in life is noted while at A = -1.0, a small increase in life is observed. These effects are small, however, and might well be within the range of reasonable scatter for data at A = ∞. In any case, no generalizations can be proposed based on these limited results since in the regime of lower strain ranges (0.80% for example) the use of A = +1.0 would be expected to lead to significant reductions in life compared to the data at A = ∞.

An interesting comparison of the low-cycle fatigue characteristics at 1200°F for the three alloys studied in this program is provided in Figure 27. This comparison can becom particularly informative when interpreted in terms of the different A - ratios involved (A = ∞ for Rene 95 and A = +1.0 for AF2-1DA and AF-115 alloys). It was pointed out in the discussion of Figure 26 that tests at an A - ratio of unity and a strain range of 1.2% gave a fatigue life at 1200°F that was not too different (just slightly lower) from that observed at A = ∞. Therefore, in this regime of strain range values, the curve for Rene 95 at 1200°F would apply equally well for A = ∞ and A = +1.0. Furthermore, it is to be noted, that in this strain range regime (about 1%) the isotherm for the Rene 95 alloy at 1200°F is nearly parallel to the 1200°F isotherm for the AF2-1DA and AF-115 alloys. It can also be seen that in this strain range regime the fatigue resistance (for A = +1.0) of the Rene 95 alloy at 1200°F appears to be superior to that of the other two alloys at this temperature. This conclusion should be tempered to some extent because of the different test specimens employed (hour glass for Rene 95 and

65

Figure 27
Comparison of Data For
Three Alloys
1200°F

△ AF2-1DA
○ AF-115

Approximation of Behavior
of AF21DA at 1200°F.

From Figure 26

$\Delta \varepsilon_t$, %

N_F, CYCLES

uniform gage section for the other alloys). Previous studies of this effect have shown that the fatigue life measured using hourglass-shaped specimens is always slightly greater than that obtained with uniform gage section specimens. In light of this result, the behavior of Rene 95 could be positioned much closer to that for the other two alloys. It would seem, however, that the fatigue resistance of Rene 95 would still be slightly superior to that of the two other materials.

In the strain range regime below 1%, the comparison in Figure 27 shows very large differences in the fatigue life of Rene 95 and the other two alloys. This is due principally to an A – ratio effect inasmuch as the endurance limit, for alloys of this type, always occurs at much higher strain range values for tests at A = ∞. It is difficult to project what the actual isotherm for Rene 95 would be at 1200°F for A = +1.0. It would be interesting to have a few tests performed at A = +1.0 for the Rene 95 alloy to directly compare LCF behavior. These tests should also include a few specimens having a uniform gage section in order to define the position of the Rene 95 curve with respect to the AF2-1DA and AF-115 curves when the same specimen design is employed. This comparison of A – ratio effects is an interesting one and will be discussed in some additional detail in a later section of this report.

A study of the effect os hold periods at peak strain on the fatigue life of Rene 95 indicated some interesting patterns. Waveforms with strain hold periods in tension, compression and both tension and compression (balanced hold) were utilized. While this testing effort focused primarily on hold period durations of one minute, there were a few tests in which ten-minute hold periods were employed. This provided the data to identify the different effects of the two hold-period durations and the effect of the location of the hold period within the cycle. An illustration of the effect of

67

a one-minute hold period in tension is provided in Figure 28 (abbreviations of the form (1/10) are employed to define the waveform imposed; the number in the numerator represents the tension hold period time in minutes and the denominator represents compression hold time). In general, the effect is negligible over the strain range regime from 0.9% to 2.0%. There are a few points at a strain range of 1.0% to indicate a beneficial effect of the one-minute tension hold period. The two, ten-minute hold-period tests shown in Figure 28 indicate essentially the same effect observed for the one-minute hold period. In summary, for Rene 95 at 1200°F (A = ∞) and at strain ranges of 1.2 and 1.4%, hold-period durations of one and ten minutes in tension have no detrimental effect on the fatigue life. This result might be viewed as being unexpected and for this reason shold be studied in more detail in future test programs.

Similar tests at 1200°F with hold periods in compression led to results that were significantly different from those described in Figure 28. This behavior is shown in Figure 29 and indicated that one-minute hold periods do exert a noticeable effect in reducing the fatigue life below that observed in continuous cycling tests at the same strain range. It is also observable in Figure 29 that the detrimental effect of a one-minute duration is increased as the hold-period duration is changed to ten minutes. When a hold-period is employed in both tension and compression, the results for one-minute durations are about the same as for the one-minute hold in compression only. This same type of behavior also seems to follow for ten-minute durations although the reduction in fatigue life is somewhat greater than that observed with one-minute durations.

A more graphic summarization of the hold-time effects noted in this study is provided by a plot of the fatigue life reduction factor as used in

68

Figure 28
Strain Range vs N_F
Hold Periods in Tension

Rene 95
1200°F   A = ∞

○ 1 min
△ 10 min

Curve from Figure 26

N_F, cycles

$\Delta \varepsilon_I$, %

Figure 29
Strain Range vs N_F
Hold Period Results

Rene 95   1200°F   A = ∞
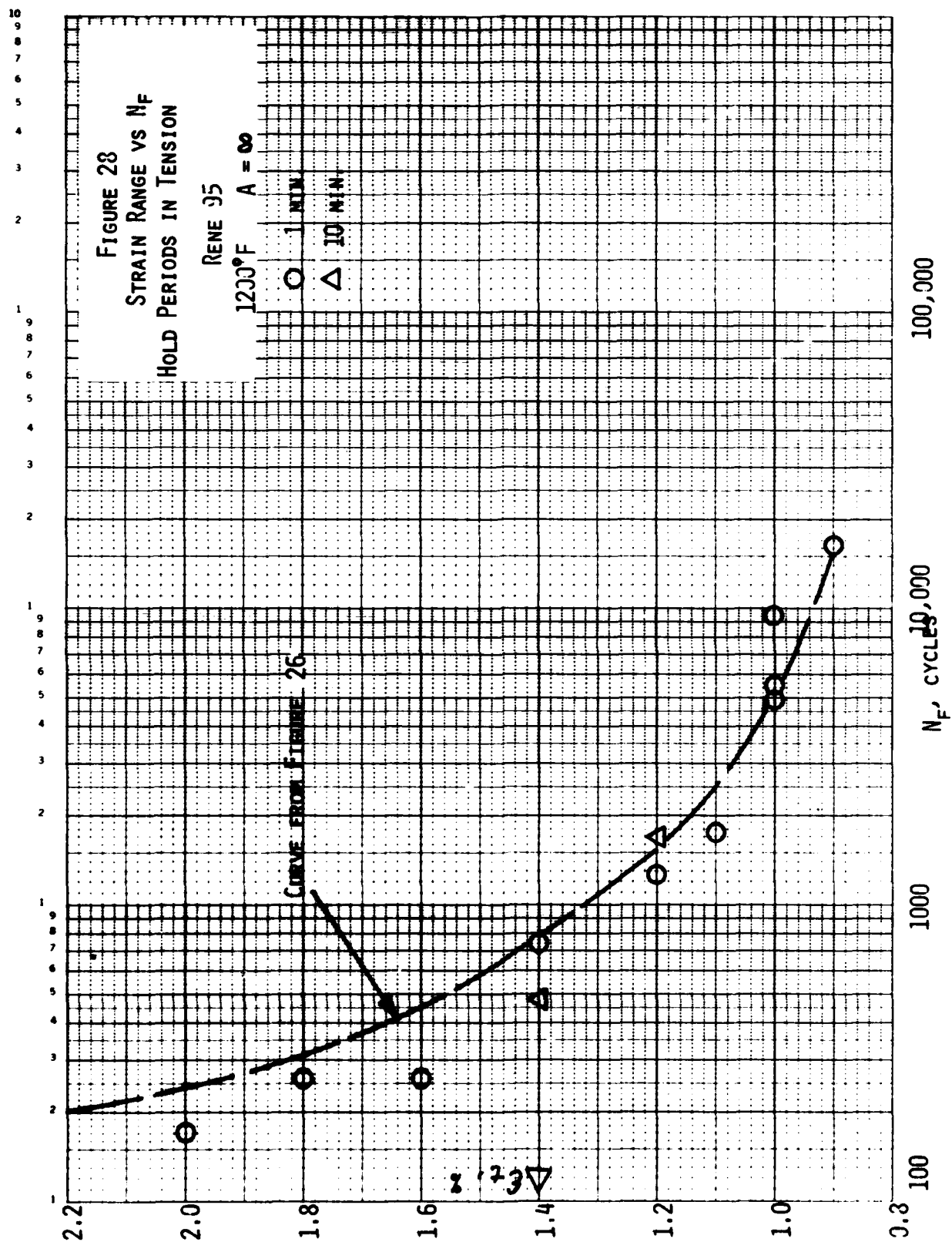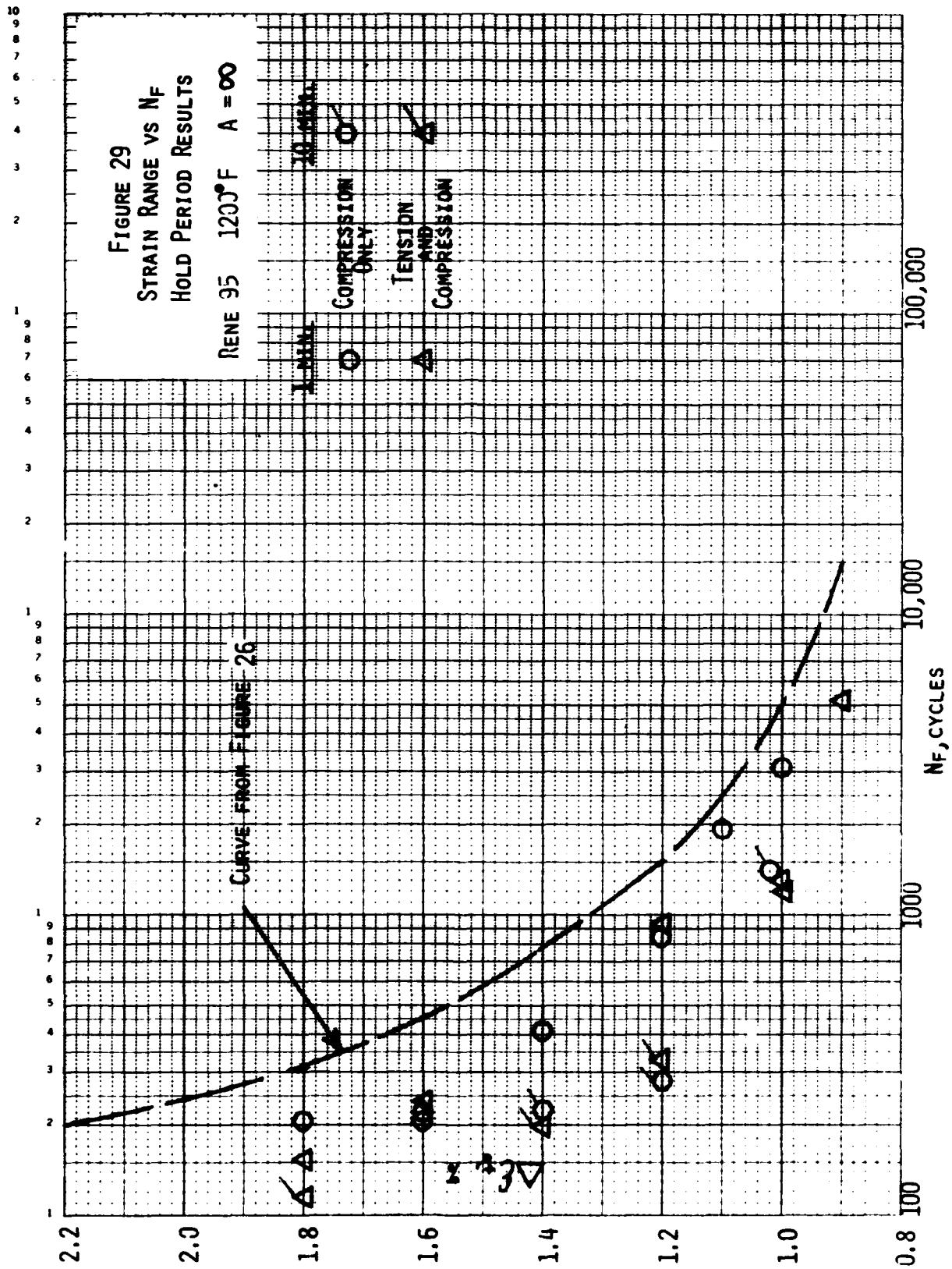
ASME Code activities. This factor is simply the ratio of the fatigue life without a hold period to the fatigue life observed when a hold period is employed. For certain waveforms the fatigue life reduction factor exhibited a definite trend toward higher values as the strain range was decreased. An example of this is shown in Figure 30A for (1/1) and (10/10) types of tests. A composite of all the hold-time results is shown in Figure 30B and within reasonable scatter the following trends are identifiable:

1) One-minute hold period in tension has a negligible effect on the fatigue life over the strain range regime from 0.9% to 2.0%;

2) One-minute hold periods in compression and in both tension and compression define a fatigue life reduction factor of 2.0 for strain ranges from 1.8% down to about 1.0%; below 1%, there appears to be a sharp increase in the slope of this trend behavior to suggest more detrimental effects in the lower strain range regime; since this lower strain range regime is in the area of special design interest (i.e. fatigue life values greater than 10,000 cycles) a more comprehensive study of hold time effects in this regime appears warranted;

3) Ten-minute hold periods in compression and in both tension and compression define a trend behavior that begins at a fatigue life reduction factor of about 5.0 in the strain range regime near 1.0%. Here again, a further study of hold-time effect is needed in the lower strain range region.

Some comment should be made at this point regarding the development of different mean stress values in the hold-time tests. A good comparison of such behavior is provided in Figure 31. In the continuous cycling tests at 20 cpm, the absolute value of the compressive stress component is always just slightly larger than the tensile stress component. This behavior is shown in Figure 31 and it will be noted that over much of the strain range regime studied a mean compressive stress of about 5 ksi is exhibited. In the region

71

Figure 30A
Fatigue Life Reduction
Factor vs Strain Range

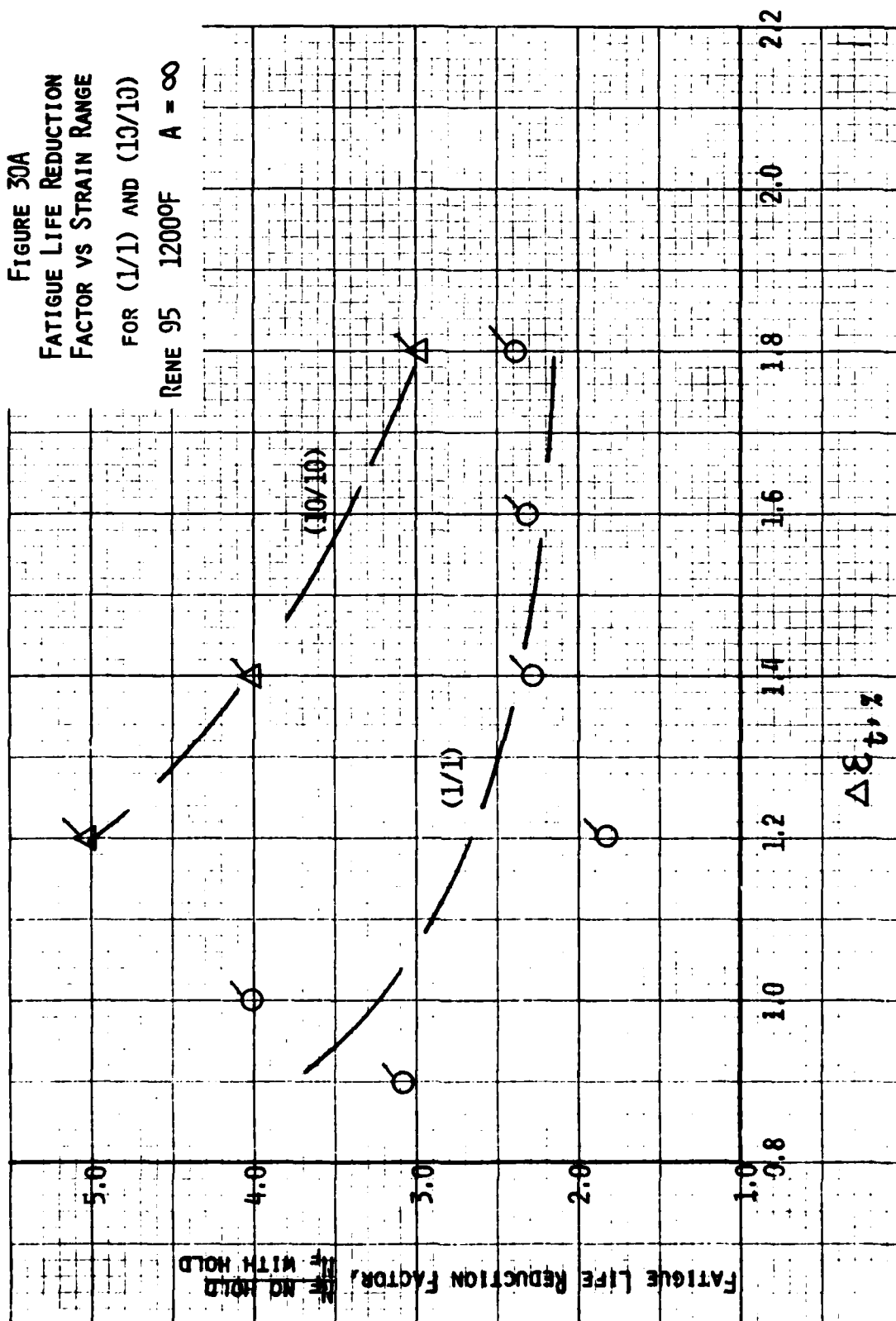For (1/1) and (10/10) A = ∞

Rene 95 1200F

Figure 30 B
Fatigue Life Reduction
Factor vs Strain Range

Rene 95   1200°F   A = ∞

73
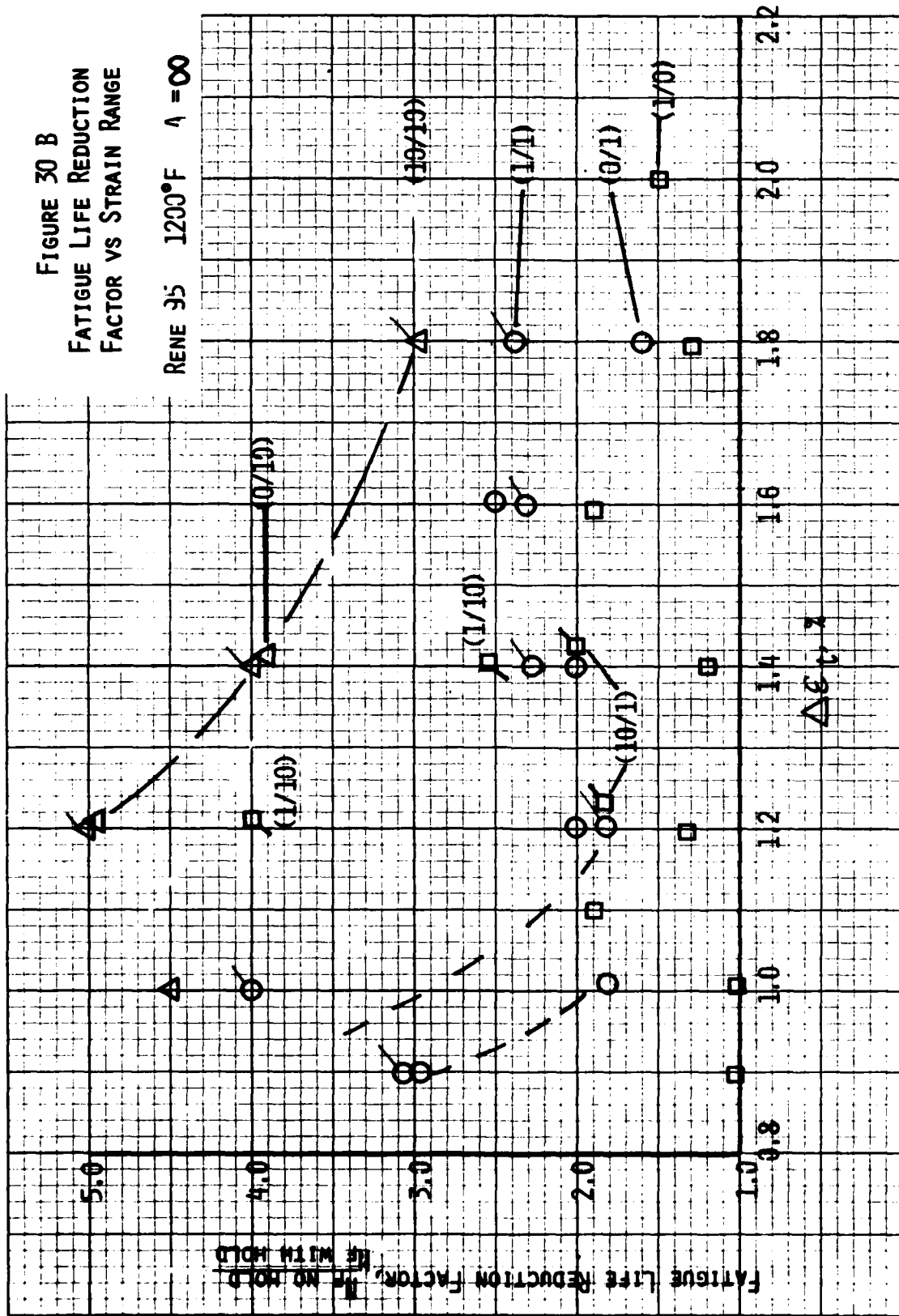
FIGURE 31
MEAN STRESS VS STRAIN RANGE
RENE 95
1200°F   A = ∞
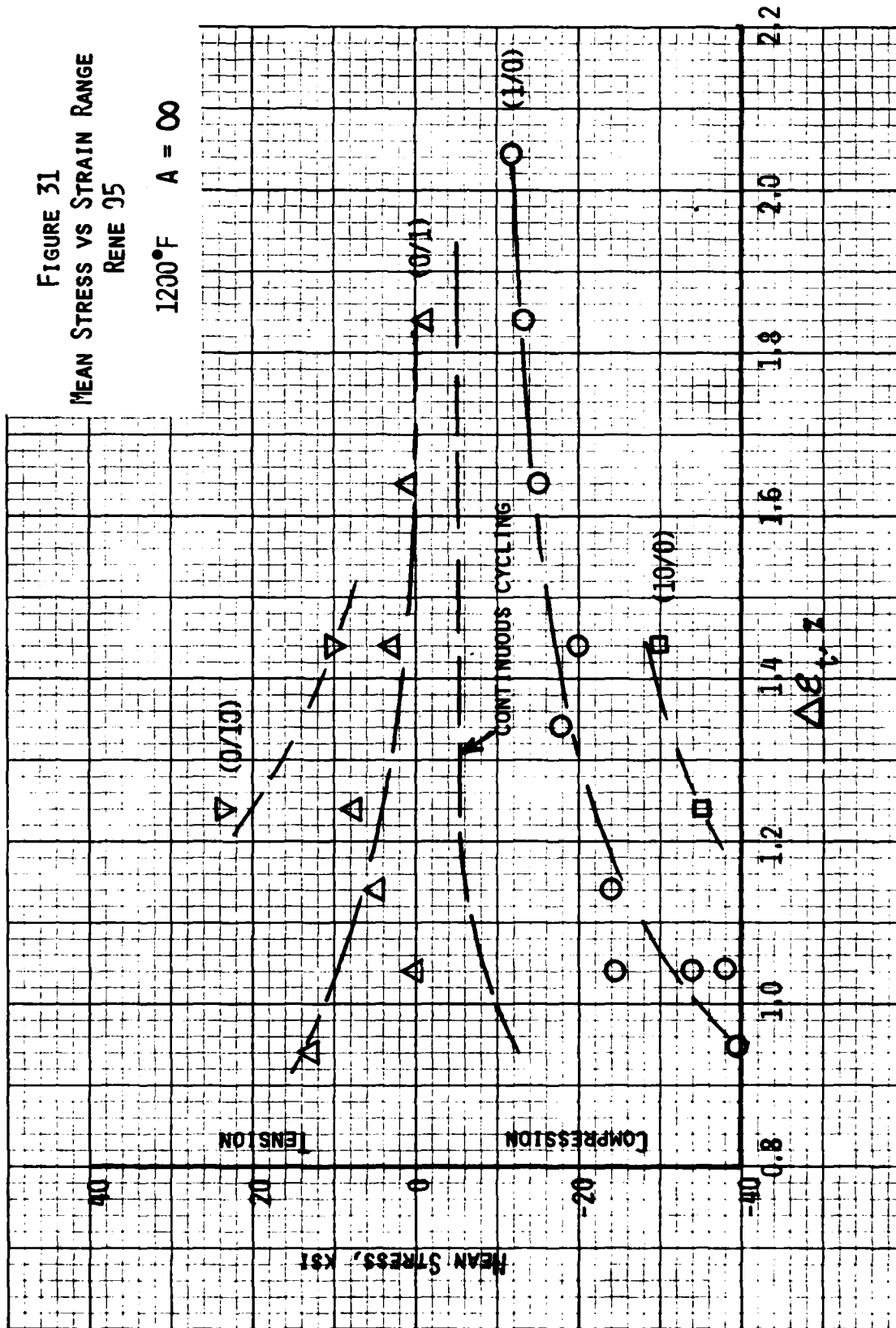
near a strain range of 1.0%, the compressive mean stress is seen to increase

to a value near 10 ksi. This result can be compared with the behavior observed

for various hold-period combinations as plotted in Figure 31. For the 1/10

combination (one minute hold in tension only) the mean compressive stress is

increased above the continuous cycling value and shows an increase to 40 ksi

compression in the low strain range regime. This mean compressive stress is

increased even more in the 10/0 combination. For the 0/1 combination (one

minute hold period in compression only) the mean stress is close to zero in the

high strain range regime and gradually increases to about 10 ksi tension at the

lower strain ranges. For 0/10, the mean tensile stress is even higher and would

appear to approach 40 ksi in the strain range regime near 1%. Data for the 1/1

and 10/10 combinations are not plotted but are not too different from the contin-

uous cycling behavior. In the case of the 10/1 combination, the mean stress

behavior is similar to that exhibited by the 1/0 combination. The effect

of hold periods on the LCF behavior of Rene 95 using this same data has been

extensively treated in previous AFML Technical Report.[3,2]

A few tests were performed at 1200°F and a strain range of 1.2% in an evaluation of the effect of A - ratio on fatigue life   To allow for convenient comparison, a summarization of these tests (reported in detail in Appendix C is as follows:

Spec. No.	A - ratio	N_f, cycles
66-B	-1/5	4,054
70-B	-1/5	5,834
69-B	-1/3	3,532
37	-1.0	2,126
67-B	+1/3	1,114
64-B	+1/5	752
36	+1/0	1,207
68-B	∞	2,369

There is a definite trend in these results in that the positive A - ratios lead to fatigue life values lower than the value observed at A = ∞, while fatigue life values greater than that at A = ∞ are observed for the negative A'- ratios. In order to remove the discontinuity associated with A = ∞, these results were analyzed in terms of 1/A as shown in Figure 32. An interesting linearity is defined to allow the A - ratio effect at this strain range to be expressed mathematically. This analysis of Figure 32 led to the following expression:

$$N_f = B \, e^{-b/A} \tag{5}$$

$$+ \, 2000 \, e^{-0.19/A} \tag{6}$$

these constants must be recognized as being dependent upon strain range since the slope (related to b) is expected to become more negative as the strain range is decreased. The interesting mathematical form in equation (5) suggests another aspect of the Rene 95 fatigue behavior that warrants additional study.

76

FIGURE 32
N_F VS $1/A$
RENE 95

1200°F; 20 CPM; $\triangle \mathcal{E}_t = 1.2\%$
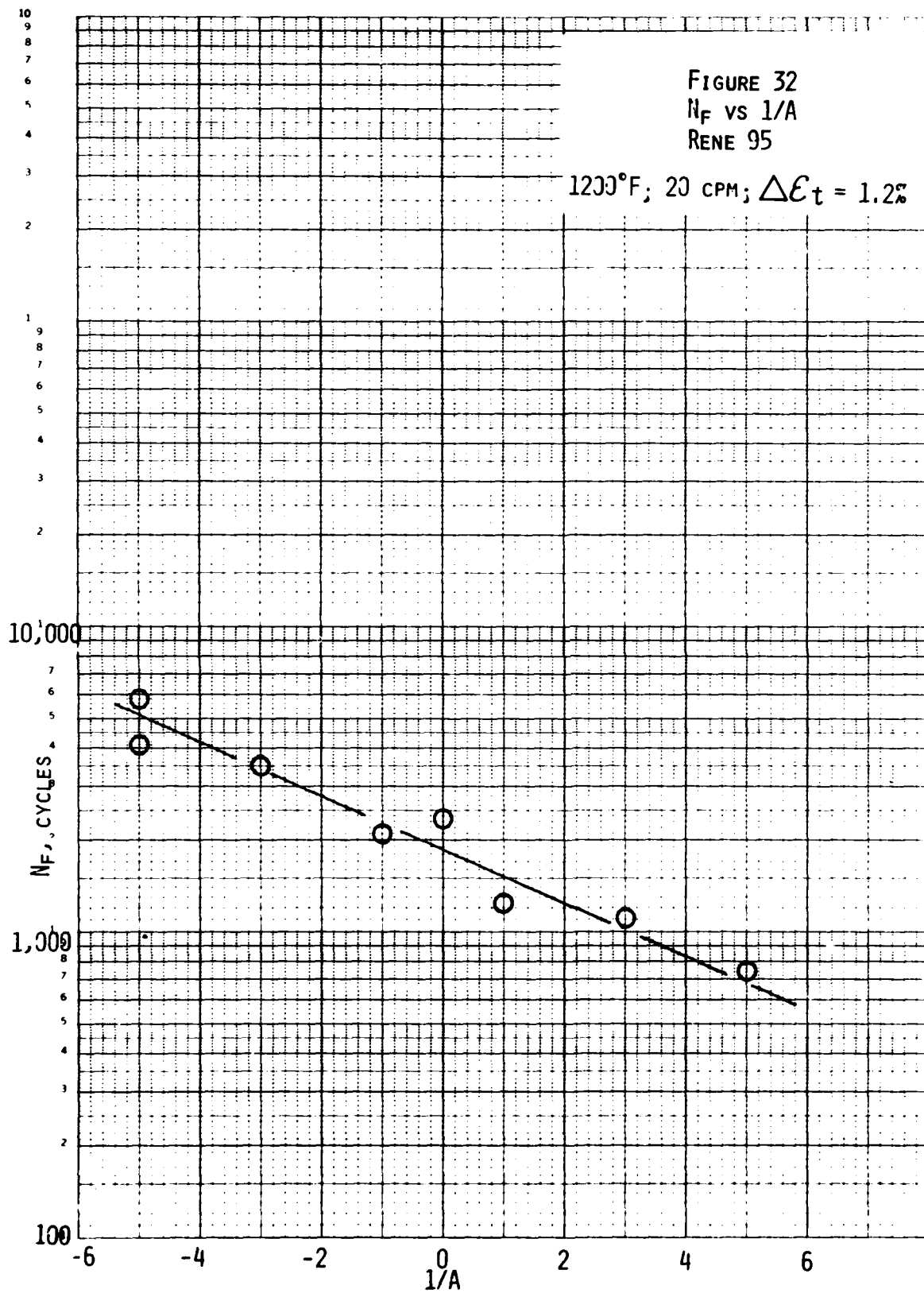
Two other interesting plots that evolved from this study of A – ratio effects are shown in Figures 33 and 34. While the stress range (at $N_f/2$) was approximately the same for all A – ratio values significant differences were noted in the tensile and compression stress components measured at half-life. These differences are shown in terms of the ten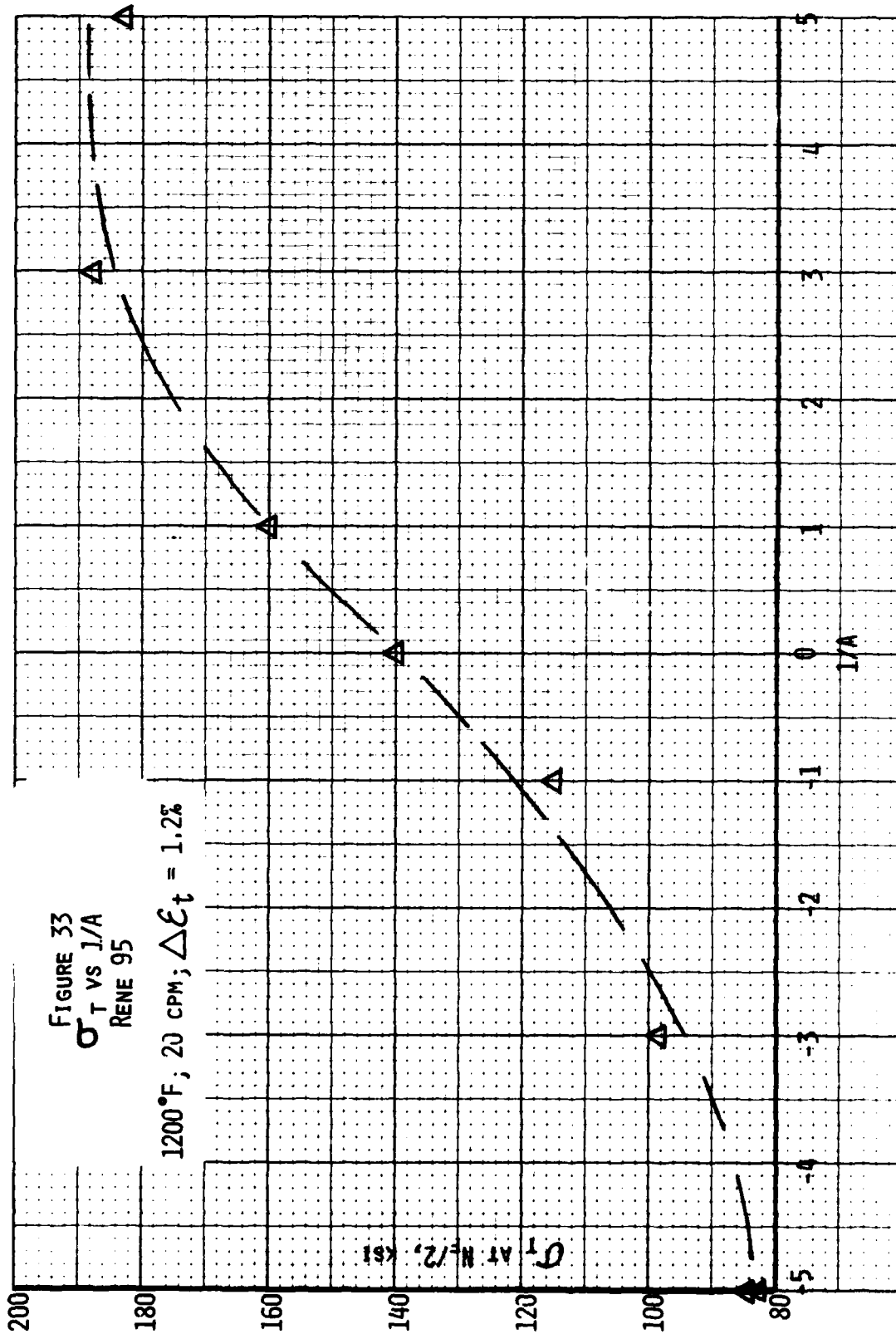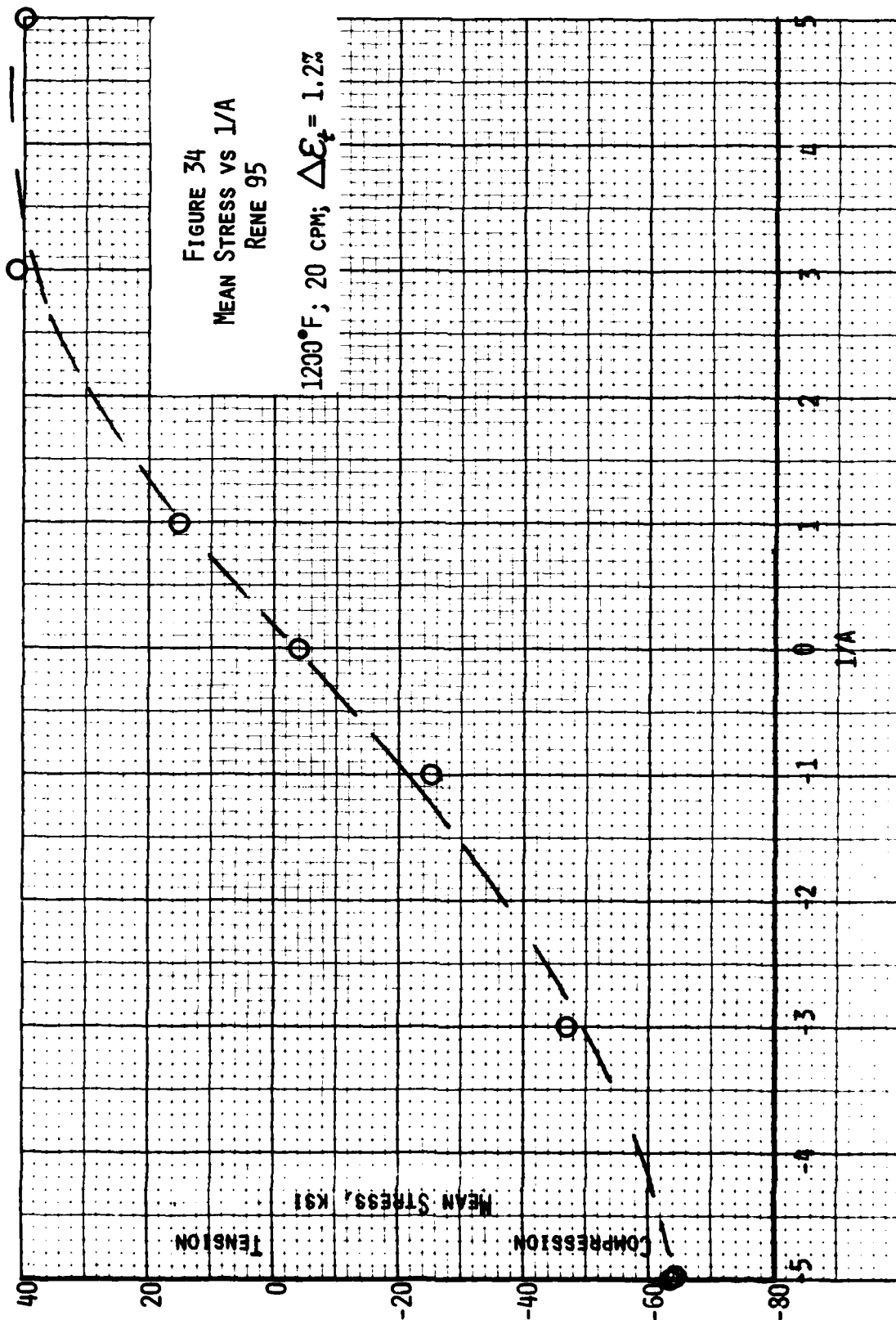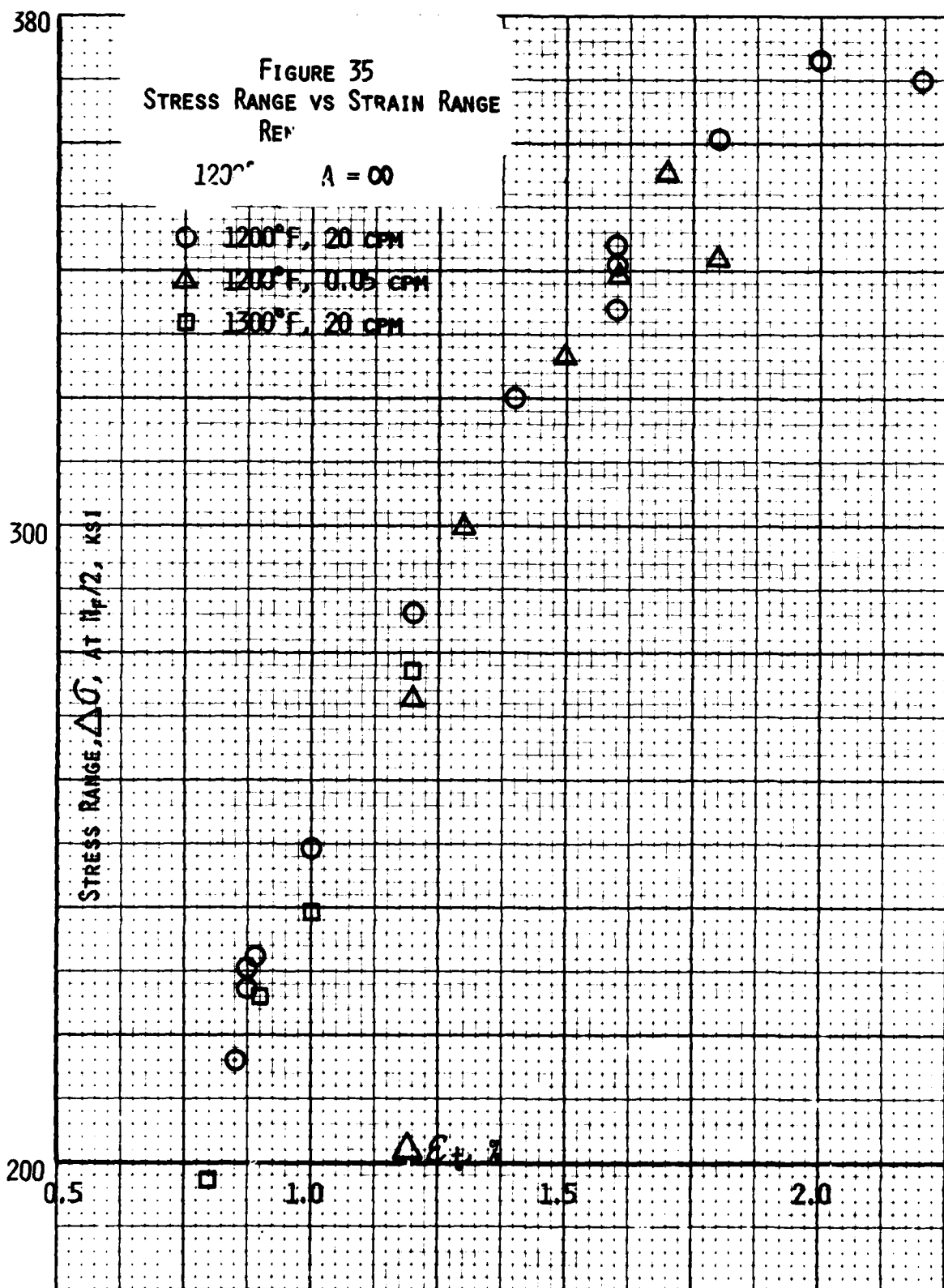sile stress component values (Figure 33) and the mean stress values (Figure 34) based on half-life information and reflect extensive variations. In the case of the σ_t plot, the overall curve shape appears to be sigmoidal, and in the A – ratio range near +1/3 an asymptotic trend is noted. The σ_t value in this regime is close to the 0.2% yield value of Rene 95 at 1200°F. Some further evaluation of this observation is in order. Sigmoidal behavior is also exhibited in the mean stress plot of Figure 34 as mean stress values range from -63 ksi at A – -1/5 to 40 ksi at A – ratio values of 1/3 and 1/5.

Cyclic stress-strain behavior derived from the data in Appendix C is displayed in Figure 35. A small frequency effect appears to be developing in the higher strain range regime but the effect is not well substantiated due to the limited number of test points. Also, a small temperature effect seems to be indicated at 1300°F but here again, the data are too limited to draw any general conclusions.

Stress range data (at $N_f/2$) at 1200°F are plotted versus fatigue life in Figure 36. These results define a linear relationship over the life range to about 10,000 cycles at which point the few data points available suggest a transition to a shallower slope and perhaps the tendency toward an endurance limit. Another interesting feature of Figure 36 involves the data at 1200°F for a test frequency of 0.05 cpm. These results define a slight reduction in fatigue life due to the lower frequency and the data points fall on a line that is parallel to that identified by the data at 20 cpm. Another consistent behavior pattern is identified by the data points at 1300°F as shown in Figure 37. Not only is a linear relationship observed in the higher stress range regime, but

FIGURE 33
σ_T VS 1/A
RENE 95

$1200°F; 20$ CPM, $\Delta\mathcal{E}_t = 1.2\%$

79

Figure 34
Mean Stress vs 1/A
Rene 95

$1200°F$; 20 cpm; $\Delta \varepsilon_t = 1.2\%$

80

FIGURE 35
STRESS RANGE VS STRAIN RANGE
REM

$1200°$ $A = \infty$

○ $1200°F$, 20 CPM
△ $1200°F$, 0.05 CPM
▣ $1300°F$, 20 CPM

STRESS RANGE, $\Delta \sigma$, AT $N_f/2$, KSI
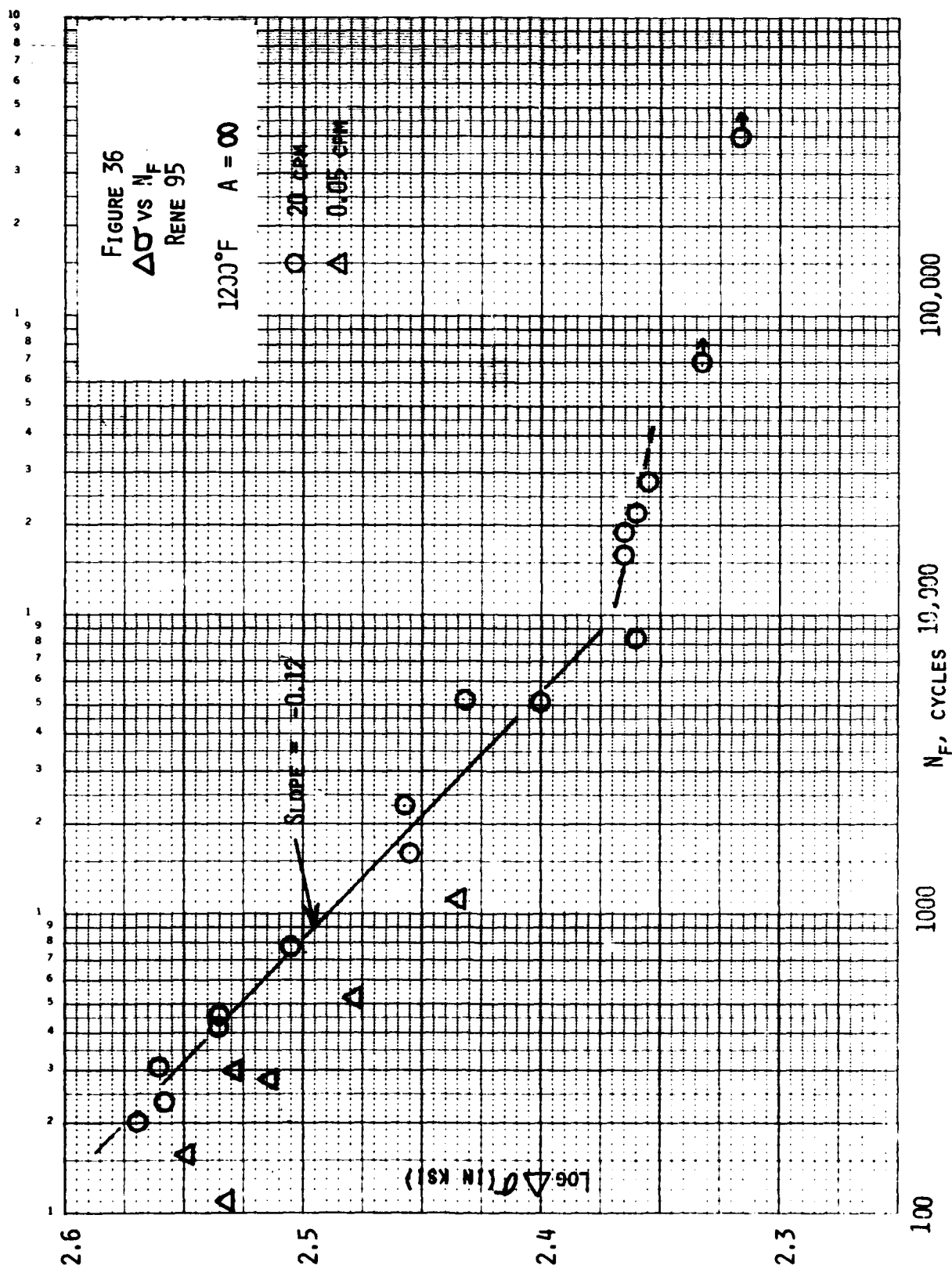
$\Delta \varepsilon_t$, %

81

this is parallel to the 1200°F isotherm. Also indicated is the transition to a shallower slope in the regime near 10,000 cycles.
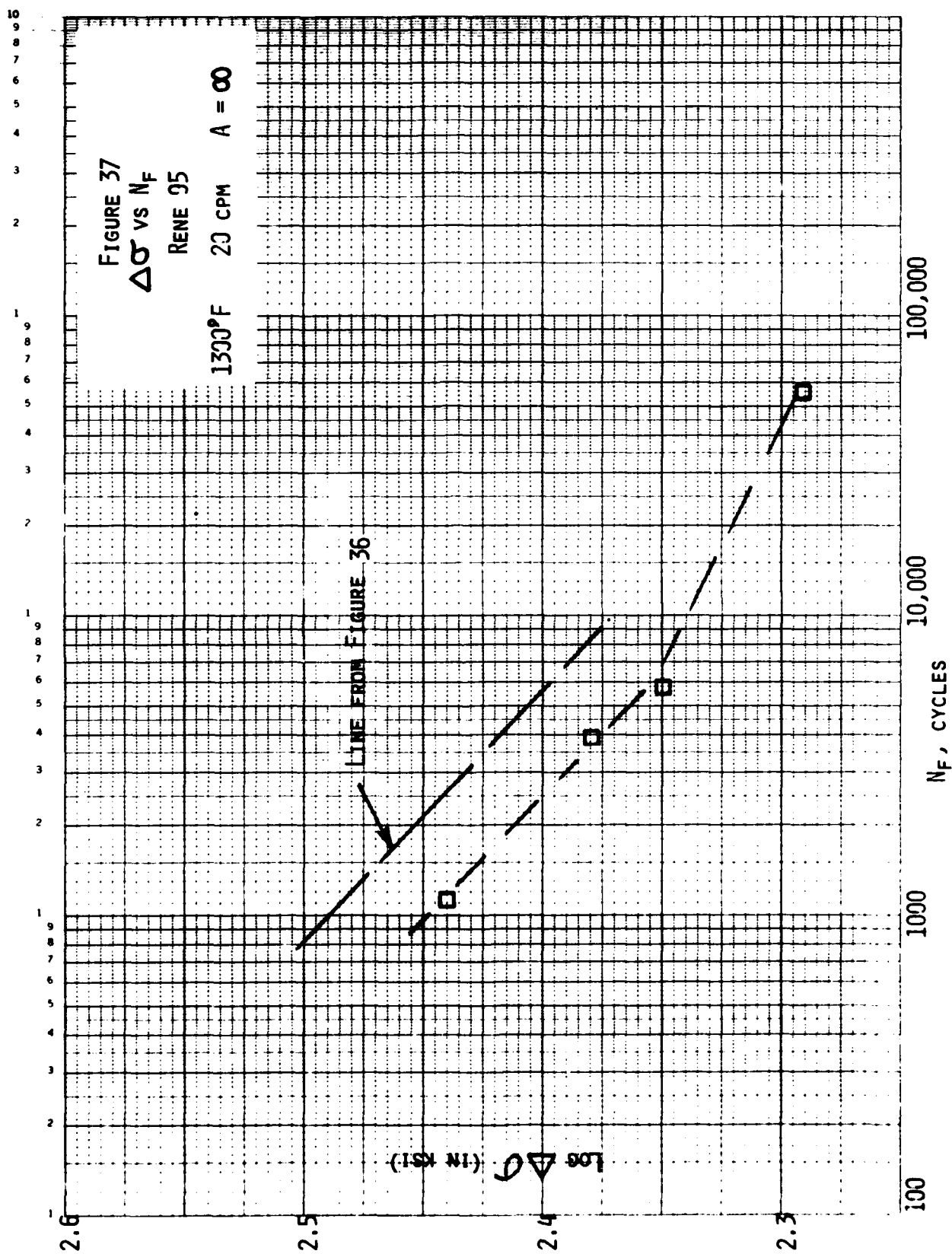
Plots comparable to Figures 36 and 37 are obtained for the data expressed in terms of elastic strain range rather than stress range. Such plots are shown in Figures 38 and 39 where it will be noted that the trend behavior for frequency and temperature effects is similar to that described in Figures 36 and 37. For comparative purposes, the elastic line for the AF2IDA alloy at 1200°F (this line is about the same as the elastic line for the AFT15 alloy at 1200°F) is positioned in Figure 38. It is interesting that in the regime to about 10,000 cycles, the line for the Rene 95 material closely parallels the line for the AF2IDA alloy. For all three materials, then, the elastic strain range lines are parallel, at least over the cycle life regime to 10,000 cycles. It is also to be noted that while the elastic line for the Af2IDA material at 1200°F remains linear out to about 40,000 cycles, the line for Rene 95 appears to develop a bilinear behavior near 10,000 cycles.

A plot showing the relationship between plastic strain range and fatigue life is presented in Figure 40. Only data below 10,000 cycles are included since beyond this point the plastic strain range values are 0.01% and less and in this regime, the values are of questionable accuracy. A definite linearity is defined in the range to 10,000 cycles and the slope is close to -1.0. As previously noted this slope is noticeably different from that usually associated with the Coffin-Manson [10,11] relationship for plastic strain range behavior. Instead of having a slope of -0.5 or -0.6, the $\Delta\epsilon_\rho$ and N_f relation exhibits a slope of -1.0 to yield the following relationship:

$$\Delta\epsilon_\rho N_f = \text{constant}$$

An intercept calculation for Figure 40 identified this constant to be 131.0 based on $\Delta\epsilon_\rho$ expressed in percent.

Figure 36
Δσ vs N_F
Rene 95

1200°F   A = ∞

○ 20 cpm
△ 0.05 cpm

Slope = -0.12

N_F, CYCLES

LOG. Δσ (IN KSI)

83

FIGURE 37
$\Delta\sigma$ VS N_F
RENE 95

1300°F   20 CPM   A = ∞

LINE FROM FIGURE 36

LOG $\Delta\sigma$ (IN KSI)

N_F, CYCLES

84

Figure 38
Elastic Strain Range vs N_F
Rene 95
1200°F   A = ∞

○ 20 cpm
△ 0.05 cpm

85

FIGURE 39
ELASTIC STRAIN RANGE VS N_F
RENE 95

1300°F   A = ∞   20 CPM

N_F, CYCLES

$LOG \triangle \varepsilon_e$

FROM FIGURE 38

86

Figure 40
Plastic Strain Range vs N_F
Rene 95

1200°F   20 CPM   A = ∞
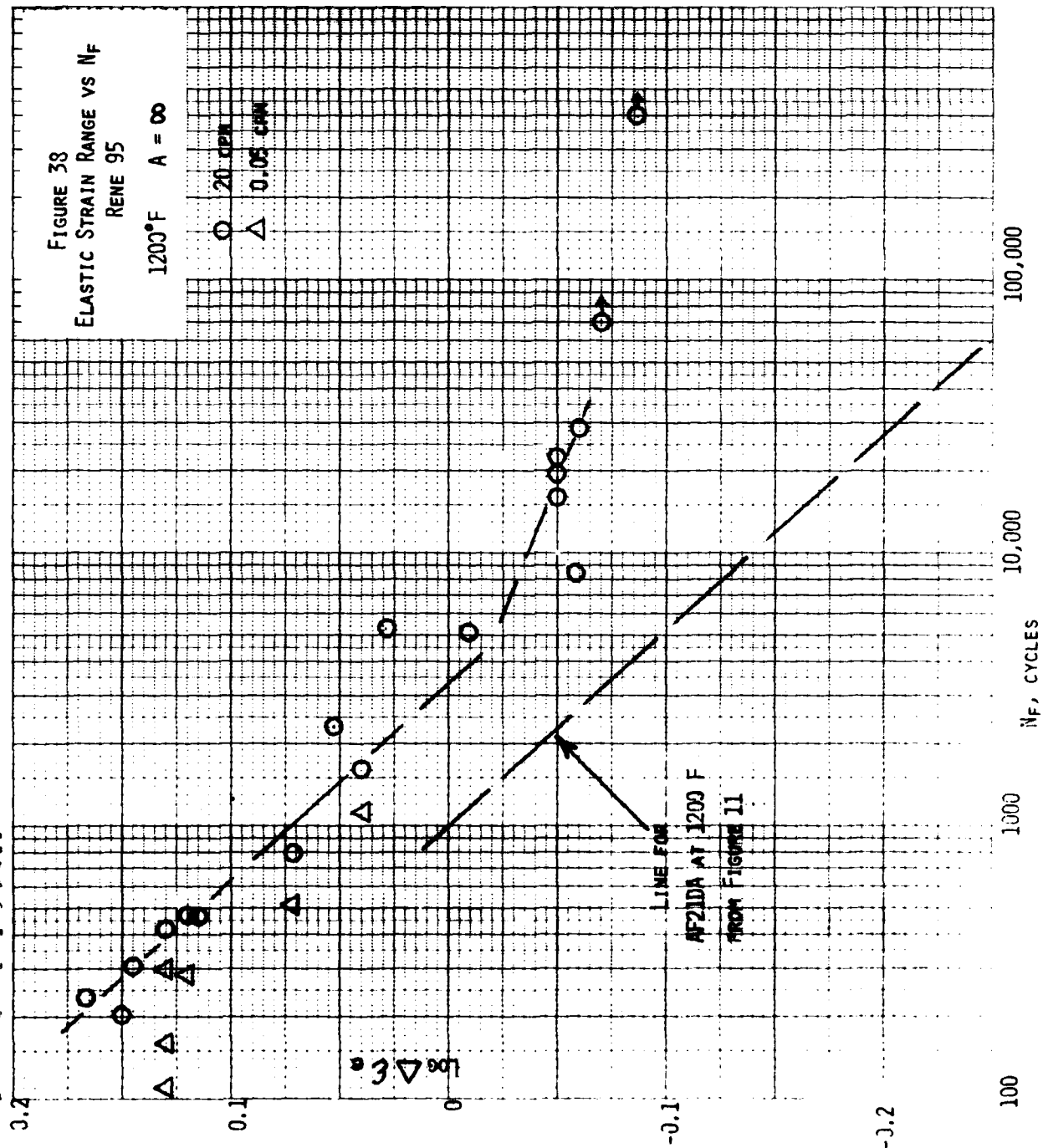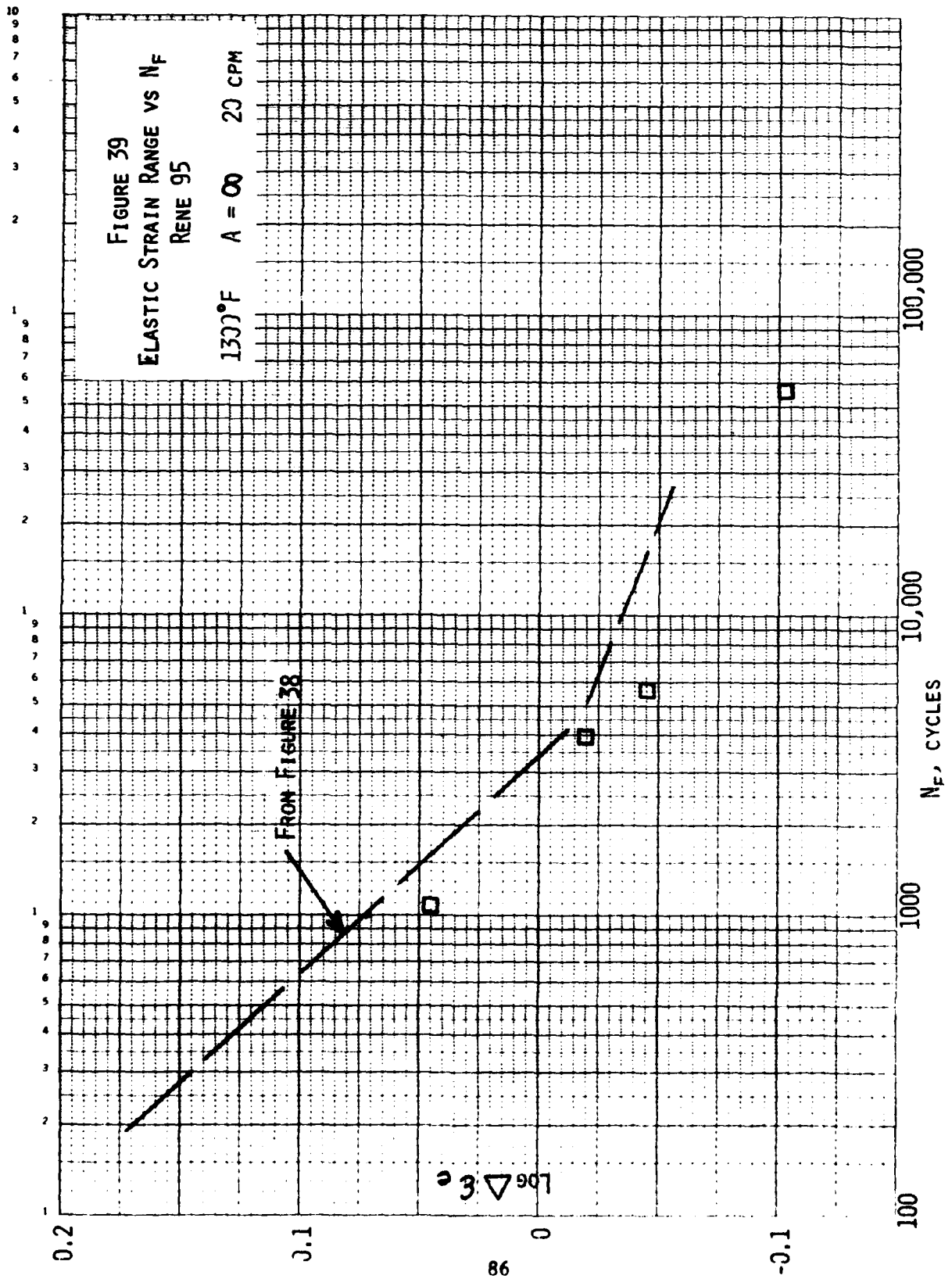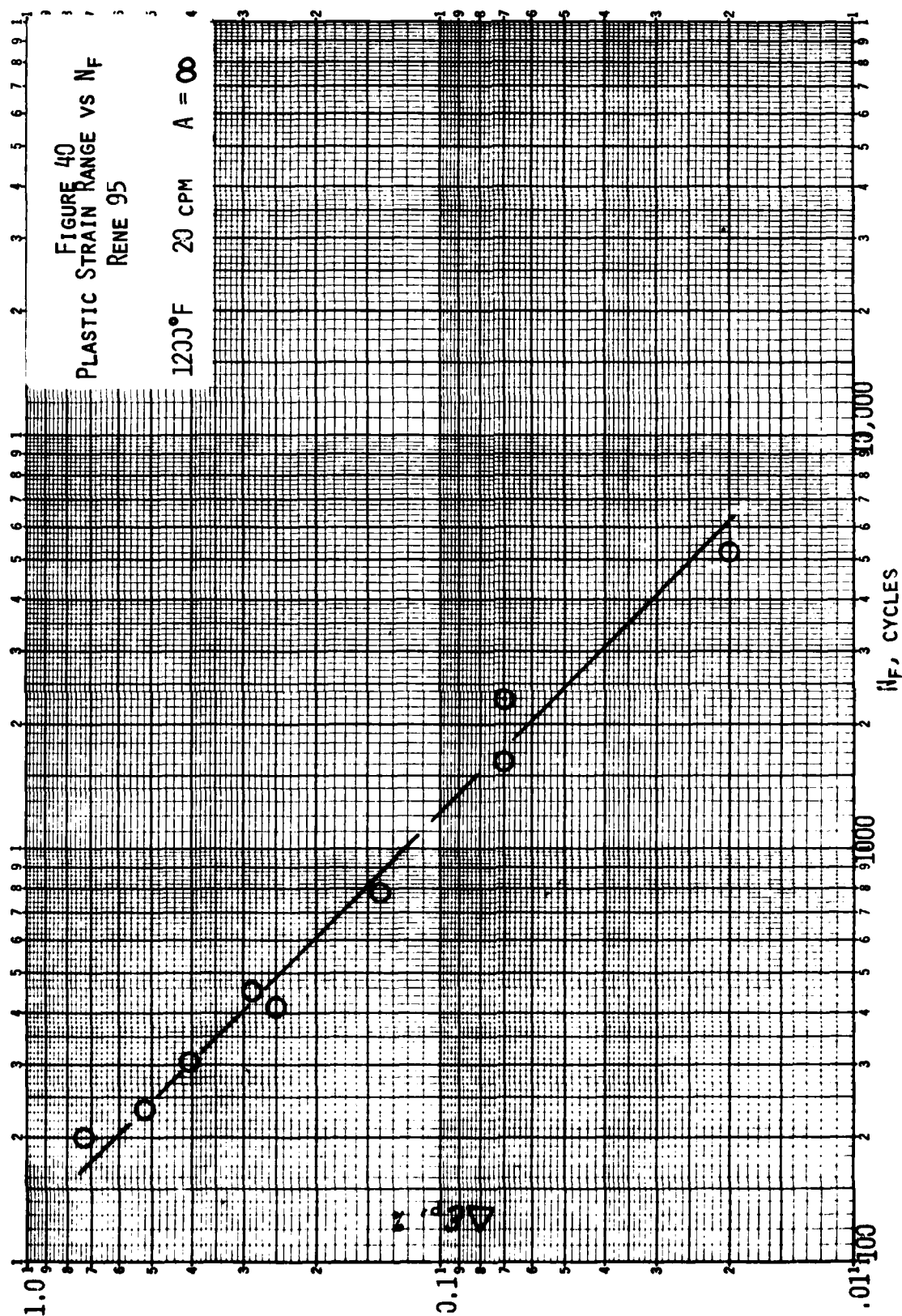
Another intersting evaluation of the hold-time results for Rene 95 stemmed from an attempt to correlate fatigue life with the tensile stress component, σ_t. One of the first plots that was prepared in this evaluation involved σ_t vs N_f on logarithmic coordinates as shown in Figure 41. For the continuous cycling results (at 20 cpm) a linear relationship was defined over the range to about 10,000 cycles. Beyond this point, the data suggested a deviation from linearity and the development of a curvature that was concave upward. Data in this long-life regime are not extensive enough to define the shape of the curve exactly, but some tendency toward an endurance limit appears to be identifiable.

Data for a 1-minute hold period in tension were found to describe a interesting behavior. A linear regime was noted that was essentially parallel to the line defined by the continuous cycling results. Secondly, this linearity persisted for only a short span of fatigue life and when deviation from linearity did occur, it defined a curvature that was opposite to that noted for the continuous cycling results. There is no explanation at the moment for these different patterns, but further study appears warranted.

Test results based on a 10-minute hold period in tension are too few to establish any meaningful conclusion, but for the data points available (see Figure 41) a line parallel to the line for 1-minute hold periods is indicated. Whether this line exhibits a deviation from linearity and a curvature to match the 1-minute hold periods results can not be stated at this time. Certainly, such behavior would be expected, but additional test results must be obtained to substantiate this tentative observation.

A significant result emerged from the use of the plot shown in Figure 41 to compare hold periods in compression. It was noted that in terms of σ_t, all these points, for 1-minute and 10-minute hold periods alike, fell along the line for the continuous cycling results for 20 cpm. This effect

is shown in Figure 42 and suggests the very interesting conclusion, that when viewed in terms of σ_t the fatigue life is closely related to the time involved with the tension portion of the cycle. This time quantity, designated here as τ_t, is equal to one-half of the cycle time (or 0.5/f) in continuous cycling tests, to one-half of the ramping time in compression hold tests, and to one-half the ramping time plus the hold-period duration in tension hold-period tests.

A further evaluation of this concept of τ_t was based on hold periods in both tension and compression (1/1. 10/1, 1/10 and 10/10) where the results should be related to the τ_t values obtained using the tension hold-period duration. This evaluation was found to be consistent with the interpretation decsribed above. Further support for this concept of τ_t was found in the continuous cycling tests at 0.05 cpm in which τ_t is 10 minutes. In this instance these results should be comparable to the results obtained with a 10-minute hold period in tension. That this is the case is shown in Figure 43.

Over the region of linearity in Figure 41 the slope is found to be -0.135 to yield the following relationship:

$$\sigma_t = B \ N_f^{-0.135} \tag{7}$$

Since each line is associated with a specific value for τ_t the determination of B values in terms of τ_t led to:

$$\sigma_t = 27.2 \ (12.1 - \log \tau_t) \ N_f^{-0.135} \tag{8}$$

for σ_t in ksi and τ_t in minutes. Rearrangement, leads to:

$$N_f = 4.22 \times 10^{10} \ (12.2 - \log \tau_t)^{7.407} \sigma_t^{-7.407} \tag{9}$$

It is significant that the term in parentheses in equations (8) and (9) has the form of the parentheses term in the familiar Larson-Miller parameter.

Whether this is truly significant or not is difficult to determine, but further assessment of the concept would appear to be warranted. Also needed are some additional data to further substantiate this tentative model. For example, further testing at 10-minute hold periods in tension is needed in the longer life region to determine if the assumed linear and parallel behavior is appropriate. It would also be very interesting to extend the testing at 0.05 cpm to determine if the curve shape follows that observed at 20 cpm (see Figure 41). Also informative, would be tests at 2 cpm to determine if these follow this pattern for the 1-minute hold-periods in tension in a certain regime and then follow the curved trend behavior noted at 20 cpm.

While Equation (9) has some interesting features it cannot be recommended for serious consideration because of its applicability to a rather narrow range of fatigue life values. Furthermore, the functional form of Equation (7) can now be recognized as not being capable of accomodating either the slope changes in the continuous cycling results or the different type of slope changes in the tension hold-time results.

One attempt to develop a more effective functional relationship for the data presented in Figure 41 involved the use of the type of semilogarithmic plot shown in Figure 44. This type of plot proved to be useful in that the data for 1-minute tension hold-period tests defined a linear relationship over the entire range of the available results. This type of linearity corresponds to the mathmatical form:

$$N_f = Be^{-m \, \sigma_t} \qquad (10)$$

However, this functional form was not completely effective since it did not accomodate the contiuous cycling results. As noted in Figure 44 the results at 20 cpm define a relation that is linear and parallel to the line for 1-minute tension hold-period results over a limited life regime, but then the same type of curvature noted in Figure 41 is exhibited. Of course, the test

90

END
DATE
FILMED
5-81
DTIC

1.0

2 8 | 2.5

3 2 | 2.2

3 6

1.1 | 2.0

1.8

1.25 | 1.4 | 1.6

MICROCOPY RESOLUTION TEST CHART

FIGURE 41
σ_T VS N_F
RENE 95

1200°F   A = ∞

○ 20 CPM
△ 1 MIN. TENSION
□ 10 MIN. TENSION

Log σ_T

N_F, CYCLES

91

FIGURE 42
σ_T VS N_F
FOR COMPRESSION HOLD PERIODS

RENE 95   1230°F   A = ∞

	20 CPM	1 MIN. COMP.	10 MIN. COMP.
	○	△	□

N_F, CYCLES

Line from Figure 41

$\text{Log } \sigma_T$

92
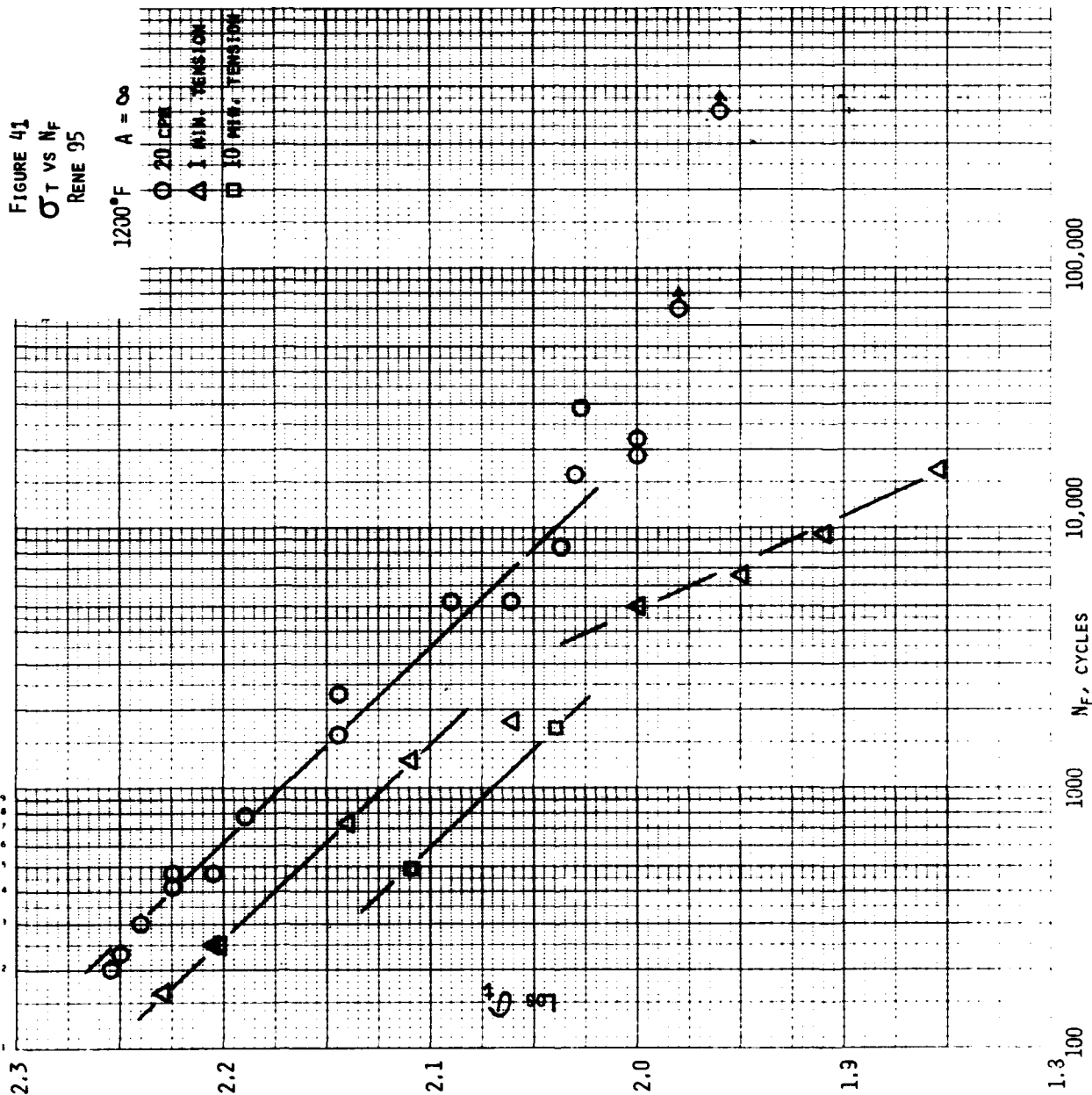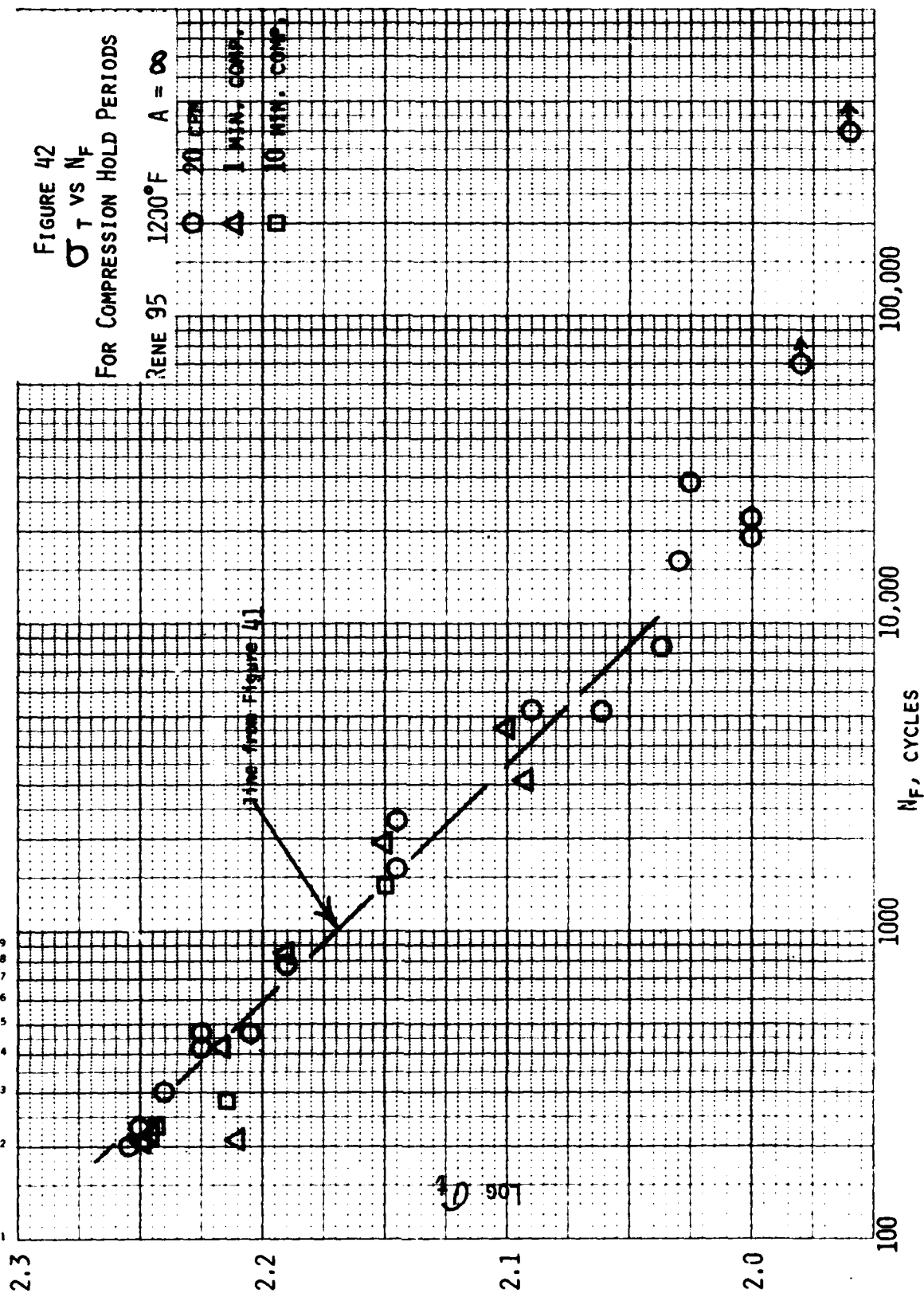
results for 1-minute and 10-minute compression hold periods fall close to the relationship defined by the 20 cpm data just as they did in Figure 42. Furthermore, the continuous cycling data at 0.05 cpm are in good agreement with the 10-minute tension hold-period results similar to the trend observed in Figure 43. These observations led to the conclusion that the concept of τ_t, cycle time tension, would again be applicable and a mathmatical form was developed to apply over the linear regions in Figure 44. This form was as follows:

$$N_f = 4.4 \times 10^5 \; \tau_t^{-0.263} \; e^{-0.0465\sigma_t} \tag{11}$$

with τ_t in minutes and σ_t in ksi.

A limited study was made to provide an addtional term in Equation 11 to describe the curve noted in the continuous cycling behavior. This study identified the following equation:

$$N_f = 4.4 \times 10^5 \; \tau_t^{-0.263} \; e^{-0.0465\sigma_t} + 4.2 \times 10^{19} \; e^{-0.354\sigma_t} \tag{12}$$

which is applicable only in the case of continuous cycling tests; for hold-period tests Equation (11) is to be used.

Actually, Equation (12) must be viewed as tentative since it is based on very limited test information. For example, as shown in Figure 44, only two data points at 20 cpm are available for the life regime above 30,000 cycles and both these are considered "run-outs" (one was a failure in the threads) and hence do not provide an exact definition of the fatigue life, but rather, a lower-bound life value. Another limitation on Equation (12) involves the application at other frequencies. Additional testing at 0.05 cpm in the longer life regime will be needed to substantiate the ability of the second term Equation (12) to accomodate the behavior at another frequency.
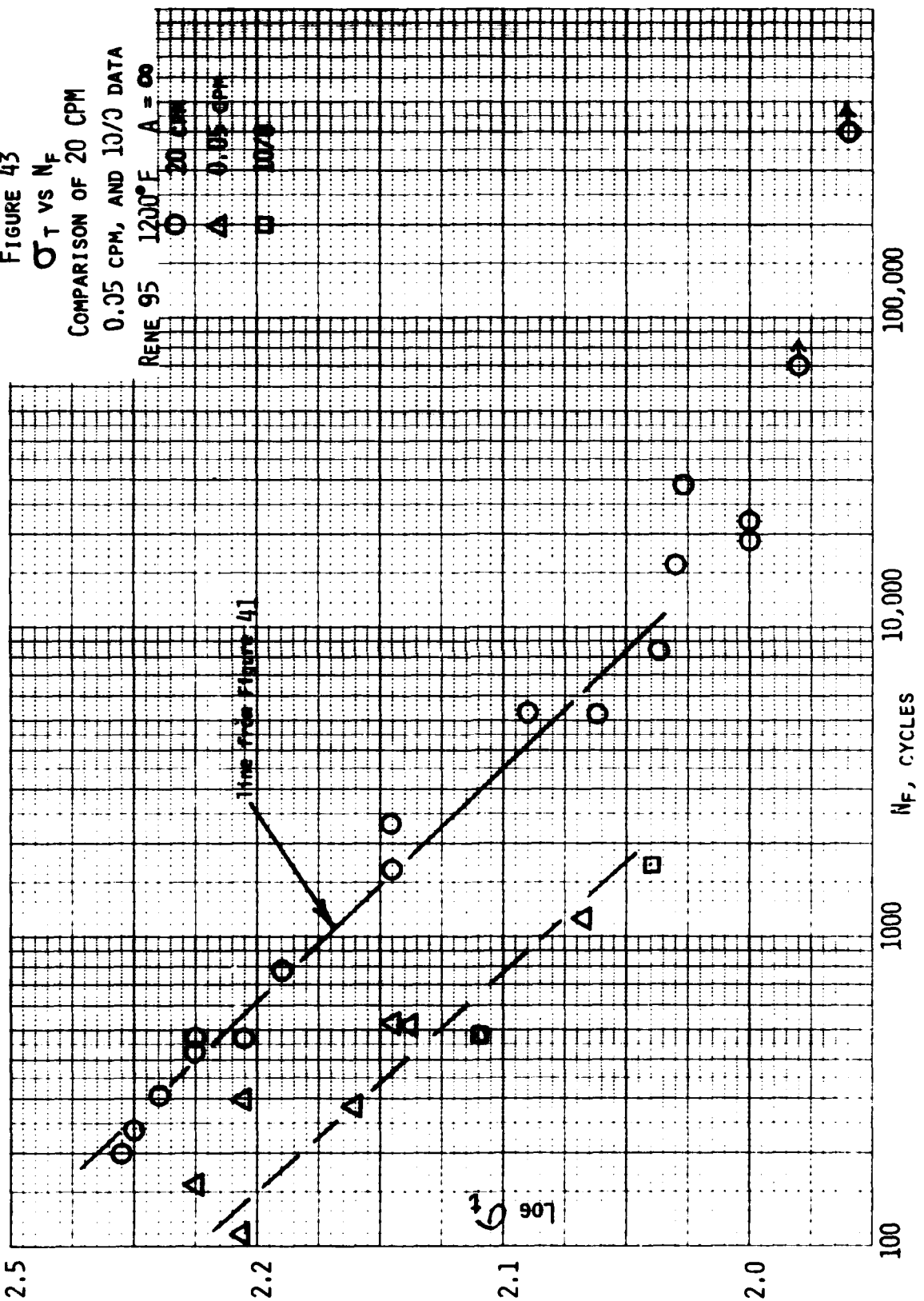
To provide some analysis of the effectiveness of Equations (11) and (12) a series of test conditions from Appendix III was selected and a comparison was made of measured and estimated values of N_f. This study led to the

93

Table X - Comparison of Experimental and Estimated Values for N_f for Rene 95 at 1200°F and A = ∞

Spec. No.	WAVE FORM	τ_t MINUTES	MEASURED N_f CYCLES	ESTIMATED N_f, Eq. (11) or (12), CYCLES
22B	0/10	0.025	224	323
23B	10/1	10.025	945	905
25B	1/10	1.025	464	390
26B	1/10	1.025	349	213
41	0/10	0.025	283	593
34	0.05 cpm	10.0	526	397
41B	0/1	0.025	1,940	1,664
53B	0/10	0.025	1,397	1,634
19	0.05 cpm	10.0	1,138	1,084
29B	1/1	1.025	5,277	5,225
51B	fast/slow	0.025	636	650
52B	slow/fast	10.025	194	107

FIGURE 43
σ_T VS N_F
COMPARISON OF 20 CPM
0.05 CPM, AND 10/3 DATA
RENE 95   1200°F   A = ∞

20 CPM   ◯
0.05 CPM △
10/3   ☐

Line from Figure 41

N_F, CYCLES

Log σ_t

95

results shown in Table X. In general, the agreement is very good and suggests
that the concept deserves a more detailed study in subsequent programs

It is to be recognized that there is some complication involved with the
use of Equations (9), (11), and (12) since the fatigue life is expressed as a
function of σ_t. However, this complication is no more serious than those
associated with correlations involving stress range and plastic strain range.
An experimental program must provide stress- strain information expressed in
terms of the tensile stress component. It should also be noted, however, that
the cyclic stress-strain behavior must be described for the various waveforms
involved since the stress-strain behavior for continuous cycling tests will
probably not be adequate for certain other waveforms. For example, in Figure
45 the data at 20 cpm would not provide a good representation for the other
waveforms. Data at 0.05 cpm appear to be close to the 1/10 data, but these all
fall below the 20 cpm data. Data for 10/0 fall even lower than the 1/10 and
0.05 cpm results. Finally, 0/1 and 0/10 data fall above the 20 cpm results
(fast-slow and slow-fast results are close to the (0/1) data) while 1/1 and
10/10 data are fairly well represented by the 20 cpm data.

If the concept of the cyclic tensile stress is to be developed the trends
identified in Figure 45, for use in Equations (9), (11) and (12), need experi-
mental verification. For instance, the behavior for 0/10 can be extended to
lower and higher strain ranges by comparison to the other curves, but how
accurate this is when used to estimate N_f values needs to be established in
laboratory tests. So do estimates for fatigue life at intermediate fre-
quencies and for longer hold periods (i.e. beyond 10 minutes).

FIGURE 44
σ_T VS N_F
ON SEMI-LOGARITHMIC
COORDINATES
RENE 95   1200°F   A = ∞

Based on equations (11) and (12)

100

97
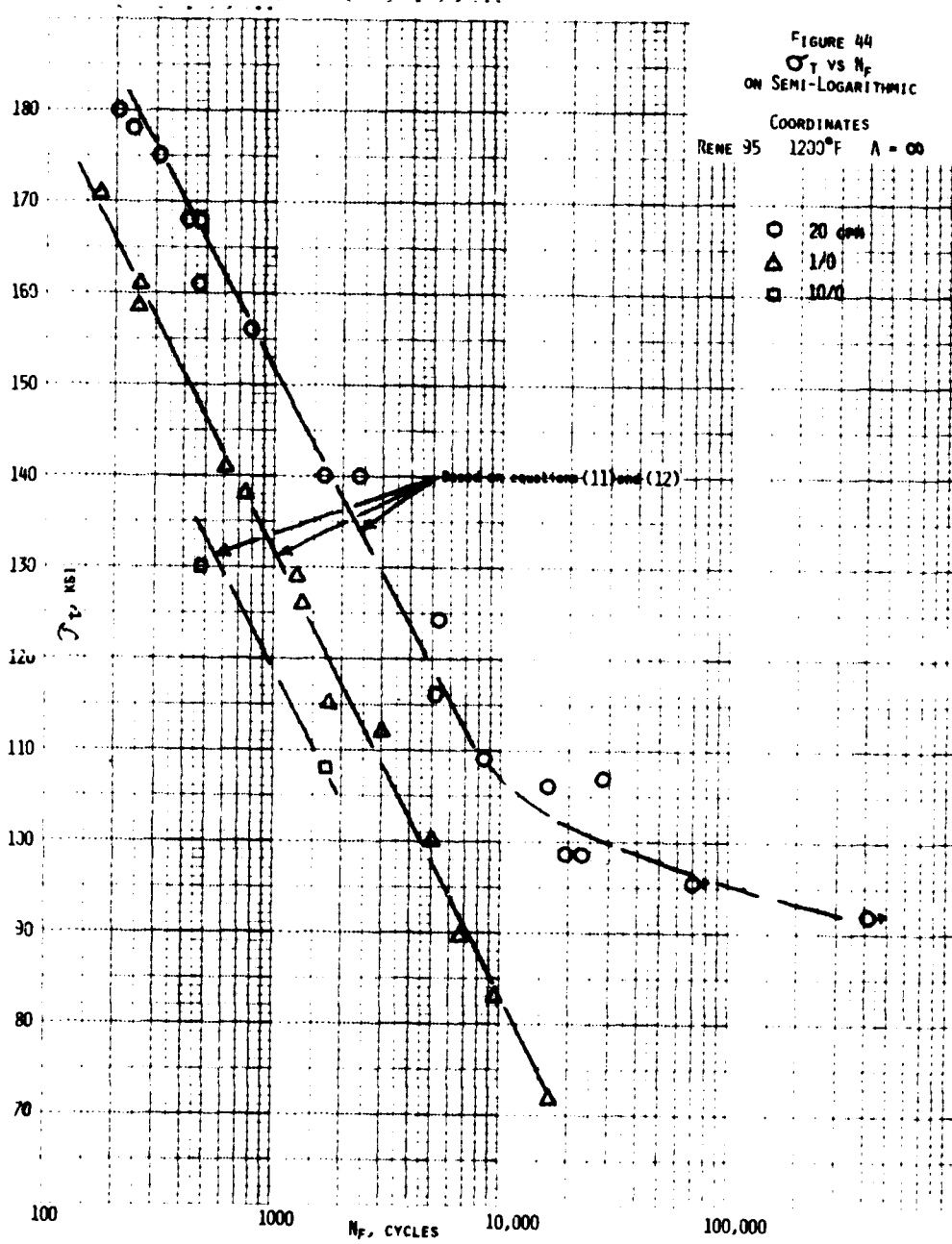
FIGURE 45
TENSILE STRESS VS STRAIN RANGE
RENE 95

1200°F   A = ∞

○ 20 CPM
△ 0.05 CPM
□ 1/0
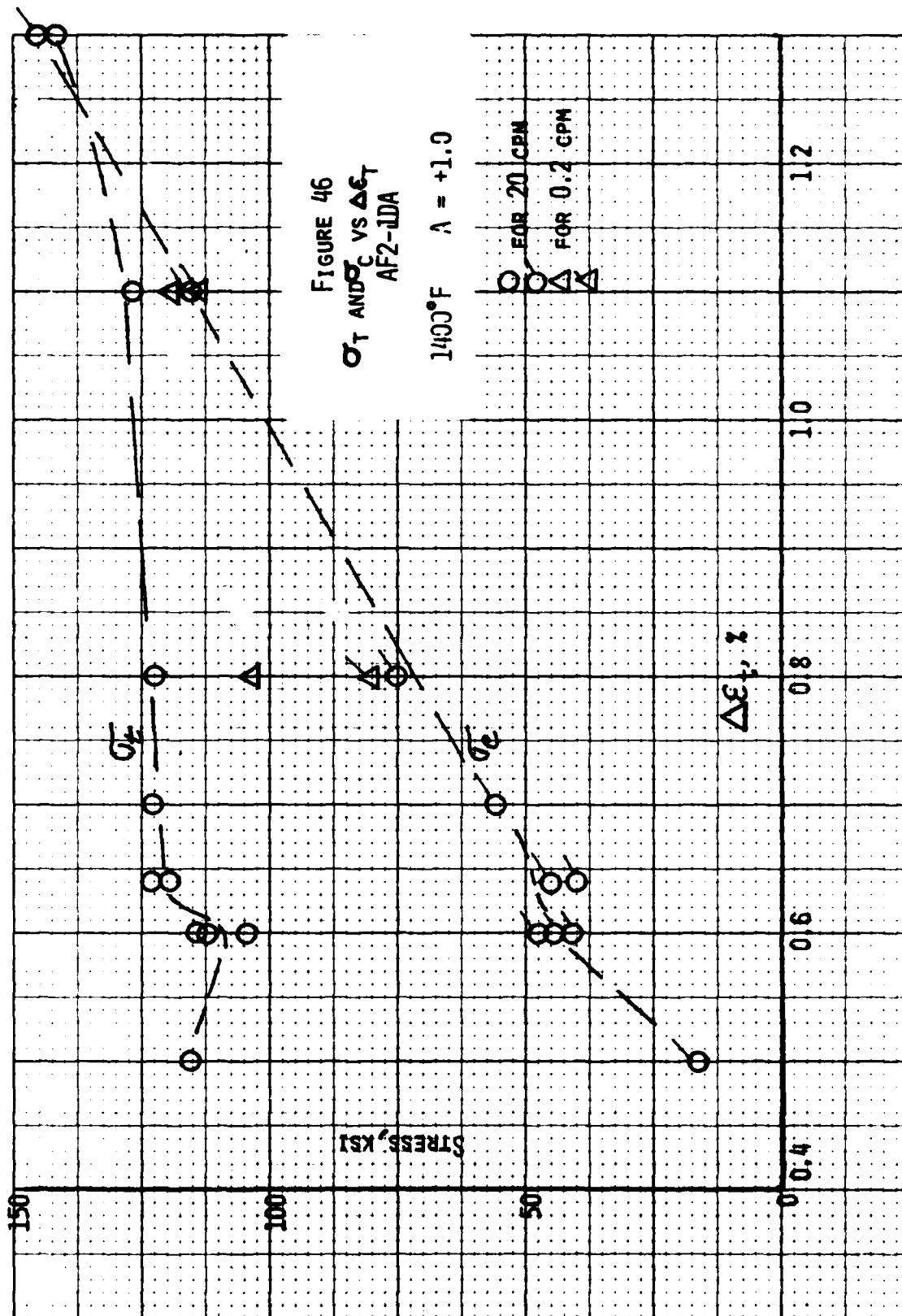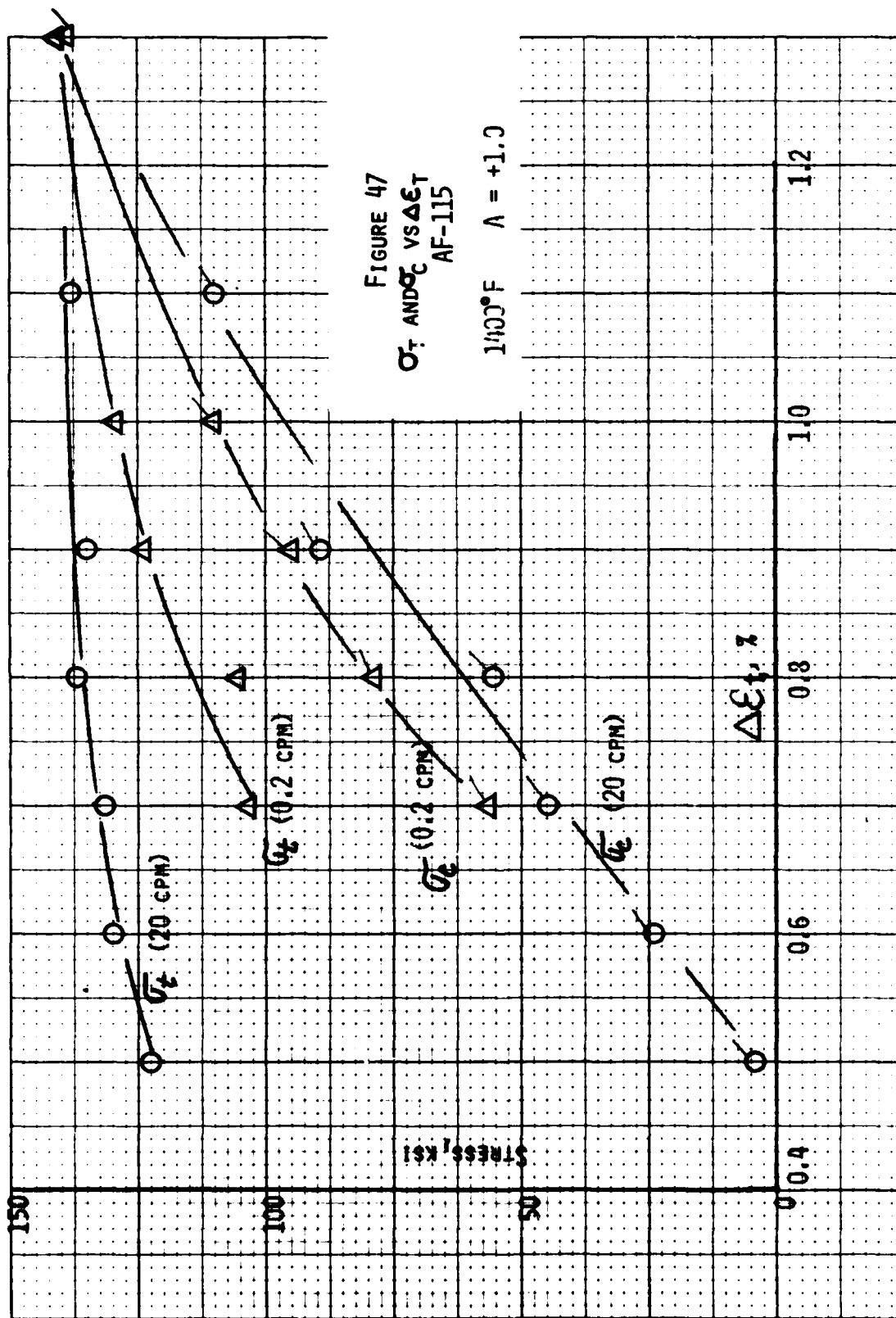▽ 0/1
◇ 10/0
◇ 0/10

σ_t KSI

$\Delta \varepsilon_t$, %
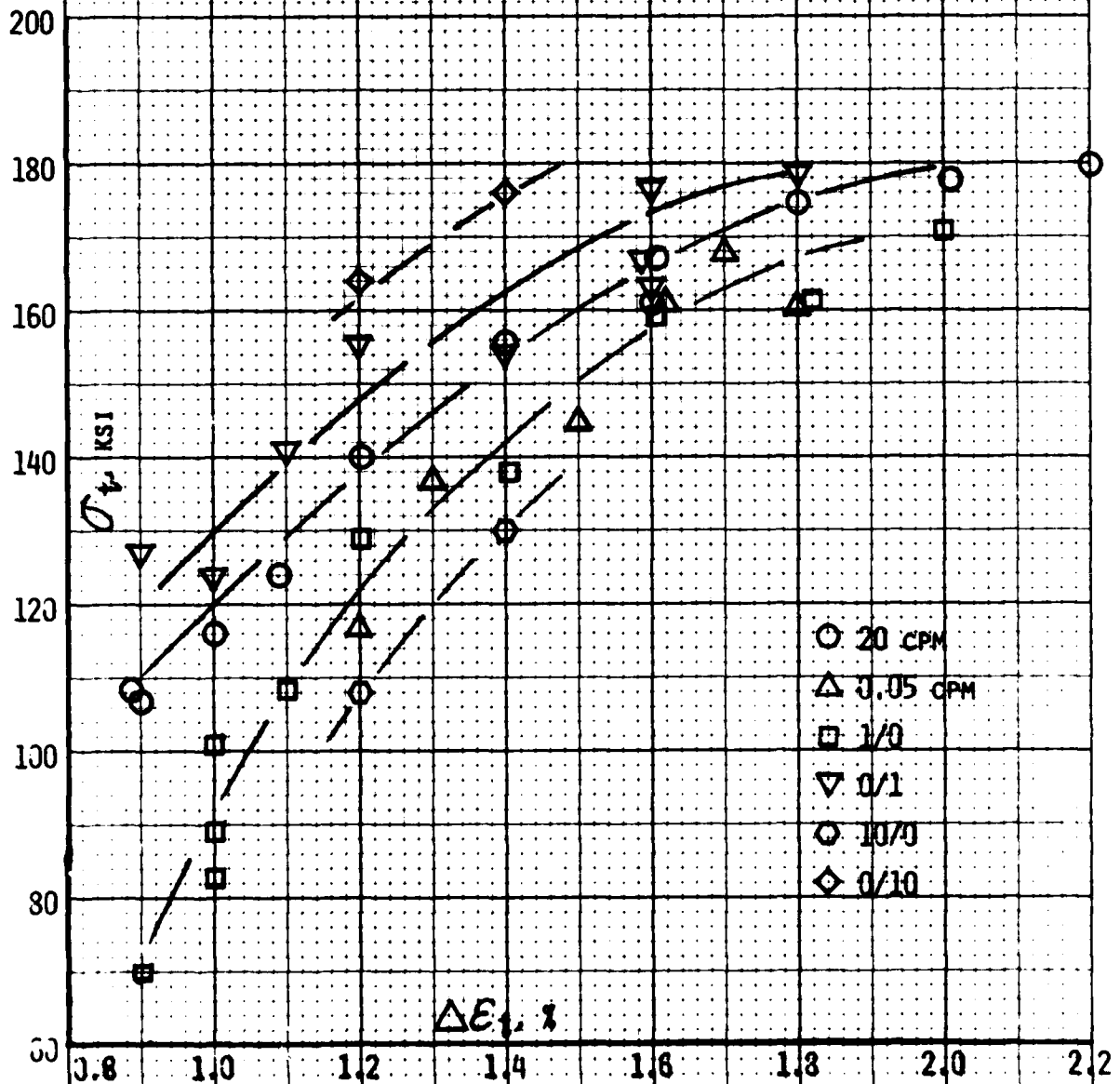
4) Special Discussion of Presentation of Stress Components

Continuous cycling tests at A = ∞ usually exhibit a mean stress close to zero. Such tests were performed in the evaluation of the Rene 95 alloy and as noted in the discussion of Figure 31, the compressive and tensile stress components were of nearly equal magnitude. Actually, a small compressive mean stress was found to exist over all the strain range values employed. However, in continuous cycling tests at A = 1.0, such as were performed for the AF2IDA and AFT15 alloys, wide variations in mean stress are observed depending upon temperature, strain range and frequency. In these situations, it is important to define the fatigue response completely by some type of graphical presentation of the tensile and compressive stress components. For example, one type of graphical display is presented in Figures 46 and 47, where it is noted that similar behavior patterns are exhibited by the two alloys. In the higher strain range regime, the magnitude of the tensile stress approaches, or becomes equal to, that of the compressive stress to define a region within which the mean stress is close to zero. As the strain range is decreased, the magnitude of the compressive stress falls below that of the tensile stress to yield a region within which a mean tensile stress is exhibited. In the totally elastic regime the compressive stress is essentially zero to correspond to a condition for which the value of the mean stress is equal to one-half the tensile stress (i.e. A = +1.0 on stress).

Some effect of cycling frequency is noted in Figures 46 and 47. At 0.2 cpm the behavior at the high strain range values does not appear to be affected, but a lower strain ranges, the σ_t and σ_c values define a condition, for a given strainrange, that is closer to a zero mean stress value than that oberved at 20 cpm.

Another method for presenting stress component data was identified in this

FIGURE 46

σ_T AND σ_C VS $\Delta \epsilon_T$
AF2-1DA

1400°F $\Lambda = +1.0$

⊙ FOR 20 CPM
△ FOR 0.2 CPM

STRESS, KSI

$\Delta \epsilon_T$, %

Figure 47
σ_T and σ_C vs $\Delta \epsilon_T$
AF-115

$1400°F \qquad A = +1.0$

program and is illustrated in Figure 48, 49, and 50. In this construction the stress amplitude ($\Delta\sigma/2$ at $N_f/2$) is ploted as a function of the strain amplitude ($\Delta\varepsilon_t/2$). Also included in this diagram is the elastic line based on the data in Appendices I and II. This, of course, allows values for pseudo-alternating stress to be read directly as points along this elastic line. A-nother important feature of Figures 48, 49, and 50 is the inclusion of the mean stress values to provide a very clear demonstration of how these quanti-ties vary with strain amplitude. An interesting aspect of this mean stress behavior is that, for the three figures shown, the variation is not only linear, but it is linear in each case over the entire strain amplitude regime, from approximately 0.2 to 0.6%. Another important feature regarding this linearity in the type of diagram presented here is the separate boundary regions estab-lished by the intersection of the mean stress line with the stress amplitude data and with the zero stress axis. Three regions are therby defined as shown in Figure 48, 49, and 50. In Region I, A_σ = +1.0 to indicate that the mean stress is equal to the alternating stress and can be read as points along the elastic line for any given strain amplitude; in the Region II, A_σ is greater than 1.0, but less that infinity, and mean stress values can be read from the mean stress line. Finally, in Region III, A_σ = ∞, and the mean stress is zero. An illustration of how the A - ratio (expressed a $1/A_\sigma$) on stress varies with strain amplitude for the date in Figure 49 is shown in Figure 51.

Frequency was found to have a definite effect on the position of the mean stress line although the data are not extensive enough to enable any more than a qualitative interpretaion to be made at this time. Based on a study of the data for AFT15 at 1400°F and 0.2 cpm, the line terminating in point "P" (Figure 50) has been positioned to represent mean stress behavior at this lower fre-quency. In the higher strain amplitudes (near 0.60%), the mean stress in near zero and as the strain amplitude is decreased, the mean stress value increases
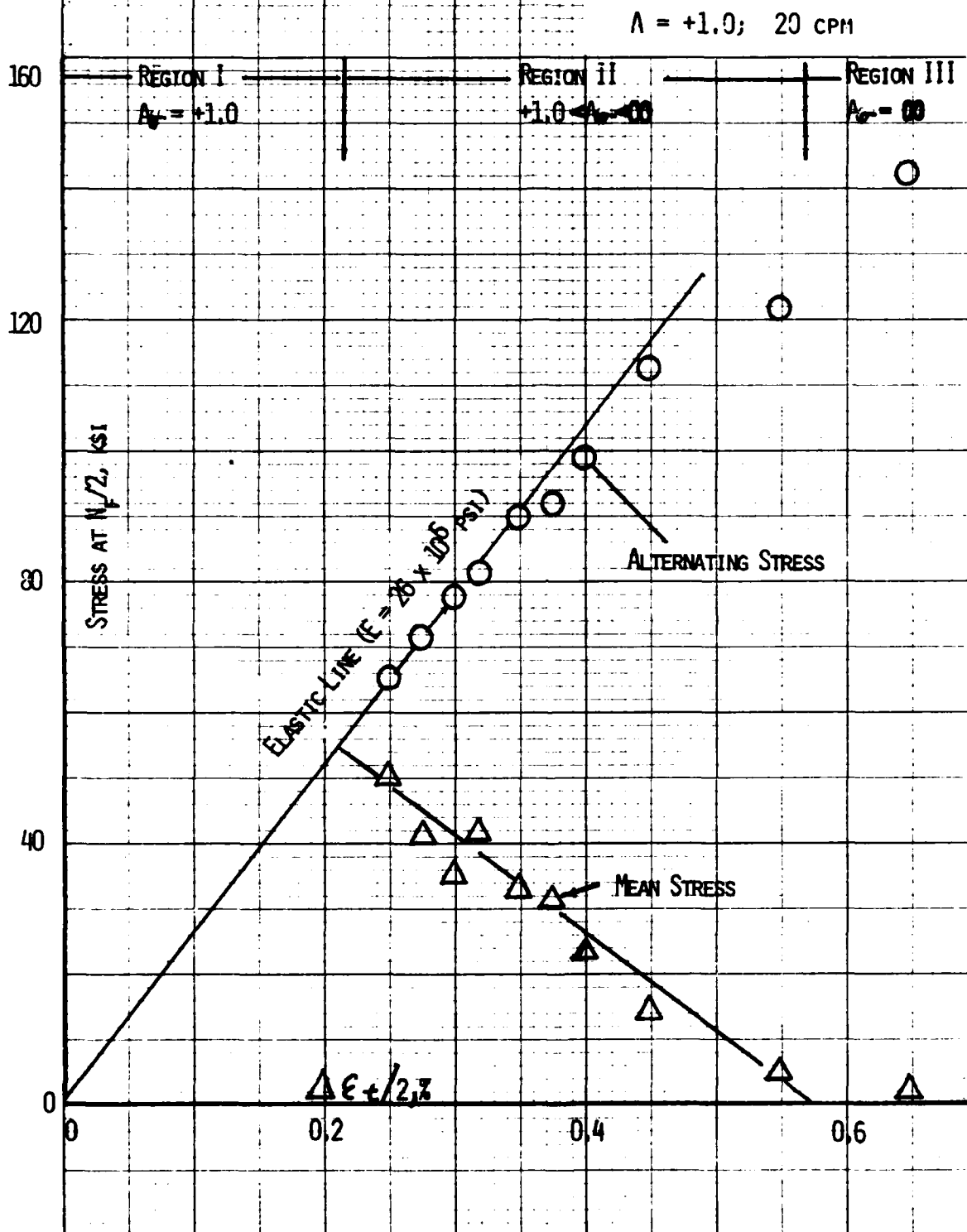
FIGURE 48
AF2-1DA
1400°F

$\Lambda = +1.0;\ \ 20$ CPM
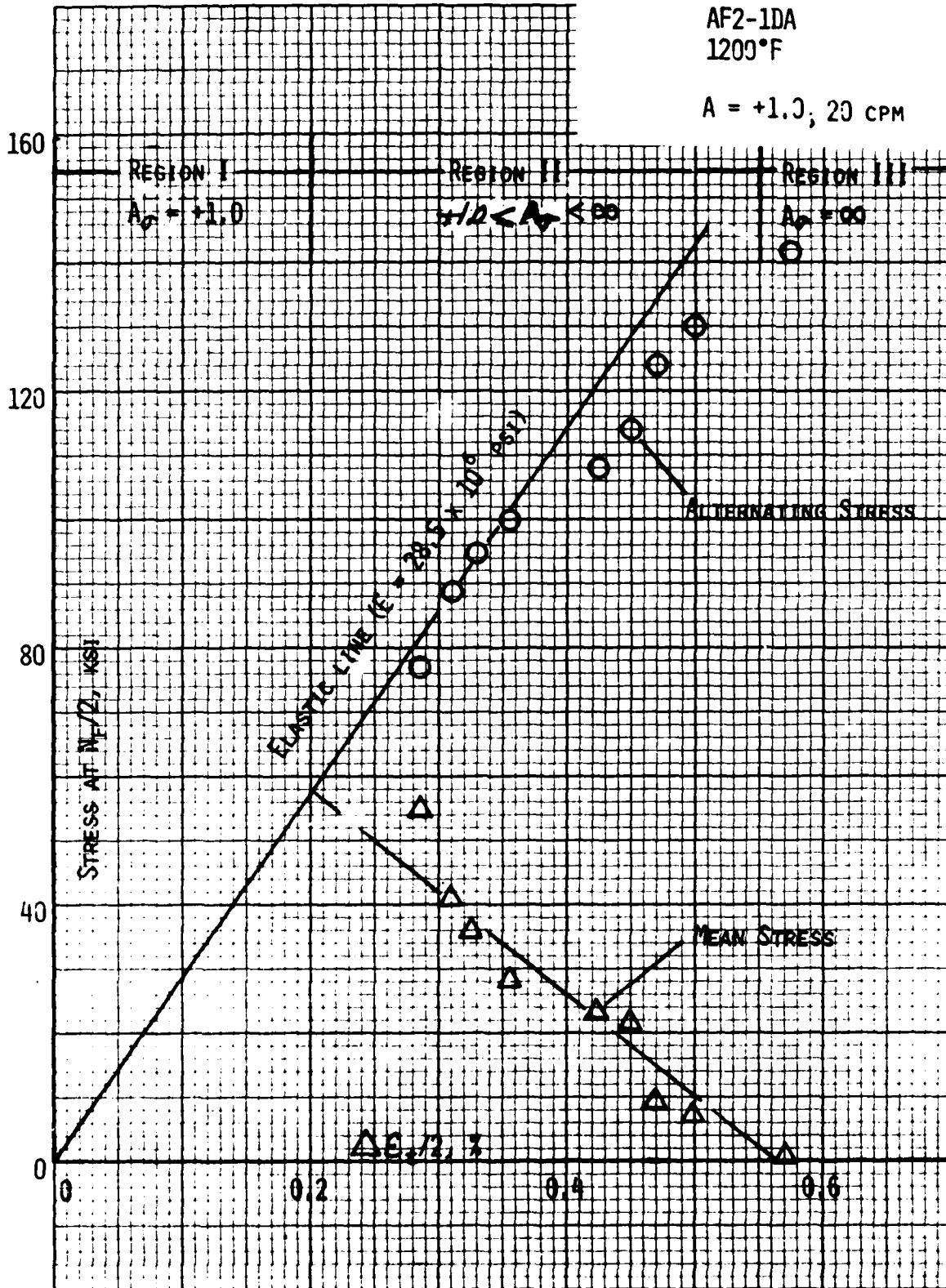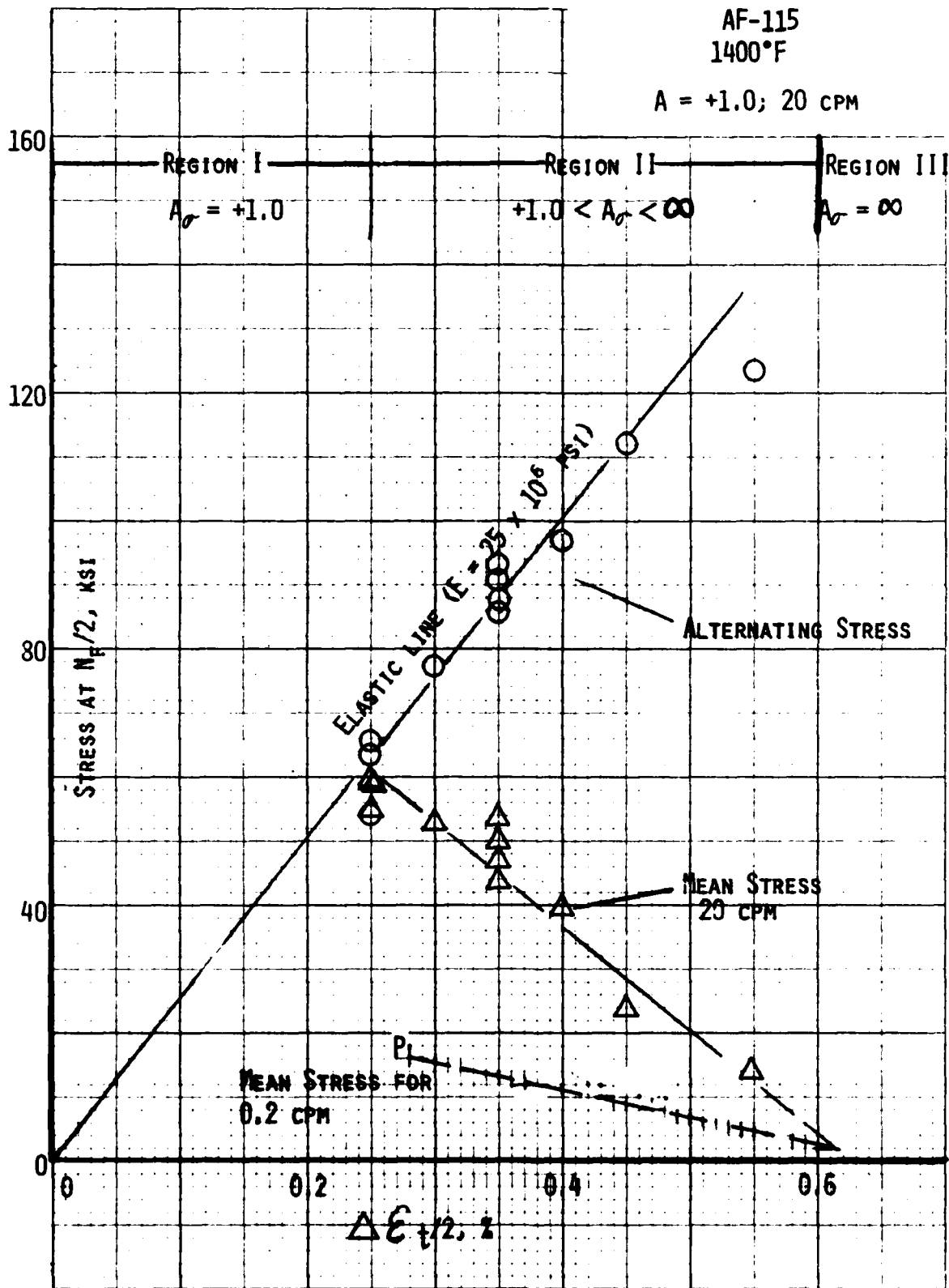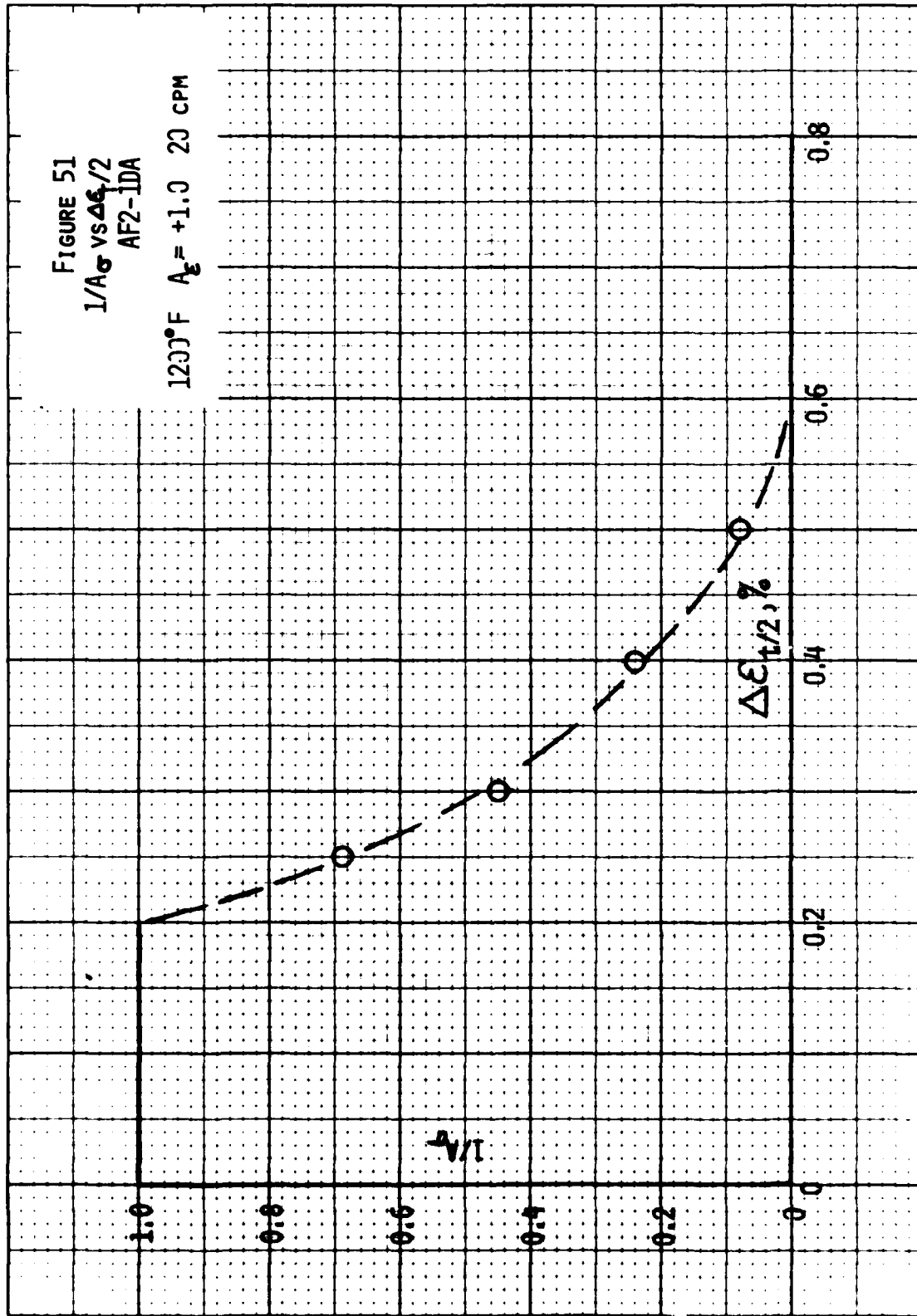
103

FIGURE 49
AF2-1DA
1200°F

A = +1.0; 20 CPM

104

FIGURE 50
AF-115
1400°F

A = +1.0; 20 CPM

in the tension direction but never to values as high as those observed at the higher frequencies. This line has been terminated at point "P" since this represents the limit of the test results. It would be reasonable to assume that this line should continue to be linear and intersect the elastic line near a strain amplitude of 0.1%, but more experimental results are needed for confirmation.

A further development of the stress-strain-amplitude plot, described in conjunction with Figures 48, 49, and 50, is illustrated in Figure 52. In preparing this example, Figure 48 was selected and is positioned in Figure 52 so that the strain amplitude axis is the ordinate. Data in this form were plotted alongside the fatigue results ($\Delta \epsilon_t$ vs N_f) of Figure 5 with the applicable stress component information. In this plot then, a complete description is provided for a given alloy tested at a given temperature, A - ratio and frequency. For example, if a certain strain range is selected, the chart given in Figure 52 is entered with the value for the strain-amplitude, and in addition to reading the fatigue life by a horizontal projection to the right, a horizontal projection to the left yields values for stress amplitude (doubling this, yields the stress range) and mean stress. Adding the stress amplitude to the mean stress leads to the value for the tensile stress component. Dividing the stress amplitude by the mean stress, allows the A - ratio on stress to be calculated. If this latter quantity is important in certain applications, the type of plot shown in Figure 51 could easily be added to the left-hand side of Figure 52 to enable this A - ratio value (on stress) to be read directly as $1/A_\sigma$. Also included in Figure 52 is an average value for the elastic modulus based on measurements made during the start-up of tests in which an axial extensometer is used. This defines the relationship between stress range and elastic strain range, and enables an elastic strain range scale to be positioned in Figure 52. A vertical pro-

106

FIGURE 51
$1/A_\sigma$ vs $\Delta\varepsilon_{t}/2$
AF2-1DA

$1200°F$ $A_\varepsilon = +1.0$ 20 CPM

$1/A_\sigma$

$\Delta\varepsilon_{t/2}$, %

jection from a given stress amplitude value yields the corresponding value for the elastic strain range. Then, the associated value for the calculated plastic strain range can easily be obtained by subtracting the elastic strain range from the total strain range. In this plot, a fairly complete definition of material response characteristics is available for a given material at a selected frequency, temperature, and A_ϵ - ratio. Similar plots at other temperatures, A - ratios (on strain) and frequencies would represent a comprehensive description of the fatigue characteristics for a material.

Another observation that has been made in conjunction with Figure 52 relates to the significance of two strain amplitude values on the stress-strain-amplitude plot. One value is associated with the deviation of the stress amplitude data from the elastic line. This is identified as point X in Figure 52 and appears to correspond to the upper slope change in the N_f plot (identified as point $\overline{X}$ in Figure 52). A second strain amplitude value is associated with the intersection of the mean stress line with the elastic line (identified as point Y in Figure 52). This point has a counterpart on the fatigue plot at $\overline{Y}$ and should correspond to the location of another slope change at which point the fatigue curve should develop a much shallower slope and tend to exhibit an endurance limit. Admittedly, this interpretation is not completely substantiated experimentally and hence must be viewed as very tentative. It seems, however, to represent an interesting concept and one that should be studied in subsequent programs. Perhaps even a third point could be indentified in Figure 52 as the point where the mean stress is zero. However, this too, must await further evaluation.

Figure 52

AF2-1DA

1400°F
A = +1.0
20 CPM
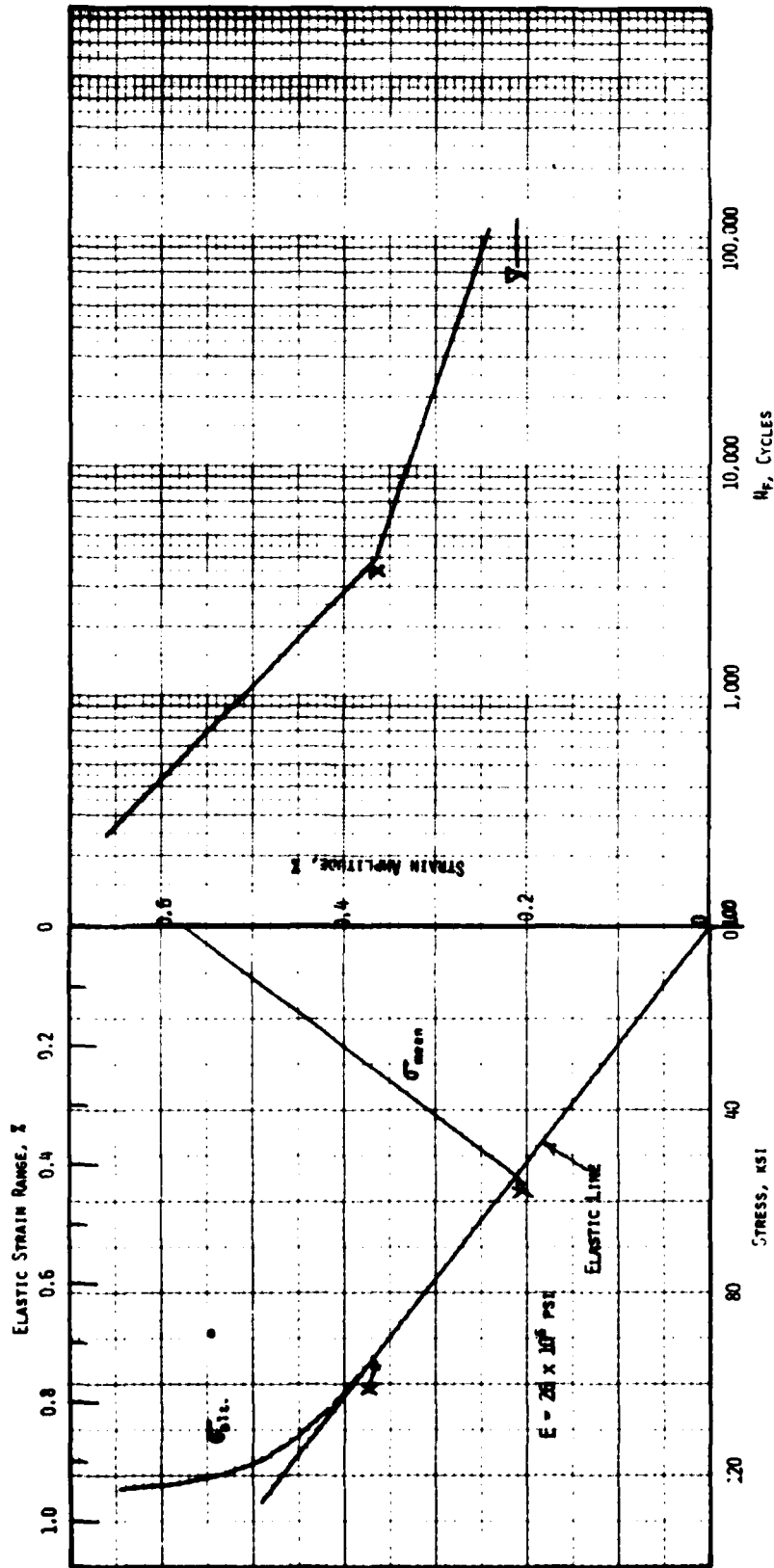
REFERENCES

1. Time Dependent Fatigue, A general Assessment (1975), ORNL 5073, Oak Ridge National Laboratory, W. L. Greenstreet Ed. 1977.

2. H. L. Bernstein: "An Evaluation of Four Current Models to Predict the Creep-Fatigue Interaction in Rene 95," AFML-TR-79-4075, Air Force Materials Laboratory, 1979.

3. J. M. Hyzak and H. L. Bernstein: "An Analysis of the Low Cycle Fatigue Behavior of the Superalloy Rene 95 by Strainrange Partitioning," AFML-TR-78-174, Air Force Materials Laboratory, 1978.

4. J. M. Hyzak and H. L. Bernstein: "An Analysis of the Low Cycle Fatigue Behavior of the Superalloy Rene 95 by Strainrange Partitioning," AGARD-CP-243, 1978, p. 11-1.

5. M. N. Menon: "Metallographic Characterization of Rene 95 Forgings," AFML-TR-73-180, Air Force Materials Laboratory, 1973.

6. M. N. Menon and W. H. Reimann: Met. Trans., 1975, Vol. 6A, p. 1073.

7. M. N. Menon and W. H. Reimann: J. Mat'ls Science, 1975, Vol. 10, p 1571.

8. S. S. Manson: Experimental Mechanics, Vol. 5, NO.7, 1965, p. 193.

9. T. Bui-Quoc and A. Biron, Comparison of Low-Cycle Fatigue Results with Axial and Diametral Extensometers, Experimental Mechanics, p 127, April, 1978.

10. S. S. Manson, Behavior of Materials under Conditions of Thermal Stress, National Advisory Committee for Aeronautics, Technical Note 2933, 1953.

11. L. F. Coffin, Jr., A Study of the Effects of Cyclic Thermal Stress, Ductile Material, Trans. ASME (Amer. Soc. Mech. Eng.), 76: 931-950 (1954).

12. H. L. Bernstein, "The Stress Behavior of Three Advanced Nickel-Based Superalloys During High Temperature, Low-Cycle Fatigue," to be published as an Air Force Materials Laboratory Technical Report, 1980.

FOOTNOTES FOR APPENDIX A

AF2-1DA

1. Relaxed Stress = Stress at beginning of hold period minus stress at end of hold period.

2. Nominal value

3. "+" indicates specimen failed outside the gage section.

4. Load control test - Strain not measured.

5. INTY = Infinity

6. Actually 4.95 minute/0 minutes

FOOTNOTES FOR APPENDIX B

AF-115

1. Relaxed Stress = Stress at beginning of hold period minus stress at end of hold period.

2. Nominal value

3. "+" indicates specimen failed outside the gage section.

4. Load control test – strain not measured.

5. INTY = Infinity

6. Actually 4.95 minutes/0 minutes.

7. 200, 400, 700 900   as HIP condition
   300   Heat #3
   500   HIP + forge

APPENDIX C

FOOTNOTES TO RENE 95

1. Nominal values

2. Relaxed tensile stress = tensile stress at beginning of hold period minus tensile stress at the end of the hold period.

3. The stress and strain at the beginning of the hold period for the intermediate hold tests. For the SLOW-FAST and FAST-SLOW tests, the stress and strain when the strain rate changed from the fast to the slow rate.

4. INTY = Infinity
   nominal value

5. Specimen was prestrained to 2% compression and then to zero strain before test began.

6. Uniform cylindrical gage section specimen of 0.25 in. Specimen was preworked by cycling it form zero to 174.4 ksi, back to zero and then to 180.0 ksi and back to zero. This pre-work resulted in a plastic strain of 0.72%. This strain was used as the zero strain level for the fatigue test. This pre-work caused a mean tensile stress to develop in the fatigue test.

7. The axial plastic strain was the controlled variable.

8. Specimen was initially cycled at $\Delta\epsilon = 0.97\%$ for 282 cycles using a 0.05-1/2-20 cpm waveform. Since this pre-cycling was not considered damaging the value of N_f does not include these cycles.

9. Test was stopped and restarted. The stress and strain was measured near 5288 cycles. The large tensile mean stress appears to be an anomaly. Specimen 263 was initially cycled under the same conditions as #257, but developed a mean compressive stress after 282 cycles.

10. Value not recorded.

11. - failed in threads. Stress and strain measured at 70,212 cycles.

12. - runnout. Stress and strain measured at 298,784 cycles.

13. - Suffixes mean: I - invalid life
                     R - runnout

14. - Test was stopped and restarted.

15. - Stress and strain measured at $N_f/4$

16. - Test was stopped and restarted at 1367 minutes.

17. - Plastic strain not recorded. Value calculated from: plastic strain = total strain minus (stress range divided by the elastic modulus).

18. - Values measured from the hysteresis loop at $N_f/2$.

DATE
ILMED
-8